UNITED STATES DEPARTMENT OF THE INTERIOR

GEOLOGICAL SURVEY

Trace element and rare earth element variation in fluorites collected from skarn and epithermal mineral deposits in the Sierra Cuchillo area, south-central New Mexico

by

Robert G. Eppinger, III

Open-File Report 88-566

U.S. Geological Survey, DFC, Box 25046, MS 973, Denver, CO 80225

1988

CONTENTS

CONTENTS (continued)

APPENDICES

FIGURES

TABLES

PLATES

(plates in back pocket)

ABSTRACT

Fluorite samples were collected in the Sierra Cuchillo region of south-central New Mexico, from the following 4 fluorite-bearing deposit types: Au-Ag veins, Ba-Pb veins, W-Be skarn, and "barren" quartz-calcite-fluorite veins apparently devoid of other metals. In addition, several fluorite samples were collected from ambiguous or "questionable" deposit types. Fluorite from both outcrop and stream sediment was collected. Samples were analyzed by quantitative and semiquantitative methods for trace and rare earth elements (REE). The trace and REE data were used to differentiate fluorites from the various deposit types.

Trace and REE patterns are unique for the different deposit types. Fluorites from Au-Ag veins have positive Eu anomalies; high Sr content; and low Be, Ba, Ti, U, and Y content. Fluorites from W-Be skarn have negative Eu anomalies; high Be, Ti, U, Y, Mn, and Mg content; and low Sr and Ba content. Fluorites from Ba-Pb veins have negative Eu anomalies; high Ba and Pb content; and low Sr and U content. "Barren" vein fluorites contain variable content in the above trace elements and exhibit variable Eu anomalies. Fluorites from "questionable" deposit type are similar to the "barren" vein fluorites. The wide chemical variation in the fluorites studied may be due in part to varying degrees of wallrock alteration.

Fluorite from "barren" veins is more abundant than fluorite from other deposits and shows wide chemical variation. One group of "barren" vein fluorites exhibits chemical characteristics similar to W-Be skarn fluorites. A second group of "barren" vein fluorites exhibits chemical affinities to Au-Ag vein fluorites. These similar geochemical signatures in the fluorite, coupled with favorable geologic settings, suggest the possibility of concealed skarn deposits underlying one and precious metal deposits underlying the other "barren" vein group. Thus, fluorite mineral separates geochemistry delineated potential concealed mineral deposits and may be a useful tool elsewhere in mineral exploration.

Fluorite exhibits a strong correlation between color and high light REE (La, Ce, Pr, and Nd) content. High content of these elements are found in both green and purple fluorites. Colorless fluorites generally do not exhibit high content of light REE, except in fluorites bleached colorless by sunlight exposure. No correlation was found between purple fluorite and uranium content.

ACKNOWLEDGEMENTS

Numerous people from the U.S. Geological Survey aided me in this study. I thank Steve Smith for his diligent field assistance, Betty Adrian for SES analyses, Al Meier for ICP-MS analyses, Jerry Motooka for ICP-AES analyses, and Jerry Gaccetta for XRD analyses. Ted Botinelly, Paul Theobald, Allen Heyl, Charlie Maxwell, Steve Smith, and Wally Griffitts provided insight and valuable expertise through numerous helpful discussions.

Personnel from the Colorado School of Mines who helped at various stages of the study include Professors Keenan Lee and Bob Hamilton. My advisor, Professor Graham Closs, is gratefully acknowledged for advice throughout the study. Graduate students at CSM provided thought-provoking and helpful discussion.

Finally, I want to thank my wife Catharine for patience and moral support, and my son Paul for sparkling smiles that motivated me immensely.

INTRODUCTION

General Statement

The use of mineral separates in geochemical exploration is developing into a promising exploration tool. Numerous workers have examined various minerals as possible guides to mineral deposits (Table 1). As undiscovered mineral deposits in the western world become ever more elusive, novel exploration techniques, such as mineral separate geochemistry, will become increasingly important.

It is well known that fluorite is found in many varied colors and habits, as attested by the multitude of spectacularly diverse fluorite specimens found in museums and private mineral collections worldwide. Of equally common knowledge is the occurrence of fluorite in a variety of mineral deposits of widely different character, from low-temperature epithermal veins, to high-temperature greissens, tactites, porphyries, and pegmatites (Table 2). The occurrence of fluorite in nature is an almost universal indicator of mineral deposits.

This study is an attempt to glean more information from fluorite. Since fluorite occurs in many different types of mineral deposits, it may have features that can differentiate these deposits.

Purpose of Study

This study addresses two questions: Do fluorites from different deposit types within a single fluorine-rich province contain different chemical or physical signatures? If so, can these features be used as exploration tools within that province?

To address these questions, fluorite mineral separates from different deposit types within a single fluorine-rich province were collected and analyzed for various trace elements and physical features. The area chosen for study contains 4 different fluorite-bearing deposit types: W-Be skarn, epithermal Au-Ag veins, epithermal Ba-Pb veins, and epithermal "barren" calcite-quartz-fluorite veins which apparently are devoid of other metals. In addition, fluorite was collected at several localities where the deposit type could not be determined.

The main thrust of this study involved trace element and rare earth element (REE) analyses of the fluorite separates. A limited study of physical properties of fluorite (involving color and fluorescence) augmented the chemical data.

Location/Accessibility/Climate

The study area, encompassing parts of the Sierra Cuchillo, Black Range, and Caballo Mountains, lies predominantly in Sierra County in south-central New Mexico. The towns of Truth or Consequences, Cuchillo, and Winston lie within the study area (Figure 1). State Highway 52 traverses the majority of the study area, and Interstate Highway 25 crosses the eastern part.

Unimproved roads provide relatively good access from the main highways. However, while the mountain ranges are generally under U.S. Forest Service and BLM control, privately held lands flank the ranges and permission must be obtained from local ranchers for access.

Table 1.--Selected mineral separate geochemical studies used in mineral exploration. Data from S. M. Smith, U.S. Geological Survey, written comm., 1987.

MINERAL OR GROUP	MAJOR METAL OR DEPOSIT TYPE	REFERENCE
Amphibole	porphyry Cu	Mason, 1978, 1979
Apatite	porphyry Cu	Williams and Cesbron, 1977
	W, Mo, Fluorite	Tsusue and others, 1981
Biotite	porphyry Cu	Al-Hashimi and Brownlow, 1970
	" "	Graybeal, 1973
	" "	Lovering and others, 1970
	" "	Mason, 1978, 1979
	" "	Jacobs and Parry, 1976
	hydrothermal Au vein	Mantei and Brownlow, 1967
	W-Mo-Cu skarn	Darling, 1971
Magnetite	general metal expl.	deGrys, 1970
	" " "	Theobald and Havens, 1960
	" " "	Theobald and others, 1967
	Zn	Theobald and Thompson, 1962
	Pb-Zn, Cu	Hamil and Nakowski, 1971
	various deposit types	Lovering and Hedal, 1987
Muscovite	Be-Nb pegmatites	Heinrich, 1962
Pyrite	various Au deposits	Auger, 1941
	various sulfide dep.	Hawley and Nichol, 1961
	massive sulfide	Johnson, 1972
	" "	Loftus-Hills and Soloman, 1967
	" "	Ryall, 1977
Rutile	porphyry Cu	William and Cesbron, 1977
Tourmaline	general metal expl.	Power, 1968
	massive sulfide	Brown and Ayuso, 1985
	" "	Ethier and Campbell, 1977
	" "	Taylor and Slack, 1984
	Cu	Birk, 1980
	hydrothermal Cu-Mo	Smith and others, 1987

Table 2.--Mineral deposit types containing fluorite. I, intermediate component (between 1 and 10 volume %); T, trace component (1 volume % or less). Data from Cox and Singer, 1986.

	Relative Volume % Fluorite
Related to alkaline intrusions	
carbonatites	I
Related to felsic phanerocrystalline intrusive rocks	
W skarn	T
Sn skarn	I
replacement Sn	I
Related to felsic porphyroaphanitic intrusions	
Climax Mo	I
Zn-Pb skarn	I
Replacement Mn	I
Sn-polymetallic veins	I
Au-Ag-Te veins	I
polymetallic veins	I
Related to subaerial felsic to mafic extrusive rocks	
hot spring Au-Ag	I
Creede epithermal vein	I
Comstock epithermal vein	I
volcanogenic U	I
rhyolite-hosted Sn	I
volcanic-hosted magnetite	I
carbonate-hosted Au	I
simple Sb	I
Deposits in clastic sedimentary rocks	
Olympic Dam Cu-U-Au	T
sandstone-hosted Pb-Zn	T
emerald veins	I
Deposits in carbonate rocks	
Appalachian Zn	T
Deposits related to regionally metamorphosed rocks	
Au-qtz veins, low sulfide	T
Homestake Au	T
Au on flat faults	T

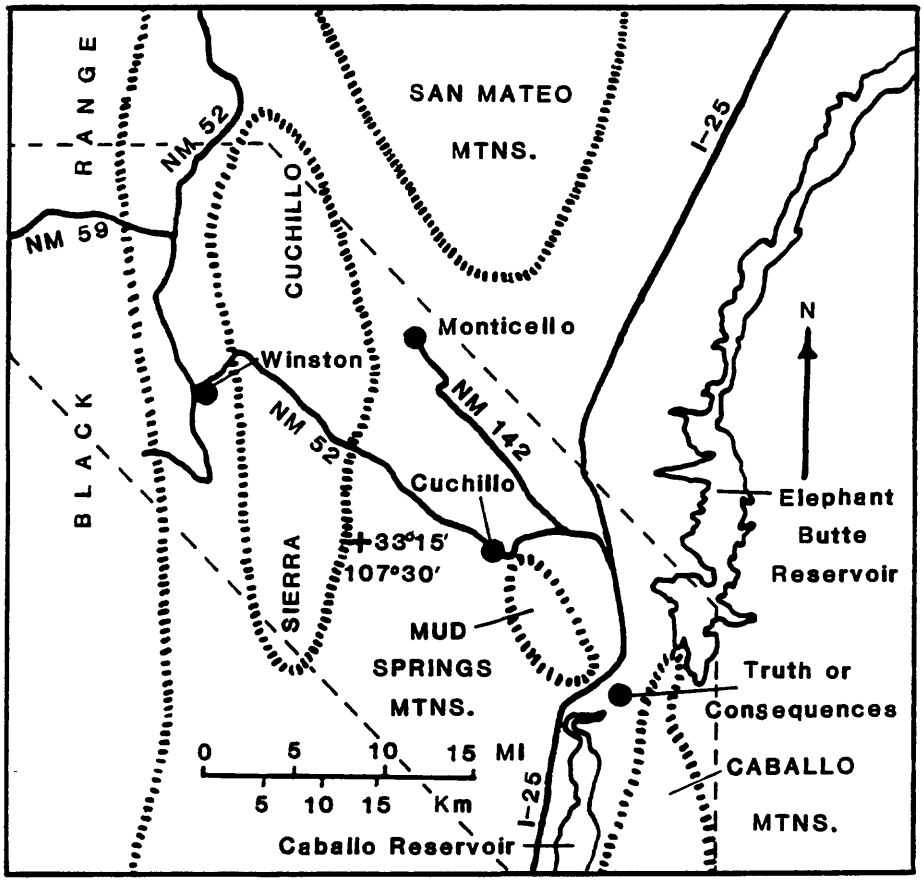

Figure 1.--Location map of study area. Dashed line indicates approximate area of coverage on Plates 1 and 2.

The study area is located in the northern extremity of the Chihuahuan Desert (Mueller, 1986). The mean annual temperature at Truth or Consequences from 1951-1982 was 59.8° F, with extremes ranging from -5° F to 106° F (Kunkel, 1984). Precipitation averages 8.77 in. annually in Truth or Consequences, the majority occurring as thunderstorms from June through October (Kunkel, 1984).

Previous Studies

Numerous geological studies have been undertaken in and around the study area. Silliman (1882) discussed active mines in the region. Brief descriptions of geology and mineral deposits in active mining districts were reported by Lindgren and others (1910). Harley (1934) provided one of the earliest comprehensive studies of the geology and ore deposits of Sierra County. Kelley (1955b) compiled a geologic map of the Sierra County region as part of a New Mexico Geological Society Guidebook. Kelley and Silver (1952) discussed geology and mineral deposits of the Caballo Mountains. Jahns (1944, 1955) thoroughly described geology and mineral deposits in the northern Sierra Cuchillo, and Jahns and others (1978) revised and expanded the earlier work. Alminas and others (1972 a-e; 1975 a-c) published maps showing anomalous metal and fluorite distributions in and around the Sierra Cuchillo. Maxwell and Heyl (1976) and Maxwell and Oakman (1984) produced detailed 1:24,000-scale geologic quadrangle maps within the region. Correa (1980) discussed fluorine and lithophile element deposits in the Sierra Cuchillo. Freeman and Harrison (1984) briefly discussed recent mining activity in the Black Range. A recent guidebook by the New Mexico Geological Society (1986) provides numerous articles on the region. Several masters theses have been undertaken in the Black Range and Sierra Cuchillo, including Woodard (1982), Abitz (1984), Davis (1986), and Robertson (1986). A colorful history of mining activity in Sierra County is provided by Glines (1982).

Studies of fluorite in the region generally are related to fluorspar resources and include brief mention by Williams (1966) and Worl and others (in Shawe, 1976), and more extensive coverage by McAnulty (1978). Masters theses on fluorite in and near the Sierra Cuchillo include those of Lamarre (1974) and Huskinson (1975).

Fluorite Structure and Composition

Fluorite is an isometric mineral of composition CaF_2, with approximately 48.7% fluorine and 51.3% calcium. The most common crystal habit is cubic, although octahedral and rarely dodecahedral habits are found. Fluorite has perfect {111} cleavage, is brittle, has a hardness of 4, a vitreous luster, and a specific gravity of about 3.2. Fluorite occurs in a variety of colors and commonly exhibits fluorescence and less commonly phosphorescence.

Chemical substitution in fluorite is minimal as it has a rather "tight" lattice. The most commonly reported cations substituting for Ca are Ce and Y (Palache and others, 1951; Deer and others, 1962). Other possible substitutes include the rare earth elements, Sr, Ba, Cd, Na, K, U, and Th (Greenwood, 1968; Palache and others, 1951). In a study of chemical and physical properties of fluorite, Allen (1952) found common occurrences of Al, Mg, Mn, Sr, and Y, and reported detection of the following additional elements: Ag, Ba, Be, Cu, Eu, Fe, La, Na, Pb, Si, Yb, and Zr. Allen (1952) suggested that the following elements probably substitute for calcium in fluorite: Ba, Eu, Fe, La, Mn, Na, Pb, Sr, Y, Yb, and Zr. Chlorine substitutes in trace amounts

for fluorine (Ford, 1926). Free fluorine has been reported in fluorite (Allen, 1952; Deer and others, 1962) and may be related to lattice defects caused by substitution of calcium by cations with higher coordination numbers.

GEOLOGY

Regional Setting

The study area is included in the eastern part of the Tertiary Mogollon-Datil volcanic field. Volcanic and volcaniclastic rocks are widespread in the region. Thick sequences of sedimentary rocks, ranging from Paleozoic to Recent are common, with all systems except the Triassic and Jurassic represented. Precambrian crystalline rocks occur locally.

The region is dominated physiographically and structurally by basins and ranges created by middle to late Tertiary normal faulting related to the Rio Grande Depression (Kelley, 1955a), more commonly referred to as the Rio Grande rift (Chapin, 1979). The rift extends as a series of well-defined en echelon asymmetrical grabens, from southern Colorado, near Leadville, through New Mexico, to El Paso, Texas, and possibly into Chihuahua, Mexico (Fig. 2). North of Socorro, New Mexico, the rift exhibits morphological and tectonic features typical for extensional rifting environments (Baldridge and others, 1984). However, south of Socorro, the rift begins to take on more of a basin and range character, with sediment-filled graben valleys separated by uplifted horsts along generally northerly-trending normal faults. The southern segment is the oldest and widest part of the rift, with extension probably beginning between 27 to 32 m.y. ago (Clemons and Osburn, 1986). The basin and range character of the study area is exemplified by the Black Range, Sierra Cuchillo, and Caballo Mountains (uplifted, generally north-trending horsts) and by the Winston-Hillsboro trough and Palomas basin/Engle basin (intervening gravel-filled graben valleys).

Local Setting

This section briefly describes the geology of the study area, based on past and ongoing studies by numerous workers. A compiled generalized geologic map is provided on Plate 1.

Precambrian Rocks

Precambrian rock exposures are sparse in the study area, restricted to the lower slopes of uplifted sides of fault-block mountains. Precambrian outcrops are found in order of decreasing abundance, in the Caballo Mountains, the Mud Springs Mountains, and the Sierra Cuchillo. Ages of the Precambrian rocks are uncertain, but most generally are believed to be from 1.2 to 1.65 b.y. (Clemons and Osburn, 1986).

Precambrian rocks in the Caballo Mountains are predominantly coarse-grained pink granite and gneissic granite. Small pegmatite dikes are common, and lamprophyre dikes are found locally. Metamorphic rocks include small patches of mica schist, metadiorite, and greenstone (Kelley and Silver, 1952).

In the Mud Springs Mountains, a few small patches of Precambrian rocks are described by Kelley and Silver (1952, p. 253) as pink granite with small pegmatite dikes and inclusions of biotite schist. Maxwell and Oakman (1986) describe the Mud Springs Precambrian rocks as a complexly contorted and interlayered sequence of reddish quartzite, quartz schist, quartz-biotite

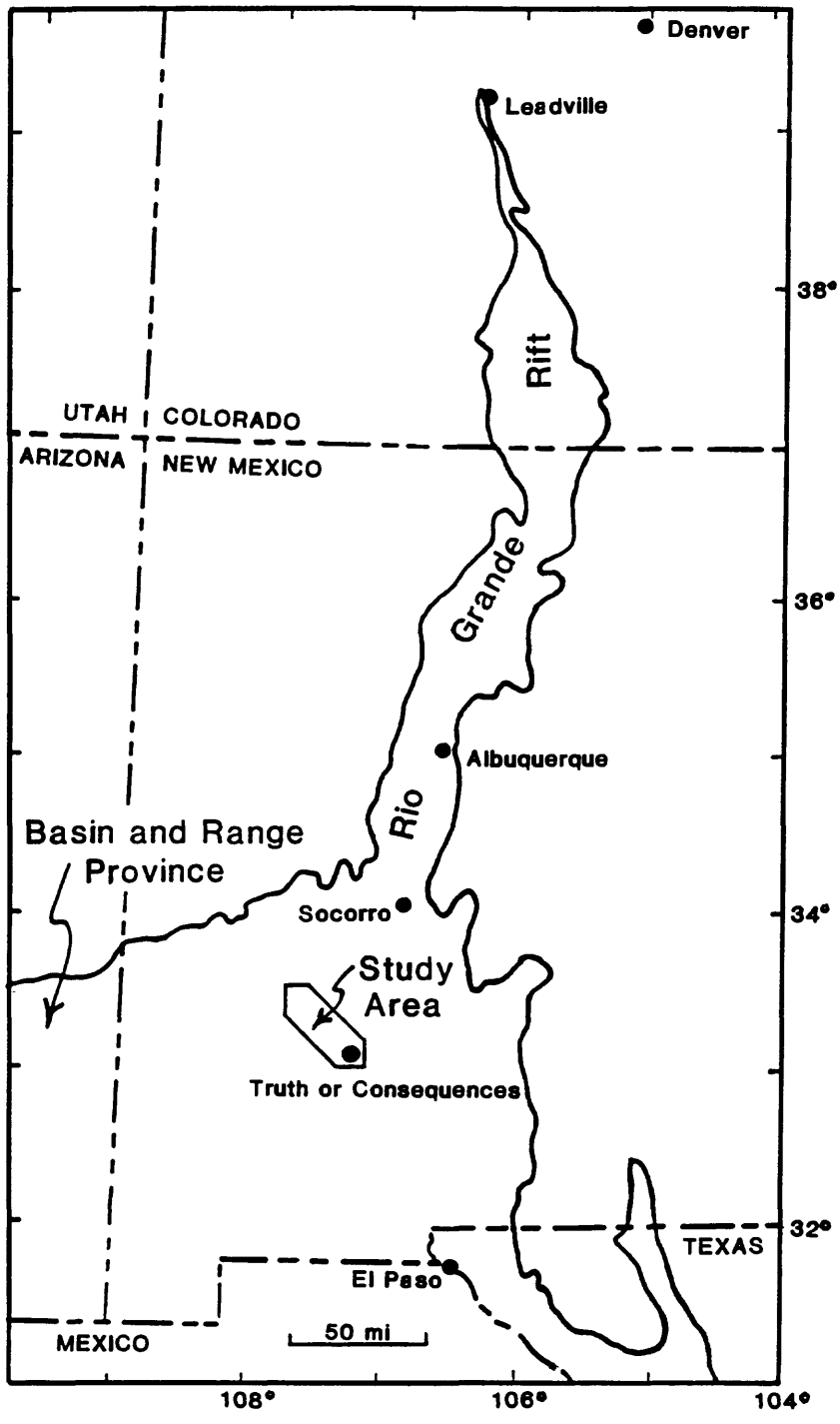

Figure 2.--Location map of study area with respect to the Rio Grande rift. Figure is modified from Figure 1 in Baldridge and others, 1984.

schist, amphibolite gneiss and schist, and intercalated reddish porphyritic granite gneiss.

Precambrian rocks in the Sierra Cuchillo are exposed in two narrow mile-long belts, one in the northern part of the range near Iron Mountain and the other east of Winston. Jahns and others (1978) note that the principal rock types are metarhyolite and amphibolite, with small bodies of metadiabase locally present. Granite is conspicuously lacking in the Sierra Cuchillo Precambrian terrane (Jahns and others, 1978).

Paleozoic Rocks

Sedimentary rocks in the study area generally are Paleozoic in age, and primarily are carbonates, with some interbedded shales and sandstones. Paleozoic rocks are most abundant in the Caballo Mountains and abundance generally decreases westward. Comprehensive summary descriptions of the Paleozoic section in the Truth or Consequences region are found in Jahns and others (1978) and Clemons and Osburn (1986). The section includes Cambrian Bliss Sandstone; Ordovician El Paso and Montoya Formations, which are predominantly limestones and dolomites with some cherty units; Silurian Fusselman Dolomite; Devonian Onate and Percha Shales; Mississippian Lake Valley Formation, a cherty, locally fossiliferous limestone; Pennsylvanian Magdalena Group, a thick, areally extensive unit which is predominantly limestone, but grades upward into shale; Permian Abo Formation, a deep reddish-brown sequence of shale, siltstone, and sandstone; Permian Yeso Formation, which consists of light-colored sandstone and gypsum, with minor siltstone, shale, and limestone; and Permian San Andreas Formation, composed of limestone, shale, and sandstone.

Mesozoic Rocks

Upper Cretaceous rocks are the only part of the Mesozoic section preserved in the study area. These rocks include, in ascending order, Dakota Sandstone, Mancos Shale, the Mesaverde Formation (sandstone, shale, siltstone, and mudstone), and the McRae Formation (locally tuffaceous sandstone, shale, siltstone, and conglomerate). The upper part of the McRae Formation may be early Tertiary (Kelley and Silver, 1952). Upper Cretaceous rocks in the Truth or Consequences region have been described in detail in several studies summarized in Clemons and Osburn (1986). Cretaceous rocks are most extensive in the Caballo Mountains. In the Sierra Cuchillo, only a few remnants of the Cretaceous (possibly equivalent to the Dakota Formation) are preserved (Jahns and others, 1978). Mesozoic rocks are not found in the Mud Springs Mountains nor in that part of the Black Range within the study area.

Cenozoic Rocks

Igneous rocks throughout the study are predominantly Tertiary, although sparse Precambrian granitic and metamorphic rocks crop out locally as described above. Cenozoic sedimentary rocks are areally extensive in the study area and are predominantly composed of sandstones and conglomerates.

Tertiary Intrusive Rocks--Tertiary intrusive rocks are most extensive in the Sierra Cuchillo, where a wide variety of generally subvolcanic rocks cut the stratigraphic section. These intrusive rocks, in order of decreasing age, include latitic tuff breccia, monzonite and latite, leucomonzonite and white felsite (leucolatite), pink felsite, pyroxene andesite, porphyritic rhyolite

and trachyte, aplite and fine-grained granite, red felsite, andesite and basalt, and olivine basalt (Jahns and others, 1978). Monzonite is the most abundant, occurring generally as white-to-gray fine-grained homogeneous sills, dikes, plugs and laccoliths. The large monzonite bodies have been referred to collectively by various workers as the Sierra Cuchillo intrusive. Jahns (1944, 1955) and Jahns and others (1978) describe a large fine-grained shallow intrusive body as leucomonzonite at Reilly Peak, south of Iron Mountain, in the northern Sierra Cuchillo. However, Davis (1986) has demonstrated chemically and petrographically that the Reilly Peak body is a high-silica intrusive rhyolite.

Numerous K-Ar ages have been reported for intrusive rocks in the Sierra Cuchillo. The Sierra Cuchillo intrusive has K-Ar ages of 50.1 ± 2.0 m.y. (Lamarre, 1974; Clemons and Osburn, 1986), 50.1 ± 2.6 m.y. (Chapin and others, 1975), and 48.8 ± 2.6 m.y. (Chapin and others, 1978). Davis (1986) reports a minimum K-Ar age of 36.0 ± 1.4 m.y. for the Reilly Peak intrusive rhyolite. Porphyritic rhyolite dikes are crosscut by aplite dikes in the northern Sierra Cuchillo (Jahns, 1944; Davis, 1986; Robertson, 1986). Davis (1986) reports a K-Ar age on microcline from a porphyritic rhyolite dike at 22.6 ± 0.8 m.y., an age which is inconsistent with a K-Ar age on biotite of 29.2 ± 1.1 m.y. from the crosscutting aplite reported in Correa (1980).

Sparse intrusive monzonite and rhyolite bodies crop out locally in the Black Range (Harrison, 1986; Allen V. Heyl, personal communication, 1987). Age determinations for these rocks have not been reported.

A 2 mi long, 0 to 90 ft thick latite sill crops out in the Mud Springs Mountains. The age of this sill may be Eocene or Pennsylvanian (Maxwell and Oakman, 1986). A small porphyritic rhyolite dike intruding the Bliss Formation has a K-Ar age on biotite of 40.8 ± 1.5 m.y. (Maxwell and Oakman, 1986). Maxwell and Oakman (1986) mapped small Miocene (?) basalt dikes and a small Eocene (?) porphyritic quartz latite dike in the northern part of the Mud Springs Mountains.

Intrusive Tertiary rocks in the Caballo Mountains are mostly dikes and sills of basalt and rhyolite. Only basalt dikes crop out in the area covered in this study. The dense fine-grained medium to dark gray basalt dikes lie in a northwestward-trending swarm in the Mesaverde Formation. Based on field relationships in the Caballos and elsewhere, Kelley and Silver (1952) suggest that the basalt dikes probably are Pliocene or younger.

Tertiary Extrusive Rocks--Extensive middle Tertiary volcanic rocks are found in the Black Range and Sierra Cuchillo. The volcanic section throughout the region shows overall similarity: (1) lower andesitic volcaniclastics and lavas, which are overlain by (2) dacite to rhyolite ash-flow tuffs, which are interlayered with and/or overlain by (3) andesite to basaltic-andesite lavas (Jahns and others, 1955); Clemons and Osburn, 1986). This roughly bimodal compositional sequence may be related to Tertiary extension in the region. Rhyolitic flow-dome complexes occur in the upper part of the sequence in both the Black Range and Sierra Cuchillo.

In the Black Range, the oldest of the volcanic rocks is the Rubio Peak Formation (up to 3000 ft thick), consisting of intermediate volcanic and volcaniclastic rocks, with numerous radiometric ages ranging from about 45 to 33 m.y. (Seager and others, 1984). Debris flow and mudflow facies volumetrically are most common in the lower part of the formation, while the upper part consists of porphyrytic and aphanitic intermediate lava flows and rhyolitic ash-flow tuffs with intercalated volcaniclastics (Harrison, 1986).

On the east flank of the Black Range, exotic blocks of Pennsylvanian limestones, up to 550 ft thick and several square kilometers in outcrop, rest

on the debris flow facies of the Rubio Peak Formation. The lower contact of the limestone blocks is brecciated locally and commonly contains abundant gouge material. These blocks are interpreted to be of gravity-slide origin (Maxwell and Heyl, 1976; Harrison, 1986). The largest of these blocks are shown on Plate 1.

Outflow facies of the Kneeling Nun tuff (up to 650 ft thick) overlies the Rubio Peak Formation in the Black Range. The tuff is a moderately welded, crystal-rich, rhyolitic ash-flow tuff with ages of 34 to 35 m.y. (Harrison, 1986). Volcaniclastic and pyroclastic rocks locally separate the Kneeling Nun tuff from the overlying basaltic andesite of Poverty Creek (Harrison, 1986). This andesite (up to 650 ft thick) consists of dark aphanitic lava flows, interbedded volcaniclastic sedimentary rocks, and pyroclastic intervals; and has radiometric ages of around 28 m.y. (Harrison, 1986). A rhyolitic interval containing numerous small flow-dome complexes and interlayered ash-flow tuffs overlies the basaltic andesite of Poverty Creek. Ages for this interval range from about 27 to 29 m.y. (Harrison, 1986). Several rhyolite flow-dome complexes occur in the study area, particularly along the east flank of the Black Range. These complexes, referred to as Moccasin John-type rhyolite flow-domes, are highly contorted flow-banded domes and flows containing sparse phenocrysts of quartz, sanidine, plagioclase, and biotite (Harrison, 1986). Hydrothermal alteration is common in upper parts of the flow-dome complexes (Harrison, 1986).

The volcanic section in the Sierra Cuchillo is similar to that in the Black Range. The section ranges from 1800 to 2500 ft thick (Jahns and others, 1978). Jahns and others (1978) divided the section into 5 volcanic sequences. The lowest is an early Tertiary latite-andesite volcaniclastic interval, consisting of several hundred feet of debris-flow deposits with lesser conglomerate and sandstone. Andesite or basaltic-andesite lavas are found in the upper part of this sequence, interbedded with ash-flow tuffs (Clemons and Osburn, 1986). Blocks of Paleozoic strata are locally abundant near the base of the section (Jahns and others, 1978).

In the Sierra Cuchillo, a relatively thin crystal-rich, quartz-rich dacite-rhyodacite ash-flow tuff unconformably overlies the andesitic interval and may be equivalent to the Kneeling Nun tuff (Clemons and Osburn, 1986). Overlying this unit is a series of thin-to-thick, mafic-to-intermediate lava flows, which may be equivalent to the basaltic andesite of Poverty Creek (Clemons and Osburn, 1986). The series of flows is overlain by an aphanitic, light-colored, phenocryst-poor, ash-flow tuff which may correlate with the Vicks Peak tuff in the San Mateo Mountains to the north (Clemons and Osburn, 1986). Two rhyolite flow-dome complexes overlie the light-colored tuff. These complexes informally are called the rhyolite of HOK Ranch and rhyolite of Willow Springs Draw. The latter complex has a fission-track age of 27.8 ± 1.0 m.y. (Heyl and others, 1983).

Latest Tertiary to Quaternary Extrusive Rocks--Young basalt flows are found in a few places in the Sierra Cuchillo and Caballo Mountains. In the Sierra Cuchillo, the alkali olivine basalt is porphyritic aphanitic, dark, and vesicular, and it commonly forms flat mesa caps. The vesicular basalt has a Pliocene K-Ar age of 4.8 ± 0.1 m.y. at Tabletop Mountain, east of Winston (Seager and others, 1984). In the Caballo Mountains, olivine basalt flows and plugs are found in the northeastern corner of the range and these are believed to be Pleistocene (Kelley and Silver, 1952). Jahns and others (1978) note that the source vents for olivine basalt flows in the region east of the Black Range appear to have been related closely to faults with northerly trends.

Tertiary and Quaternary Sedimentary Rocks--The Santa Fe Group sedimentary deposits overlie volcanic rocks throughout the region. The group is extensive and ages range from Miocene to Pleistocene. Sandstones and conglomerates are most common, with lesser siltstones and local interbedded volcanic rocks. Miocene Santa Fe Group rocks are commonly tilted, reflecting basin-and-range tectonism in the region.

Structure

Deformation in the region occurred in Precambrian, Paleozoic, Laramide, and middle to late Tertary times. Precambrian penetrative and non-penetrative deformation probably occurred at mid-crustal depths (Clemons and Osburn, 1986). Four Paleozoic deformational events were reported by Kelley and Silver (1952), recorded by regional wedging out of units, by unconformities and missing sections, and by erosional relief. Complex Laramide deformation and faulting were important elements in the region, and numerous studies of Laramide structure in the Caballo Mountains, the Fra Cristobal Mountains to the north, and the Mud Springs Mountains are summarized in Clemons and Osburn (1986).

Middle to late Tertiary extensional faulting is largely responsible for the present topographic relief in the region. Major ranges were apparently near their present elevations by 4 or 5 m.y. ago (Chapin and Seager, 1975; Seager and others, 1984). Extension probably began 27 to 32 m.y. ago, although data documenting this are sparse (Clemons and Osburn, 1986). Late Miocene and younger extensional structures are well documented (Lozinsky, 1986; Seager and others, 1984) and indicate that most faulting and range uplift took place between 10 to 13 and 5 to 3 m.y. ago.

MINERAL DEPOSITS

Past/Present Mining Activity

Epithermal gold and silver mineral deposits were discovered in the 1880s in the Chloride mining district, along the east flank of the Black Range. A flurry of mining activity ensued, continuing until the Great Depression in the 1930s. Harley (1934) reports that from 1880 to 1932 the district produced an estimated $1,000,000 in Au and Ag (minor Cu, Pb, and Zn) at the then-prevailing prices.

Minor silver-bearing base metal skarn was discovered in the Sierra Cuchillo in the 1880s (Glines, 1982). Renewed interest in the region occurred in the 1940s with discovery of Be-W-Fe skarn at Iron Mountain. Reserves in Be and W were found to be minimal, and mining activity waned in the late 1940s.

Prospecting continued in the region into the 1960s with discoveries of small base metal and fluorspar deposits. Numerous fluorspar deposits were discovered near Truth or Consequences in the Caballo Mountains, but little production has occurred in the area since 1954 (McAnulty, 1978). Development of fluorspar deposits in the Chise district began in the late 1960s, but high silica content presented milling problems, and the project was abandoned in 1973 (McAnulty, 1978).

Prospecting for Au and Ag in the Chloride area resumed in the 1960s and 1970s, resulting in development of the St. Cloud and U. S. Treasury Mines near Chloride (Freeman and Harrison, 1984). From 1982 to 1985, the St. Cloud, U. S. Treasury, Great Republic, and Minnehaha mines produced over 2 million ounces Ag; 9,000 ounces Au; 3,000 tons Cu; and several thousand tons each of lead and zinc (Harrison, 1986).

Fluorite-Bearing Mineral Deposits

Four distinct types of fluorite-bearing deposits are found in the study area.

(1) Epithermal Au-Ag-Cu-Pb-Zn-bearing quartz-calcite fissure veins, locally containing fluorite, barite, and amethyst, are found in the Chloride mining district along the eastern flank of the Black Range. The veins are steeply dipping, intruding along high-angle normal faults of various trends. Host rocks generally are mid-Tertiary intermediate volcanic and volcaniclastic rocks. The veins are believed to be the result of hydrothermal convection cells generated by intrusion of Moccasin John-type rhyolite flow-dome complexes (Harrison, 1986). Some of the veins are hosted in radial and tangential fractures produced during arching of country rock by the flow-dome complexes, although these features commonly are obscured by later faulting associated with the Rio Grande rift. Vein adularia at the Minnehaha mine yields a K-Ar age of 26.2 ± 2 m.y. (M. Bauman, unpublished report for FRM Minerals, in Harrison, 1986).

(2) Fluorite-bearing W-Be skarn is found at Iron Mountain in the northern part of the Sierra Cuchillo Range. The helvite-scheelite-magnetite-fluorite skarn is described in detail by Jahns (1944). Robertson (1986) demonstrated that mineralized skarn at Iron Mountain is related to intrusions of two principal compositions: an older rhyolite porphyry dike, associated with early Sn-garnet skarn, and a younger aplitic rhyolite dike, associated with W-Be-fluorite skarn. Robertson (1986) found that both of the intrusives are highly differentiated, based on trace element and REE patterns. As described under Tertiary Intrusive Rocks, inconsistent ages have been obtained for these dikes. Davis (1986) reports that an adularia separate from a vug in scheelite ore at Iron Mountain gave a K-Ar age of 27.3 ± 0.6 m.y. Jahns (1944) considered the scheelite veins to be very late stage. Small pockets of mineralized skarn (generally base metal) occur elsewhere throughout the Sierra Cuchillo Range, all along the contact between calcareous Paleozoic sedimentary rocks and Tertiary intermediate to felsic intrusives.

(3) Epithermal calcite-chalcedonic silica-fluorite fissure veins are found throughout the Sierra Cuchillo range, generally following the north-south trend of the range-front normal faults. This is the most abundant type of fluorite-bearing deposit in the study area. The veins do not contain any known base or precious metals, and thus are termed "barren" in this study. Quartz in these veins generally is extremely fine-grained, in contrast to quartz in the precious metal veins in the Black Range, which varies from cryptocrystalline, to drusy, to coarse-grained. Amethyst was not found associated with the "barren" veins. No age determinations have been made on these veins, although they crosscut mineralized skarn in the Vindicator Mine area.

(4) Fluorite-bearing epithermal Ba-Pb veins are found in the Caballo Mountains, as quartz-calcite-barite-fluorite- galena fissure veins cutting Paleozoic sedimentary rocks. No igneous rocks are found in the area. The veins commonly occupy normal faults paralleling the Rio Grande rift. Drusy quartz overgrowths on fluorite and on platy barite are common. No age determinations have been made on these veins.

Fluorite in ambiguous or unclear deposit types is found locally in the study area. The Vindicator mine area provides a good example. Here, mineralized skarn is found along a gently dipping contact of monzonite overlain by Paleozoic limestone. Fluorite, secondary copper minerals, and calc-silicate minerals are common in mine tailings. Steeply dipping "barren"

quartz-calcite-fluorite veins are found crosscutting the skarn. Thus, the source of fluorite in the mine tailings is unclear. Fluorite of an ambiguous origin is termed "questionable" in this study.

SAMPLE COLLECTION AND PREPARATION

Collection

Fluorite was collected from 64 sites representing all 4 deposit types, predominantly from bedrock, although a few stream sediments were collected below bedrock sources. The stream-sediment fluorite samples were collected below sampled mineralized bedrock to monitor any differences in trace element behavior in fluorite from the two sources. Sample site duplicates were collected, and analytical splits were made to monitor site and analytical variation. Table 3 lists types and quantities of samples collected in the study.

Grab rock samples were collected from prospects, mines, and mineralized outcrops. In general, megascopically visible fluorite was collected but, on a few occasions where fluorite was not evident, bulk rock samples were collected for concentrating fluorite in the laboratory.

Stream sediment samples were composited from active drainages in areas exhibiting either heavy mineral streaks (magnetite) or coarse gravel accumulation. Approximately 5 kg of minus 10-mesh (1.7 mm) sediment was collected and panned until indicator heavy minerals such as magnetite or garnet were visible. Samples were placed in bags, air-dried, and saved for further preparation.

Preparation

An extensive sample preparation procedure was undertaken in the laboratory to provide pure, homogeneous fluorite mineral separates for chemical analysis. Final samples were estimated to be approximately 99% pure CaF_2. Figure 3 shows a sample preparation flowchart; a discussion of the preparation procedure follows.

Preparation began with crushing and coarse grinding the rocks. From this point on, both rocks and stream sediments were prepared identically.

Samples were sieved, and the minus 10-mesh (1.7 mm) to plus 35-mesh (0.4 mm) fraction was saved for further preparation. This size fraction was used because grains larger than 10-mesh commonly were not mono-mineralic, and grains smaller than 35-mesh were difficult to identify microscopically with certainty.

Samples were gravity separated using bromoform, a heavy liquid with specific gravity of approximately 2.85. Fluorite, with a specific gravity of

Table 3.--Listing of quantity and types of samples collected for analysis, by deposit type. A = total number of samples collected from specified deposit type; B = number of samples in which fluorite was not found in lab; C = number of samples for analysis (A minus B).

		SAMPLE TYPE					
		Stream Sediment			Rock		
	Total # samples collected	26			68		
		A	B	C	A	B	C
DEPOSIT TYPE	Au-Ag vein	10	2	8	17	6	11
	Ba-Pb vein	2	0	2	3	0	3
	"Barren" vein	8	1	7	32	1	31
	W-Be skarn	3	0	3	8	1	7
	"Questionable" deposit type	3	0	3	8	0	8
*Total For Analysis				23			60
Analytical Duplicates				4			16
Grand Total For Analysis		103	=	27	+		76

*includes 10 stream sediment and 16 rock sample site duplicates

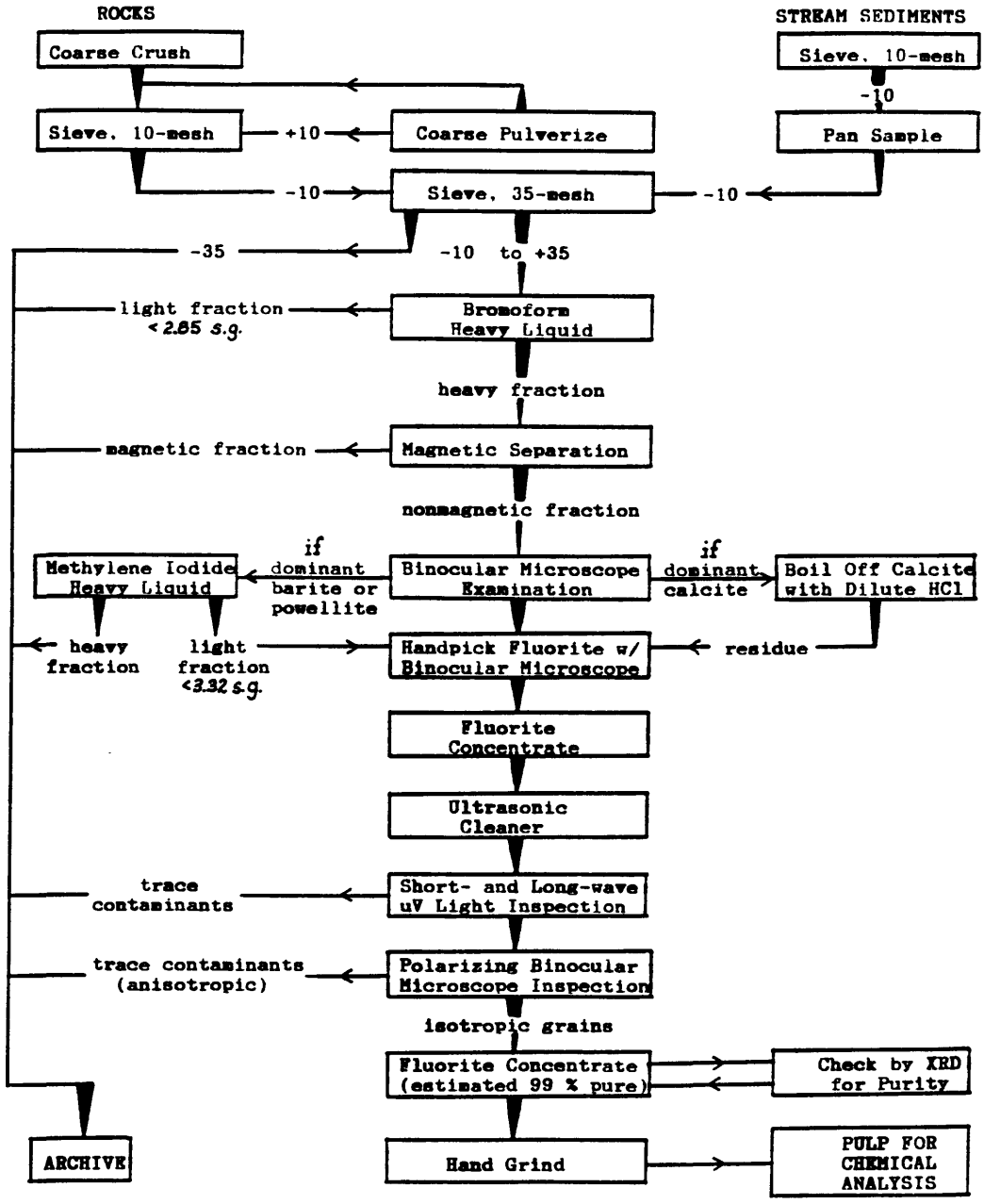

Figure 3.--Flowchart of sample preparation procedures.

approximately 3.2, sinks while common rock-forming minerals such as quartz and feldspar float. The heavy mineral concentrates then were separated magnetically using a Frantz isodynamic separator. Fluorite concentrates in the non-magnetic fraction.

Fluorite samples were next examined using a binocular microscope and fluorite was hand-picked for analysis. Samples composed predominantly of calcite (>95%) were digested in dilute HCl and fluorite was hand-picked from the residue. Samples composed predominantly of barite (s.g. 4.3-4.6) or powellite (s.g. 4.2) were gravity separated using methylene iodide (s.g. 3.3); fluorite was hand-picked from the light residue. When possible, 0.5 g samples of fluorite (herein referred to as fluorite separates) were isolated for analysis. Several 1 g samples were handpicked for duplicate analyses. A few samples contained insufficient fluorite for analysis.

Fluorite separates were cleaned using an ultrasonic vibrator in demineralized water for 30 minutes. This procedure removed loosely adhered surficial iron oxide, clay and other grains adhered to the fluorite by static electricity. This step was particularly useful in cleaning cleavage recesses.

Fluorite separates were next scanned with short- and long-wave ultraviolet light to record fluorescence characteristics, to remove other fluorescing minerals, and to look for fluorescing mineral inclusions in fluorite. This step was useful in removing trace contaminants such as apatite, scheelite, calcite, powellite, willemite, and zircon from the hand-picked fluorite separates.

As a final check for purity, fluorite separates were scanned under a binocular microscope equipped with polarizing filters and transmitted light--in effect a low-power petrographic microscope. Since fluorite is essentially the only transparent isotropic mineral commonly found in nonmagnetic heavy-mineral concentrates, this step was very effective in assessing purity of the sample. Trace anisotropic grains were removed, and tiny anisotropic inclusions were noted. Fluorite grains with large anisotropic inclusions were removed and the inclusions were identified by X-ray diffractometry. X-ray diffractometry also was used to ascertain purity of several of the fluorite separates.

Finally, fluorite separates were weighed and hand-ground for chemical analysis using an agate mortar and pestle. Clean quartz sand was ground between each fluorite separate to minimize contamination. After hand-grinding, the 1 g fluorite separates were split using a small Jones splitter to monitor analytical variance.

A map of sample sites is shown on Plate 2. Initially, samples were collected from 64 sites, but insufficient fluorite was found at 7 of the sites (sites 01, 03, 04, 16, 23, 25, and 33). Analytical (20 total) and sample site (26 total) duplicates brought the total number of samples for analysis to 103, representing 57 sites (Table 3).

Appendix E lists the following physical properties identified during microscopic examination of the fluorite samples: color in white light, short- and long-wave ultraviolet fluorescence, and relative amounts of anisotropic inclusions.

SAMPLE ANALYSIS

Several analytical methods were used in chemical analysis of the fluorite separates. These methods include inductively coupled plasma mass spectrometry (ICP-MS), inductively coupled plasma atomic emission spectrometry (ICP-AES), and semiquantitative emission spectrography (SES). Figure 4 shows the

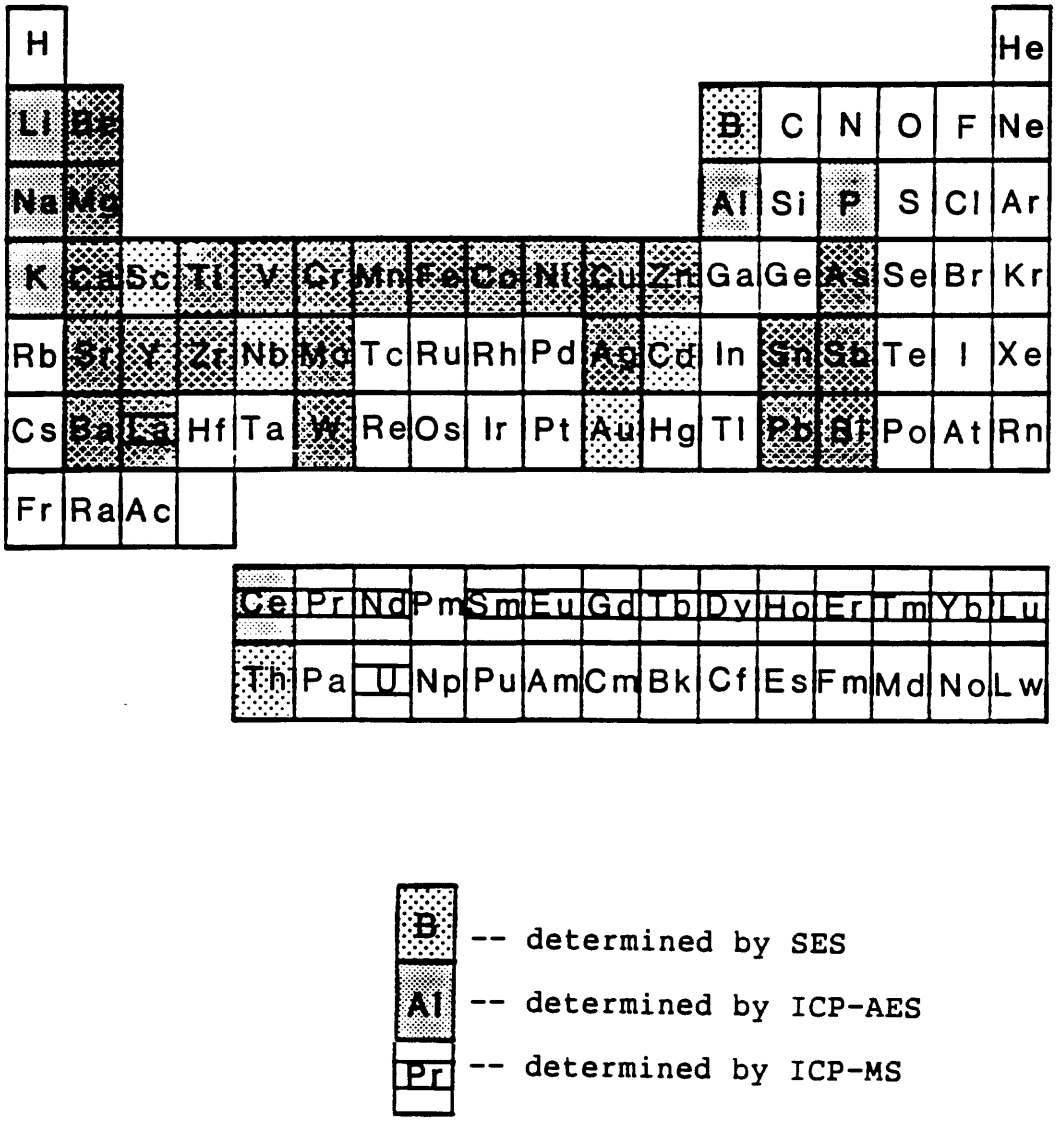

Figure 4.--Periodic chart showing elements determined in this study.

elements determined by each of the methods. In addition, X-ray Diffraction (XRD) was used to assess sample purity and to identify inclusions in the fluorite separates. Methodology used with each of the above techniques is discussed briefly below.

Inductively Coupled Plasma Mass Spectrometry (ICP-MS)

Thirty-one fluorite separates were selected for analysis by ICP-MS for the rare earth elements (REE = La, Ce, Pr, Nd, Sm, Eu, Gd, Tb, Dy, Ho, Er, Tm, Yb, and Lu) and for uranium. As a cost-saving measure, these 31 fluorite separates were selected from the total of 103 separates. Separates were selected to include: samples from the Au-Ag vein, Ba-Pb vein, W-Be skarn, and "barren" and "questionable" deposit types; samples exhibiting physical differences, such as color and fluorescence; and analytical (2 total) and site duplicates (4 total) to monitor site/analytical variance.

The 31 fluorite separates were put into solution following a method devised for this study based on a brief description in Feigl (1958). The dissolution method is explained in Appendix A. Briefly, the method consisted of digesting 0.1 g of fluorite in a warm dilute boric/nitric acid solution for several hours. The dissolution method is specific for fluorite; oxide or silicate inclusions are not dissolved, but accumulate as residue.

Solutions were analyzed for the REE using the newly devised method of Lichte and others (1987). Uranium was determined from the same solutions. Table 4 shows lower detection limits for the REE and U by determined ICP-MS. Appendix B lists REE and U data determined by ICP-MS.

Inductively Coupled Plasma Atomic Emission Spectrometry (ICP-AES)

The same 31 solutions were analyzed by ICP-AES for the following 31 elements: Al, Ca, Fe, Mg, K, Mn, Na, Ag, As, Ba, Be, Bi, Ce, Co, Cr, Cu, La, Li, Mo, Ni, P, Pb, Sb, Sn, Sr, Ti, V, W, Y, Zn, and Zr. The method used is a modification of the method described in Church (1981). Since B, Cd, and Th standards were added to the solutions for analysis by ICP-MS, these elements were not determined by ICP-AES. Table 5 shows lower detection limits for the elements determined by ICP-AES. Appendix C lists the data obtained by ICP-AES.

Semiquantitative Emission Spectrography (SES)

All 103 fluorite separates were analyzed using semiquantitative, direct-current arc emission spectrography for the following 31 elements: Ag, As, Au, B, Ba, Be, Bi, Ca, Cd, Co, Cr, Cu, Fe, La, Mg, Mn, Mo, Nb, Ni, Pb, Sb, Sc, Sn, Sr, Ti, Th, V, W, Y, Zn, and Zr. The method used is described in Grimes and Marranzino (1968) and lower limits of determination are shown in Table 6. Spectrographic results were recorded on glass plates and visually compared with standards. Spectrographic results are reported as approximate geometric midpoints: 0.15, 0.2, 0.3, 0.5, 0.7, 1.0 (or multiples of these by 10) of intervals whose respective boundaries are: 0.12, 0.18, 0.26, 0.38, 0.56, 0.83, 1.2 (or multiples of these by 10). The precision of the analytical method is approximately plus or minus one interval at the 83% confidence level and plus or minus two intervals at the 96% confidence level (Motooka and Grimes, 1976). Appendix D lists the data determined by SES.

Table 4.--Lower detection limit for REE and U determined in rocks by ICP-MS. Lower detection limits for REE are based on a 1 g sample in a 200 ml solution, as reported in Lichte and others (1987). Lower detection limit for U is from A. Meier (U. S. Geological Survey, personal communication, 1988). Values are in parts per million unless noted otherwise.

Element		Lower detection limit
Lanthanum	(La)	0.002
Cerium	(Ce)	0.002
Praseodymium	(Pr)	0.002
Neodymium	(Nd)	0.009
Samarium	(Sm)	0.006
Europium	(Eu)	0.003
Gadolinium	(Gd)	0.011
Terbium	(Tb)	0.002
Dysprosium	(Dy)	0.007
Holmium	(Ho)	0.002
Erbium	(Er)	0.007
Thulium	(Tm)	0.002
Ytterbium	(Yb)	0.006
Lutetium	(Lu)	0.002
Uranium	(U)	0.1 ppb

Table 5.--Lower detection limit for several elements determined in rocks and stream sediments by ICP-AES. Values are based on a 0.1 g sample in a 10 ml solution. Values are in parts per million.

Element		Lower detection limit	Element		Lower detection limit
Silver	(Ag)	6	Manganese	(Mn)	80
Aluminum	(Al)	30	Molybdenum	(Mo)	7
Arsenic	(As)	30	Sodium	(Na)	20
Barium	(Ba)	0.6	Nickel	(Ni)	10
Beryllium	(Be)	0.2	Phosphorus	(P)	100
Bismuth	(Bi)	80	Lead	(Pb)	50
Calcium	(Ca)	10	Antimony	(Sb)	50
Cerium	(Ce)	30	Tin	(Sn)	30
Cobalt	(Co)	8	Strontium	(Sr)	0.2
Chromium	(Cr)	8	Titanium	(Ti)	2
Copper	(Cu)	2	Vanadium	(V)	3
Iron	(Fe)	70	Tungsten	(W)	30
Potassium	(K)	60	Yttrium	(Y)	2
Lanthanum	(La)	6	Zinc	(Zn)	2
Lithium	(Li)	0.8	Zirconium	(Zr)	6
Magnesium	(Mg)	46			

Table 6.--Limits of determination for various elements for the spectrographic analysis of rocks and stream sediments. Values are in parts per million unless noted otherwise, and are based on a 10 mg sample.

Element		Lower determination limit	Upper determination limit
Silver	(Ag)	.5	5,000
Arsenic	(As)	200	10,000
Gold	(Au)	10	500
Boron	(B)	10	2,000
Barium	(Ba)	20	5,000
Beryllium	(Be)	1	1,000
Bismuth	(Bi)	10	1,000
Calcium	(Ca)	0.05%	20%
Cadmium	(Cd)	20	500
Cobalt	(Co)	5	2,000
Chromium	(Cr)	10	5,000
Copper	(Cu)	5	20,000
Iron	(Fe)	0.05%	20%
Lanthanum	(La)	20	1,000
Magnesium	(Mg)	0.02%	10%
Manganese	(Mn)	10	5,000
Molybdenum	(Mo)	5	2,000
Niobium	(Nb)	20	2,000
Nickel	(Ni)	5	5,000
Lead	(Pb)	10	20,000
Antimony	(Sb)	100	10,000
Scandium	(Sc)	5	100
Tin	(Sn)	10	1,000
Strontium	(Sr)	100	5,000
Thorium	(Th)	100	2,000
Titanium	(Ti)	0.002%	1%
Vanadium	(V)	10	10,000
Tungsten	(W)	50	10,000
Yttrium	(Y)	10	2,000
Zinc	(Zn)	200	10,000
Zirconium	(Zr)	10	1,000

X-Ray Diffraction (XRD)

Mineral identification by XRD was used at three different stages during preparation and analysis of the fluorite, as described below. (1) Coarse-pulverization, during sample preparation, exposed anisotropic inclusions along fluorite cleavage planes in a few fluorite separates. Several of these inclusions were identified using XRD. (2) After sample preparation, a scan of the fluorite separates was done with a petrographic microscope to visually estimate sample purity. This visual estimate was confirmed using XRD on several fluorite separates. Interestingly, the petrographic visual scan is much more sensitive than XRD in identifying sample impurities (T. Botinelly, U. S. Geological Survey, written comm., 1988). (3) Selected insoluble residues (principally insoluble inclusions) from the fluorite dissolution procedure were identified by XRD.

RESULTS

Trace and REE data on the fluorite separates are grouped by analytical method and found in Appendices B (REE and U, ICP-MS), C (trace elements, ICP-AES), and D (trace elements, SES). Appendix E lists several physical characteristics of the fluorite samples. This section begins with a discussion of sample site and analytical variance. Then, results of each analytical procedure and X-ray diffraction studies are discussed. Throughout this study, the term "correlation" is used qualitatively, not in a rigorous statistical sense.

Sample Site and Analytical Quality Control

Total variance in this study is the sum of: (1) variation between deposit types, (2) variation within a given deposit type, (3) variation at the sample site, and (4) analytical variation. Optimum conditions are those of maximum variation at the deposit type level and minimum combined analytical and site variation.

Sample site and analytical variation is addressed qualitatively here because of the large amount of qualified data ("qualified" indicates data where an element is detected, but has a value lower than the determination limit and is thus termed "L") for the samples analyzed by SES, and the relatively sparse duplicate data for the ICP-MS and ICP-AES methods. Sample site duplicates were collected at 5 stream sediment sample sites (yielding 10 samples total) and 8 rock sample sites (yielding 16 samples total), to monitor element variation at sampling sites. After sample preparation, 20 samples were split using a small Jones splitter to monitor analytical variation. The entire suite of sample site and analytical duplicates were analyzed by SES. However, only 2 analytical duplicate pairs and 4 site duplicate pairs were analyzed by ICP-MS and ICP-AES.

Quality Control--SES Data

The following elements were not detected by SES in either the sample site or analytical duplicates: Ag, As, Au, B, Bi, Cd, Co, Cr, Cu, Mo, Nb, Ni, Sb, Sc, Sn, W, Zn, and Th. Calcium was reported in all samples as greater than 20%. Duplicate sample results for the remaining 12 elements determined by SES

are presented in Table 7, and a rough estimate of variation is indicated by the following:
(1) 96% of the combined analytical and site duplicate determinations are within one reporting step of each other.
(2) 98% of the analytical duplicate determinations are within one step.
(3) 93% of the site duplicate determinations are within one step.

Overall, both site and analytical variation are remarkably minimal for the semiquantitative emission spectrographic method used in this study. Analytical duplicates vary only slightly, and this variation appears most extreme for Zr and Be. Site variation is slightly higher, with Zr and Pb having the most variablity at the sample site. The sample site pair SC037H1-SC037H1 exhibit the most overall variation, with 4 of 12 elements having step differences of 2 or more (Ba, Be, La, and Sr). However, this relatively extreme variation probably is due to the fact that only 5 mg of sample SC037H2 was available for analysis, while the normal 10 mg was analyzed for sample SC037H1. The smaller sample size reduces precision for the SES method (B.M. Adrian, U.S. Geological Survey, personal communication, 1987).

Fluorites collected from heavy mineral concentrates have higher sample site variability than fluorites collected from rocks. Fluorites from concentrates exhibit 9 instances where step differences are greater than 1, while fluorites from rocks exhibit just 1 instance (Table 7). This feature probably reflects diverse origins for fluorite grains (with corresponding diverse trace element content) which are concentrated locally within a given drainage basin. An example of this phenomenon is the sample site pair SC006H-SC045H from Iron Mountain, where drainages contain fluorite derived from numerous fluorite-bearing pods of skarn.

Quality Control--ICP-MS Data

Duplicates analyzed by ICP-MS include 4 site duplicate pairs and 2 analytical duplicate pairs. Site and analytical variation for the REE are shown in chondrite-normalized plots in Figure 5. Uranium is discussed in the ICP-AES section with trace element data. Three of the site duplicate pairs (SC010R1-SC028R5, SC030R5-SC030R9, SC056R1-SC056R3) exhibit very sympathetic patterns. This suggests minimal REE variation due to sample site differences. Since analyt-ical variation generally is contained within sample site variation, minimal analytical variation is implied for these 3 duplicate pairs. Average REE variation is within ± 9% for these three site duplicate pairs. Variation increases slightly in the heavy REE for site duplicate pairs SC010R1-SC028R5 and SC030R5-SC030R9 (Lu variation: ± 16% and ± 13%, respectively) (Fig. 5).

The fourth site duplicate pair (SC007R1-SC007R2) was chosen randomly to split in order to monitor both site and analytical variation by ICP-MS. Both the site and analytical duplicates (SC007R1-SC107R1, SC007R2-SC107R2) exhibit much more variation than the former 3 site duplicate pairs (Figure 5). Average REE variation for site duplicate pair SC007R1-SC007R2 is within ± 31%. For analytical duplicate pair SC007R1-SC107R1, average REE variation is within ± 28%; while average REE variation for analytical duplicate pair SC007R2-SC107R2 is within ± 7%.

Unlike the rest of the samples selected for REE analysis, the SC007R-107R-suite of samples happened to be the only samples containing REE concentrations generally below chondrite abundances. Values below chondrite abundances, and particularly those below about 0.5-times chondrite abundances are at the lower end of the working range for the analytical method (Al Meier,

Table 7.--Reproducibility of sample site and analytical duplicates analyzed by SES, illustrated by the difference in reported steps. *

DUPLICATES	Fe	Mg	Ti	Mn	Ba	Be	La	Pb	Sr	V	Y	Zr
Site Duplicates												
SC002H -SC017H	(-)	(1)	1	(-)	(-)	(-)	1	(-)	-	-	1	(5)
SC006H -SC045H	(-)	-	1	-	(-)	1	-	(3)	-	-	2	(4)
SC035H1-SC035H2	(-)	(1)	-	(-)	(-)	(-)	-	(-)	1	-	-	4
SC037H1-SC037H2	(1)	(1)	1	(-)	6	2	3	(-)	2	(1)	-	(1)
SC057H1-SC057H2	(-)	(-)	1	(-)	(-)	(1)	-	(-)	-	-	1	1
SC007R1-SC007R2	(-)	(-)	-	(1)	(-)	(-)	-	(-)	(1)	-	(-)	(-)
SC010R1-SC028R5	(-)	1	1	(1)	(-)	-	1	(3)	1	1	-	(-)
SC010R2-SC028R4	(-)	-	-	(-)	(-)	1	-	(-)	-	-	1	(-)
SC026R1-SC026R2	(-)	-	1	(-)	(-)	(-)	-	(-)	-	1	1	(-)
SC030R1-SC030R7	(-)	-	-	(-)	(-)	(-)	-	(-)	-	1	-	(-)
SC030R3-SC030R8	(-)	-	1	(-)	(-)	(-)	1	(-)	-	-	1	(-)
SC030R5-SC030R9	(-)	(-)	-	(-)	(-)	(-)	1	(-)	-	-	1	(-)
SC056R1-SC056R3	(-)	(-)	-	(-)	(-)	(-)	-	(-)	-	-	1	(-)
Analytical Duplicates												
SC007R1-SC107R1	(-)	(-)	1	-	(-)	(3)	-	(-)	(1)	-	(-)	(-)
SC007R2-SC107R2	(-)	(-)	-	(-)	(-)	(-)	-	(-)	-	-	(-)	(-)
SC010R1-SC110R1	(-)	-	-	(-)	(-)	-	-	(-)	1	-	-	(-)
SC010R2-SC110R2	(-)	(1)	-	(-)	(-)	1	-	(-)	-	-	1	(1)
SC026R1-SC126R1	(-)	-	2	(-)	(-)	(-)	1	(-)	-	-	1	(1)
SC026R2-SC126R2	(-)	-	1	(-)	(-)	(-)	1	(-)	1	1	-	(-)
SC028R4-SC128R4	(-)	-	-	(-)	(-)	1	-	(-)	-	-	-	(1)
SC028R5-SC128R5	(-)	-	1	1	(-)	2	-	1	-	1	1	(-)
SC030R1-SC130R1	(-)	-	1	(-)	(-)	(-)	1	(-)	-	1	-	(2)
SC030R3-SC130R3	(-)	-	-	(-)	(-)	(-)	-	(-)	-	-	-	(-)
SC030R5-SC130R5	(-)	(1)	1	(-)	(-)	(-)	-	(-)	1	-	-	(-)
SC030R7-SC130R7	(-)	-	-	(-)	(-)	(-)	-	(-)	-	-	1	(-)
SC030R8-SC130R8	(-)	-	1	(-)	(-)	(-)	1	(-)	-	-	1	(-)
SC030R9-SC130R9	(-)	(-)	1	(-)	(-)	(-)	-	(-)	-	-	-	(-)
SC056R1-SC156R1	(-)	(-)	-	(-)	(-)	(-)	-	(-)	-	-	1	(-)
SC056R3-SC156R3	(-)	(-)	-	(-)	(-)	(-)	-	(-)	-	-	-	(-)
SC035H1-SC135H1	(-)	(1)	1	(-)	(-)	(-)	-	(-)	-	-	-	-
SC035H2-SC135H2	(-)	-	-	(-)	(-)	(-)	-	(-)	1	-	1	4
SC057H1-SC157H1	(-)	(1)	-	(-)	(-)	(-)	-	(-)	-	-	1	-
SC057H2-SC157H2	(-)	(1)	-	(-)	(-)	(1)	1	(-)	-	-	1	-

* Analyses by SES are reported in steps of 0.15, 0.2, 0.3, 0.5, 0.7, and 1.0 (or multiples of 10). 1 step = 0.2 to 0.3, 2 steps = 0.2 to 0.5, etc.; N (at 0.5) to L = 1 step; L (at 0.5) to 0.5 = 1 step. - indicates no difference between analyses for that element. ( ) denotes a comparison where at least one analysis did not detect that element. For sample numbers, R denotes fluorite collected from rock and H denotes fluorite collected from heavy mineral concentrates.

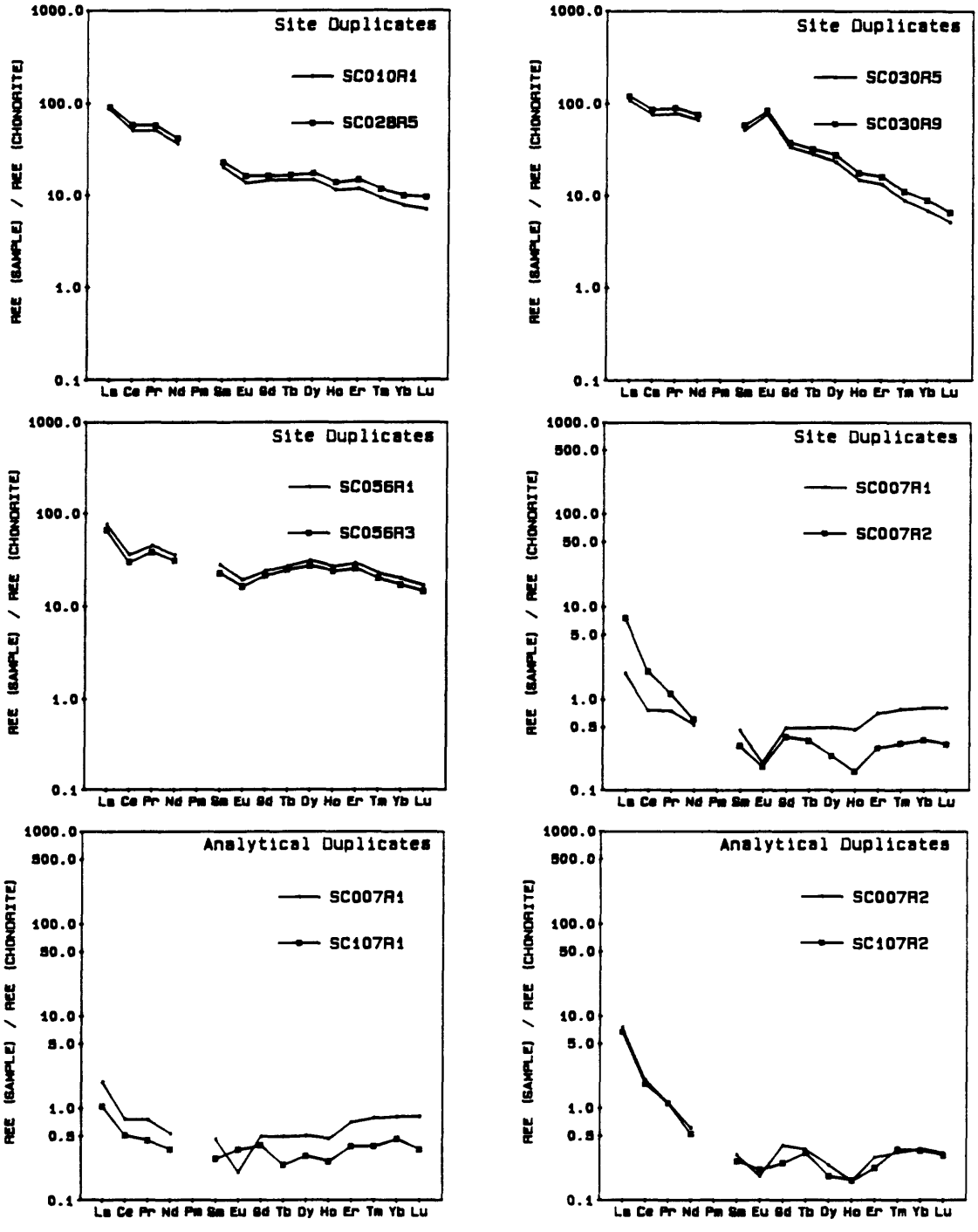

Figure 5.--Chondrite-normalized rare earth element plots for duplicate samples analyzed by ICP-MS. Chondrite REE values are from Wakita and others, 1971.

U.S. Geological Survey, personal communication, December, 1987). Therefore, the variation observed in the SC007R-107R suite of site and analytical duplicates may be due to analytical limitations. Instrumental and/or procedural error (sample splitting, sample dissolution, sample dilution, etc.) contribute to the analytical variation. Procedural error is likely the source for the large REE variation in analytical duplicate pair SC007R1-SC107R1 (avg. REE variation = ± 28%), when compared to the analytical duplicate pair SC007R2-SC107R2 (avg. REE variation = ± 7%). All other samples analyzed by ICP-MS generally had REE concentrations well above chondrite abundances, and analytical problems likely are minimal as suggested by the first 3 site duplicate pairs.

Quality Control--ICP-AES Data

Duplicates analyzed by ICP-AES are the same 4 site and 2 analytical duplicate pairs analyzed by ICP-MS. Of the 31 elements determined by ICP-AES, 10 (Ag, As, Bi, Co, Mn, Mo, P, Sb, V, and W) were not detected in any samples and 7 (Ce, Cr, Cu, Li, Ni, Pb, and Sn) were not detected in duplicate samples. Samples and duplicates for the remaining 14 elements (Al, Ba, Be, Ca, Fe, K, La, Mg, Na, Sr, Ti, Y, Zn, and Zr) plus U, are plotted against one another in Figures 6a-6o, respectively. Qualitative estimates of precision are based on whether at least 4 of the 6 combined site plus analytical duplicate pairs lie within ± 10% (good precision), ± 20% (fair), or greater than 20% (poor) of each other. Using these criteria, good precision is found for Al, Ba, Be, Ca, K, Na, and Sr; and fair precision is found for Ti, Y, and U. Lanthanum was detected in only 3 of the duplicate pairs, and has a fair precision estimate. Poor precision in duplicate pairs is found for Fe, Mg, Zn, and Zr. Thus, data for these 4 elements may not be reliable and must be used with caution.

Results--Inductively Couple Plasma Mass Spectrometry

Two of 31 samples analyzed by ICP-MS are analytical duplicates discussed in the quality control section. The remaining 29 samples are discussed here.

Rare earth elements were detected in all 29 fluorite samples, exhibiting a wide variation ranging from hundredths to hundreds of parts per million (ppm). In general, fluorites contained more light REE (La, Ce, Pr, Nd, Sm) than heavy REE (Gd, Tb, Dy, Ho, Er, Tm, Yb, Lu). Uranium was detected in all 29 samples, but all contained 1 part per billion (ppb) or less. Results of the uranium analyses by ICP-MS are discussed in the ICP-AES section, along with other trace elements. Table 8 lists univariate statistics for REE and U determined by ICP-MS.

Rare earth elements in the fluorite samples were normalized against rare earth abundances found in chondrite meteorites. The basis for this common practice is the generally held belief that chondrites represent the original cosmic abundances of the REE, with no fractionation between light and heavy REE. Using chondrite REE values as a common reference datum, noticeable abundance variations between REE of odd and even atomic number are eliminated, and the extent of fractionation between REE elements within a given sample is discernable. Chondrite values chosen for this study are those of Wakita and others (1971). Chondrite-normalized plots for the 29 samples are shown in Appendix F. The gap in the plots for Pm reflects the fact that promethium does not occur in nature.

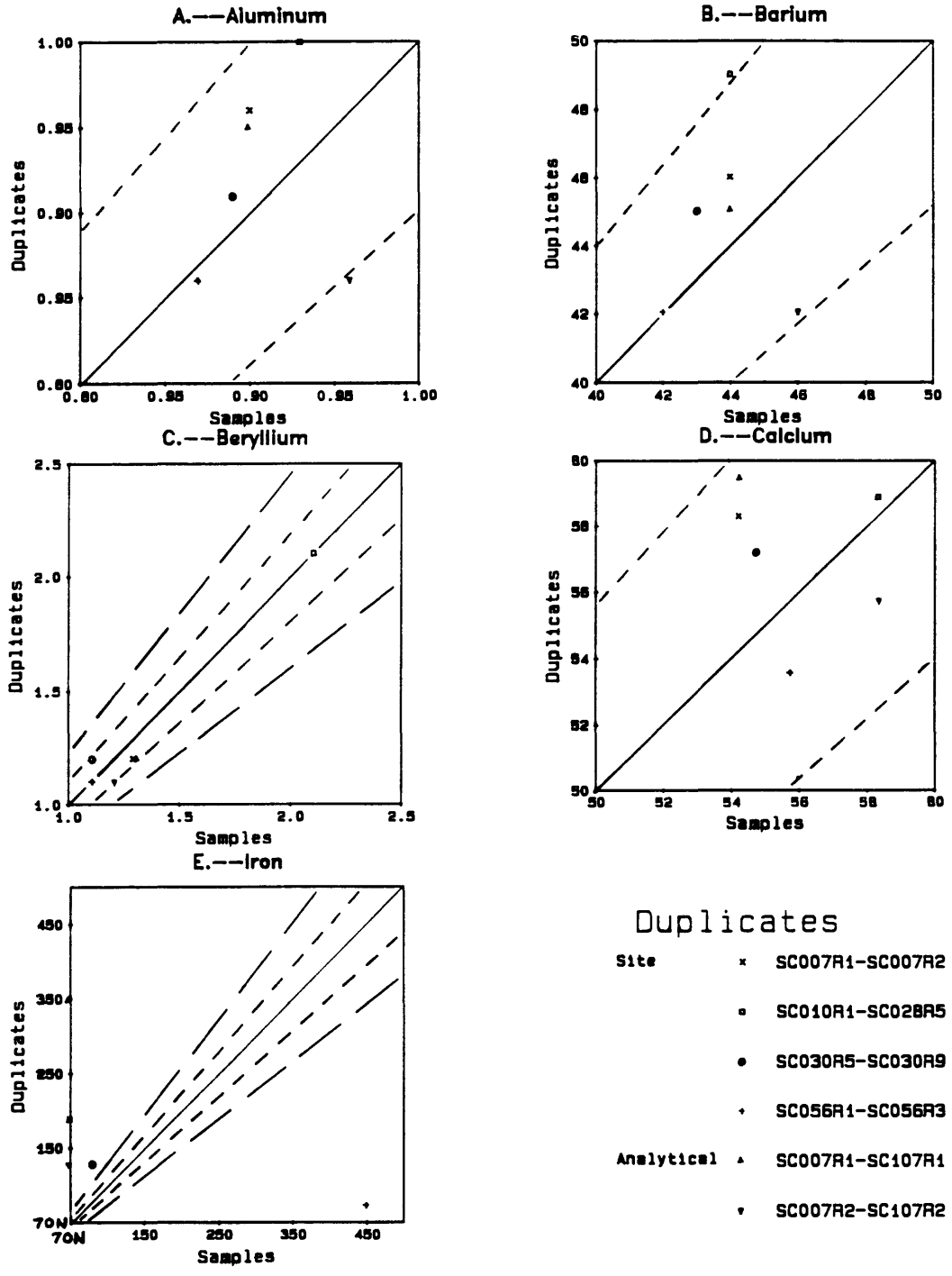

Figure 6.--Scatter plots for duplicate samples analyzed by ICP-AES. Values are in ppm except for Al, Ca, and Na (percent); and U (ppb). Short dashes enclose duplicates within ± 10%; long dashes enclose duplicates within ± 20%. 70N = not detected at 70 ppm.

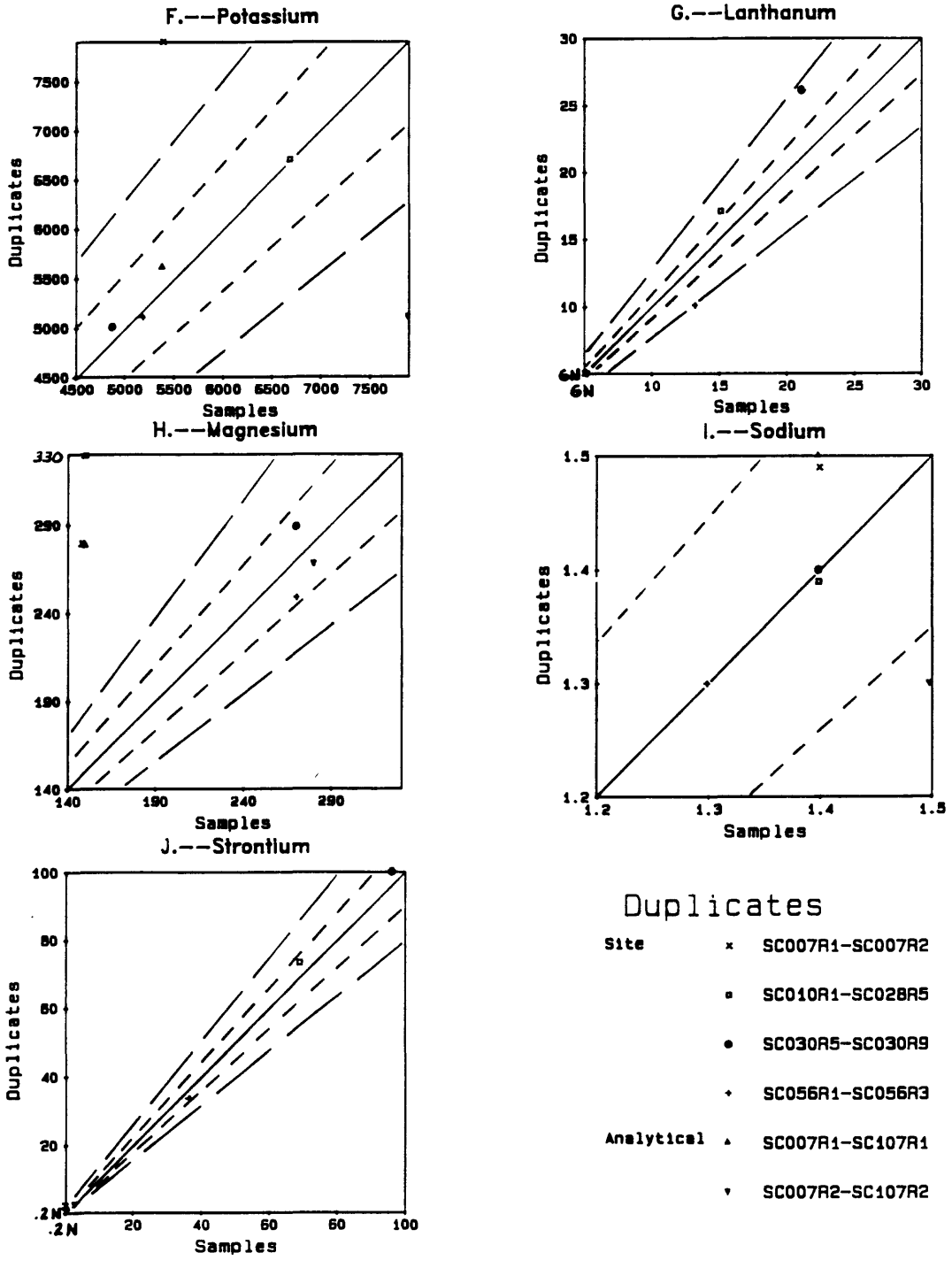

Figure 6.--(continued).

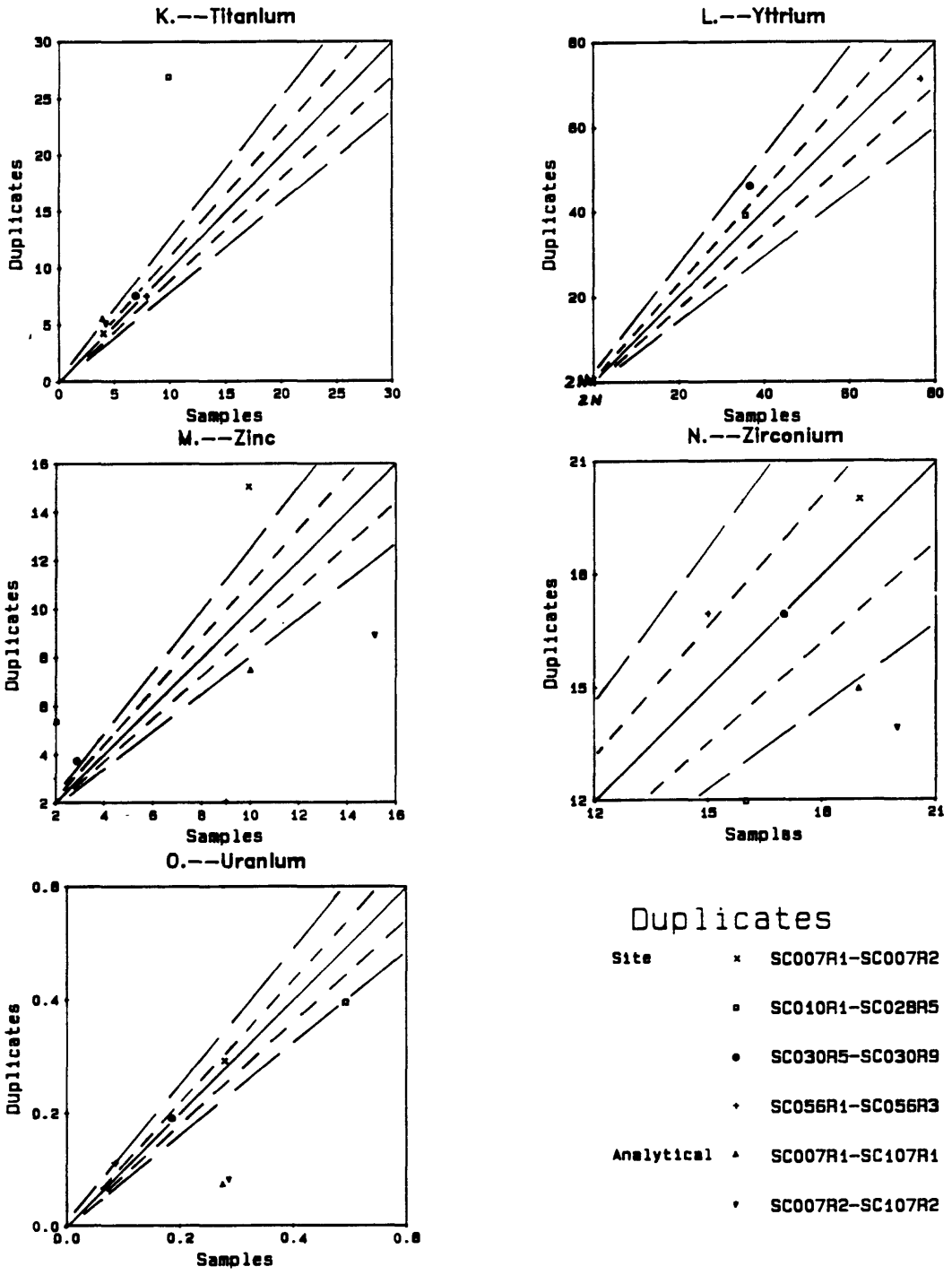

Figure 6.--(continued).

Table 8.--Univariate statistics for REE and U determined by ICP-MS. Values are in ppm, except for U (ppb).

Var.	Minimum	Maximum	Mean	Standard Deviation	Valid
La	6.400E-01	7.758E+01	2.038E+01	1.8260E+01	29
Ce	6.900E-01	1.981E+02	3.819E+01	4.3079E+01	29
Pr	9.000E-02	2.826E+01	5.330E+00	5.8637E+00	29
Nd	3.400E-01	1.208E+02	2.276E+01	2.4874E+01	29
Eu	1.000E-02	6.230E+00	1.514E+00	1.6265E+00	29
Sm	6.000E-02	4.309E+01	5.816E+00	8.1188E+00	29
Gd	1.000E-01	5.346E+01	6.335E+00	9.7915E+00	29
Tb	2.000E-02	1.281E+01	1.271E+00	2.3375E+00	29
Dy	7.000E-02	9.797E+01	8.863E+00	1.7950E+01	29
Ho	1.000E-02	2.335E+01	1.962E+00	4.2947E+00	29
Er	6.000E-02	7.956E+01	5.961E+00	1.4689E+01	29
Tm	1.000E-02	1.370E+01	9.000E-01	2.5332E+00	29
Yb	8.000E-02	1.033E+02	6.264E+00	1.9161E+01	29
Lu	1.000E-02	1.483E+01	8.707E-01	2.7533E+00	29
U	9.000E-02	1.090E+00	3.476E-01	2.4261E-01	29

The numerous chondrite-normalized plots in Appendix F exhibit a wide variety of shapes. However, there are three features which can be used to characterize the overall variation in the patterns: slope, behavior of Eu, and behavior of Ce. Slopes most commonly are negative, reflecting higher light REE content, although some patterns are flat to slightly positive. The behavior of Eu is quite variable, exhibiting strong negative anomalies (such as SC005R), positive anomalies (such as SC040R5), and no apparent anomaly (such as SC024R2). Variability in Ce behavior also is evident, although it is not as strong as that for Eu. Negative Ce anomalies are common in most of the patterns, but the intensity of the negative anomalies ranges from slightly to markedly negative (such as SC005R and SC028R4, respectively).

These three features can be observed and quantified more readily by looking at various chondrite-normalized (n) REE ratios. A ratio of (La)n to (Yb)n will give an indication of the overall slope of the curve. A number greater than 1 reflects light REE enrichment (relative to chondrites) and a corresponding negative slope, while a number smaller than 1 reflects heavy REE enrichment and a positive slope. Care must be taken in using this ratio, however, since the straight-line slope between La and Yb will not reflect curvature in chondrite-normalized patterns. The behavior of Eu can be expressed by looking at a ratio of the (Eu)n value obtained to the expected value for Eu (hereafter signified as [Eu/Eu*]n). The expected value (Eu*)n is obtained by interpolating between (Sm)n and (Gd)n. Thus, (Eu/Eu*)n values greater than 1 reflect positive Eu anomalies, while values less than 1 reflect negative Eu anomalies. Magnitude of the Eu anomaly is reflected by the amount of divergence from 1. The same procedure can be used to model Ce behavior, obtaining (Ce*)n by interpolating between (La)n and (Pr)n. Table 9 lists values for chondrite-normalized ratios used in the following discussion and for constructing Figures 7 and 8.

Figure 7 plots Eu behavior, (Eu/Eu*)n, against overall slope of the curve, (La/Yb)n. Several populations can be discerned in the plot, and these generally define different deposit types, with some overlap. The W-Be skarn fluorites from the Iron Mountain area exhibit wide variation in slope, with (La/Yb)n ranging from 0.49 (SC005R, endoskarn sample) to nearly 21 (SC007R2, exoskarn sample). This variation reflects both heavy REE and light REE enrichment for Iron Mountain skarn fluorites. Speculation on the cause for this apparently contradictory behavior is touched upon in the Discussion of Results. Europium anomalies are consistently negative for the skarn fluorites, with (Eu/Eu*)n ratios ranging from a moderately negative value of 0.53 (SC007R2) to a very strong negative value of 0.03 (SC005R).

Fluorites from the Au-Ag veins differ markedly from the W-Be skarn fluorites. The (La/Yb)n values, ranging from 7.5 (SC040R5) to 55.9 (SC014R6), indicate consistently strong negative slopes which reflect light REE enrichment. In contrast to the skarn fluorites, europium anomalies are consistently positive, with (Eu/Eu*)n ratios ranging from a slightly positive value of 1.19 (SC015R2) to a moderately strong value of 1.73.

The Ba-Pb vein fluorites exhibit both slightly positive and slightly negative slopes, with (La/Yb)n values 0.68 (SC046R1) and 2.81 (SC047R1). However, the chondrite-normalized plots for these samples in Appendix F reveal convex humps in the patterns, indicative of middle REE enrichment, a feature which is not indicated by the (La/Yb)n ratio. Fairly strong negative europium anomalies also characterize the Ba-Pb vein fluorites.

The metal-deficient "barren" vein fluorites exhibit flat and, more commonly, strong negative slopes, indicating a preference for light REE enrichment. The widely variable (La/Yb)n values range from 1.02 (SC024R2) to

Table 9.--Chondrite-normalized rare earth element ratios. Deposit type code: 1, Au-Ag vein; 2, Ba-Pb vein; 3, "barren" vein; 4, W-Be skarn; 5, "questionable" deposit type.

SAMPLE	Deposit Type	Eu*	Eu/Eu*	La/Yb	Ce*	Ce/Ce*
SC005R	4	213.28	0.03	0.49	230.87	0.94
SC007R1	4	0.47	0.42	2.32	1.31	0.57
SC007R2	4	0.35	0.53	20.93	4.32	0.46
SC009R2	3	61.91	0.67	5.11	148.35	0.98
SC010R1	3	17.42	0.78	11.19	68.70	0.74
SC014R6	1	21.71	1.29	55.94	86.29	0.86
SC015R2	1	22.27	1.19	9.93	43.37	0.83
SC018R1	1	15.57	1.42	19.08	38.77	0.76
SC024R2	3	3.43	1.04	1.02	3.20	0.66
SC027R2	3	8.06	0.75	1.13	5.46	0.86
SC027R3	3	3.94	0.79	13.99	18.24	0.77
SC028R4	3	42.44	0.70	1.84	60.90	0.54
SC028R5	3	19.81	0.83	9.29	75.43	0.78
SC030R1	3	34.58	1.65	16.84	85.77	0.83
SC030R5	3	42.88	1.81	15.79	93.76	0.81
SC030R9	3	48.85	1.75	13.56	106.91	0.82
SC031R4	3	21.57	1.42	10.12	56.13	0.84
SC032R2	3	27.57	1.38	8.99	48.29	0.82
SC040R5	1	3.24	1.73	7.52	3.63	0.76
SC045H	4	40.42	0.08	0.53	50.62	0.93
SC046R1	2	6.45	0.48	0.68	2.85	0.88
SC047R1	2	3.69	0.35	2.81	4.17	0.81
SC051R1	5	44.14	0.80	1.56	64.73	0.68
SC051R4	5	11.91	0.98	5.81	33.12	0.70
SC052R1	3	16.96	0.82	4.37	46.46	0.61
SC054R1	5	2.08	1.08	4.53	7.60	0.56
SC055R1	5	2.43	1.28	3.73	4.82	0.60
SC056R1	3	26.07	0.74	3.85	61.32	0.60
SC056R3	3	22.16	0.74	3.90	52.59	0.57

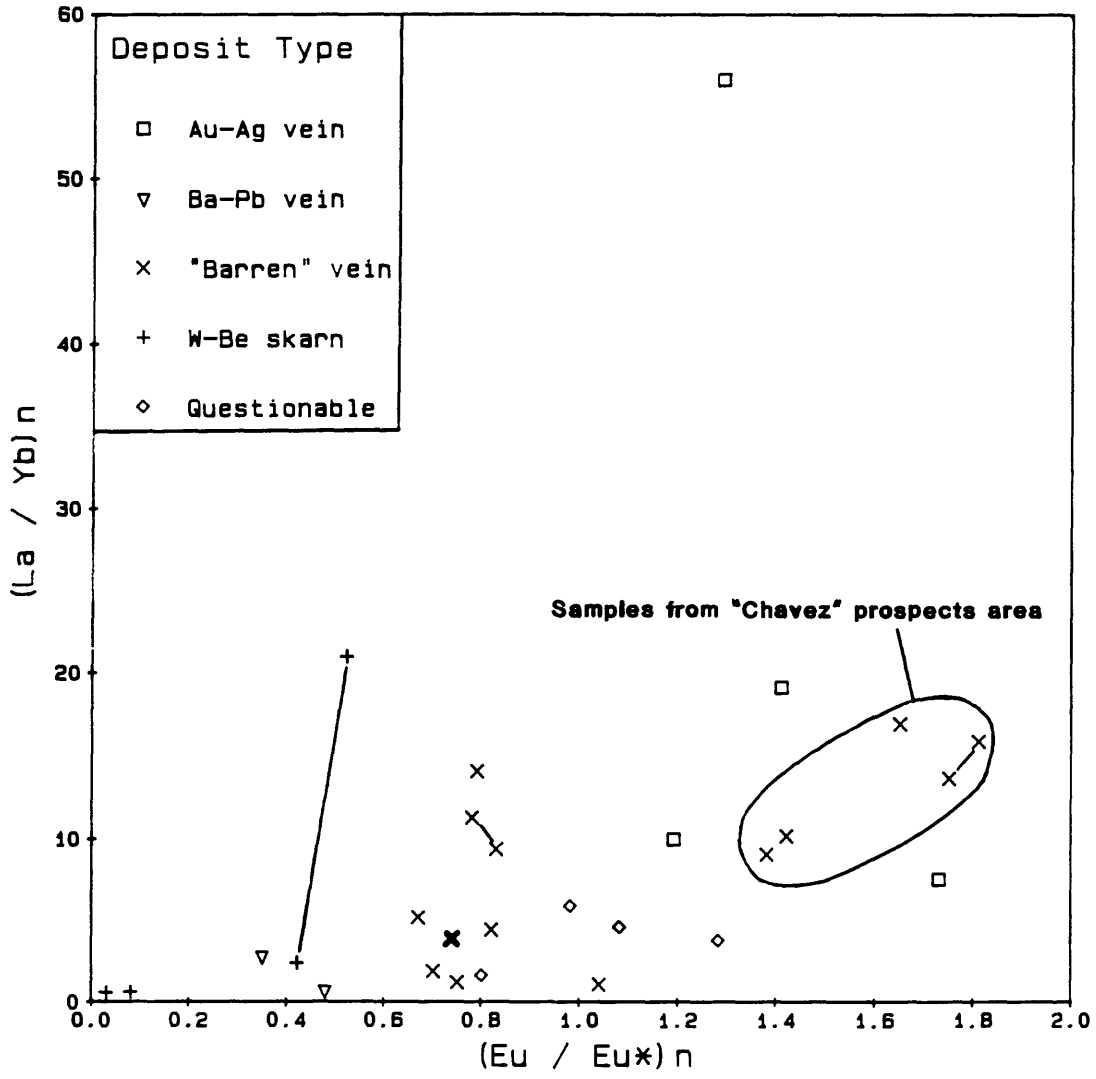

Figure 7.--Chondrite-normalized plot of slope, (La/Yb)n, versus europium behavior, (Eu/Eu*)n. Line segments link sample site duplicates. Bold "X" identifies 2 superimposed site duplicates.

16.84 (SC030R1). The (Eu/Eu*)n values also are quite variable, ranging from 0.67 (SC009R2) to 1.81 (SC030R5).

Fluorites from mineral deposits of "questionable" affinity exhibit consistently negative slopes, with (La/Yb)n values ranging from 1.51 to 5.81. Europium anomalies vary from slightly negative to moderately positive. In general, the "questionable" deposit type fluorites occupy the same field as the "barren" vein fluorites.

Fluorites from the different deposit types plotted in Figure 7 overlap considerably in slope, (La/Yb)n, limiting the usefulness of this parameter. However, the behavior of europium, (Eu/Eu*)n, clearly differentiates W-Be skarn and Ba-Pb vein fluorites from Au-Ag vein fluorites. "Barren" vein fluorites fill in a gap expressed by (Eu/Eu*)n, with W-Be skarn and Ba-Pb vein fluorites at the negative end, and Au-Ag vein fluorites at the positive end. "Barren" vein fluorites do not overlap W-Be skarn and Ba-Pb vein fluorite (Eu/Eu*)n fields. Considerable overlap occurs between "barren" vein and Au-Ag vein fluorites. The five encircled "barren" vein fluorite samples in Figure 7 are all from the same general area, informally called the "Chavez" prospects (Plate 2, samples SC030R1, SC030R5, SC030R9, SC031R4, and SC032R2). These samples exhibit slopes and Eu behavior very similar to those of Au-Ag vein fluorites.

Figure 8 is a plot of cerium behavior (Ce/Ce*)n versus europium behavior, (Eu/Eu*)n. The Au-Ag vein and Ba-Pb vein fluorites occupy fairly tight fields, with respect to cerium behavior, with (Ce/Ce*)n ranges of 0.76 to 0.86 and 0.81 to 0.88, respectively.

The W-Be skarn fluorites exhibit the widest variation for cerium behavior of all the samples, with ratios ranging from 0.46 (SC007R2) to 0.94 (SC005R). Cerium versus europium behavior identifies two groups of W-Be skarn fluorite samples, one with very slight cerium negative anomalies (endoskarn samples) and one with rather strong negative anomalies (exoskarn samples). A close inspection of the (La/Yb)n versus (Eu/Eu*)n plot (Figure 7) subtly reveals the two groups of samples.

"Barren" vein fluorites also exhibit fairly wide variation in cerium behavior, with (Ce/Ce*)n values ranging from 0.57 (SC056R3) to 0.98 (SC009R2). The five "barren" vein fluorites from the "Chavez" prospects again cluster with Au-Ag vein fluorites.

Results--Inductively Coupled Plasma Atomic Emission Spectrometry

The 29 fluorite samples were analyzed for 31 elements by ICP-AES. Univariate statistics for these elements are summarized in Table 10. Ten elements were not detected by ICP-AES: Ag, As, Bi, Co, Mn, Mo, P, Sb, V, and W. The remaining 21 elements are discussed individually below.

Six elements, Li, Sn, Ce, Pb, Cr, and Ni, were detected in only a few samples, and Cu and La were detected in fewer than half of the samples. Table 11 lists samples, deposit types, and abundances for these 8 elements. Infrequent detection of Li and Sn (1 observation each) and of Ce (2 observations) limits the usefulness of these data. Lead, with only 4 observations provides very limited information, but of interest are the occurrences of Pb in a sample from Ba-Pb veins and in 2 samples from W-Be skarn. However, it should be noted that 2 of the Pb observations are at the lower end of the working range of the analytical method. Sample SC05R, which contained the highest total REE values, also contained the highest Ce and Pb values, and the only Li value. Chromium and Ni were both found in 4 samples, two from "questionable" and two from "barren" deposit types. Copper was

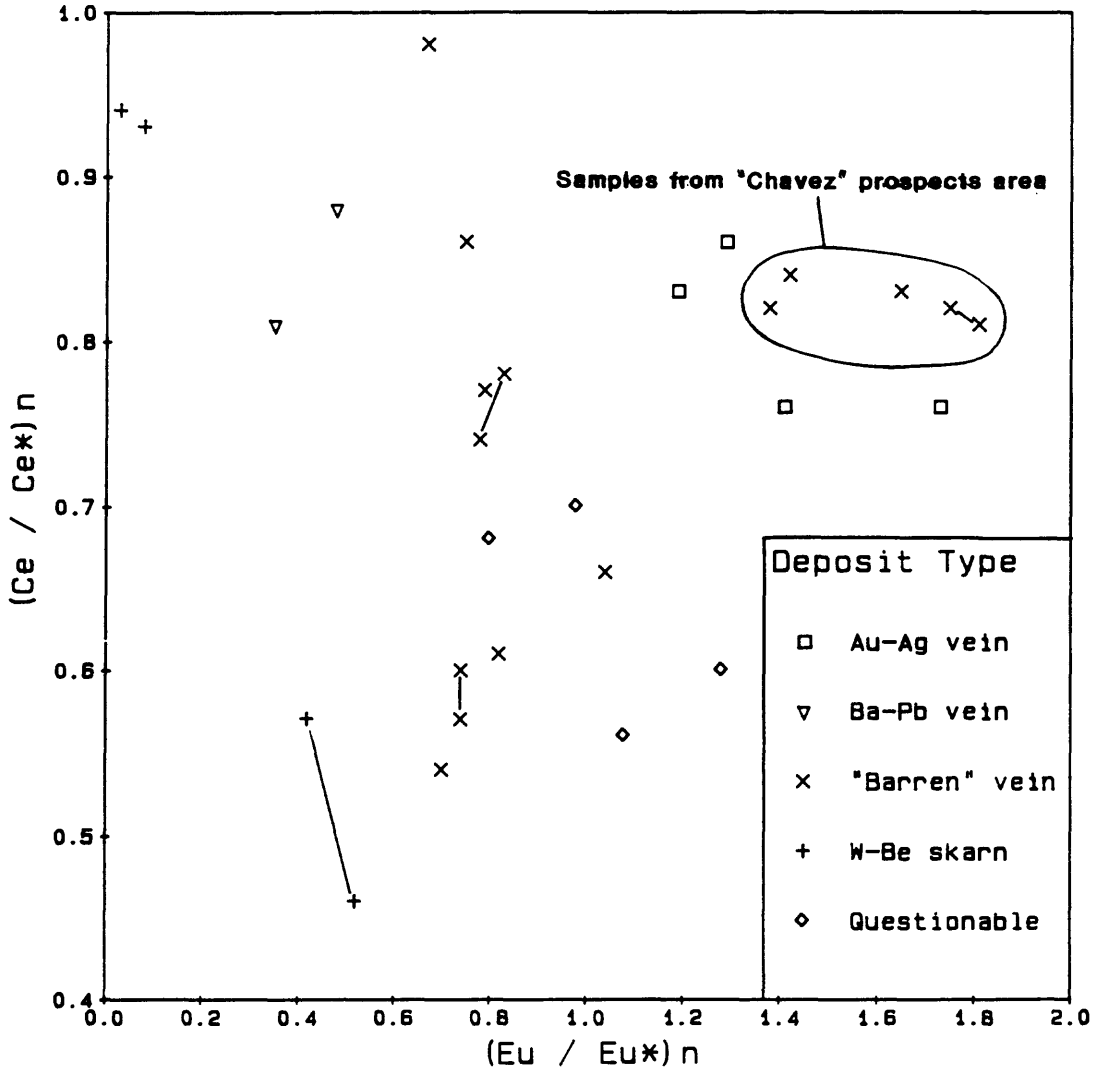

Figure 8.--Chondrite-normalized plot of cerium behavior, (Ce/Ce*)n, versus europium behavior, (Eu/Eu*)n. Line segments link sample site duplicates.

detected in 12 samples, ranging from just above the detection limit (2 ppm) to 15 ppm. However, 9 samples have Cu values at the lower end of the working range of the analytical method. Lanthanum was detected in 14 samples, ranging from 8 to 57 ppm. In agreement with the ICP-MS results, sample SC005R had the highest La value detected by ICP-AES. No correlation was noted in plotting these various 8 elements against deposit type.

The following 13 elements were detected in more than 20 of the 29 samples (Table 10): Al, Ba, Be, Ca, Fe, K, Mg, Na, Sr, Ti, Y, Zn, and Zr. Histograms for these elements plus Cu and La are provided in Appendix G. These elements are discussed below in order of least to most useful in differentiating deposit types.

All 29 samples contained Al, ranging in concentration from 0.8% to 1%, with 25 of the samples uniformly containing 0.9% Al. However, since aluminum hardware was used extensively throughout the sample preparation procedures, contamination is certain. Thus, no further mention of Al will be made, except to note that the narrow range in Al concentrations may indicate fairly uniform contamination throughout the samples.

Iron was detected in 21 of the samples, with all but 3 ranging from 75 to 190 ppm. The latter 3 samples contained 360 (SC054R1), 450 (SC056R1), and 1900 (SC055R1) ppm Fe. In comparing the Fe data with the data in Table 11, it is evident that, except for sample SC030R1, there is a one-to-one correlation between high Fe and detectable Ni and Cr. The sample containing the highest Fe contents (SC055R1) also contains the only detected Sn (36 ppm) and the second highest Cu value (11 ppm). Surficial iron oxide was noted on all 3 samples high in Fe during binocular microscopic scans of the samples. Iron-oxide-stained grains were removed, but the above data suggest that trace amounts of iron oxide remained. The Cr, Cu, Ni and Sn in these samples may reflect metal adsorption onto the iron oxide. However, Cr, Ni and Pb in sample SC030R1 (Table 11) cannot readily be attributed to iron oxide, since no Fe was detected. Trace amounts of iron oxide were noted in most samples during the binocular microscopic scan. While most was removed prior to analysis, it is possible that Fe detected in the 21 samples is due to trace iron oxide coating grains and in cleavage recesses. No correlation of Fe content with deposit type was found.

Fairly uniform amounts of Mg was detected in all 29 samples. A narrow range of 250 to 300 ppm was found for 22 of the samples. Only 1 sample was higher at 330 ppm and the other 6 samples ranged from 140 to 210 ppm. No correlation was noted with deposit type or Fe contents. The large amount of analytical and site variation for Mg possibly overwhelms any obvious correlation with deposit type.

Zinc was found in 27 samples ranging from 2.8 to 15 ppm. Some 22 of the samples contained less than 9 ppm Zn, limiting the usefulness of this element. Poor precision was found in site and analytical duplicates and this probably is related to difficulties in resolving differences in concentration over such a narrow range. No correlation between Zn content and deposit type was found.

Zirconium was detected in all 29 samples, in a narrow range from 8 to 20 ppm, with just one sample having less than 12 ppm Zr. As with Zn, poor precision found in site and analytical duplicates may be related to difficulties in resolution over such a narrow range. The highest Zr values were found for W-Be skarn samples (SC005R, 19 ppm; SC007R1, 19 ppm; SC007R2, 20 ppm), but these values were not repeated with analytical duplicates (SC107R1, SC107R2). No other correlations between Zr content and deposit type were found.

Table 10.--Univariate statistics for trace elements determined by ICP-AES. Values are in ppm, except for Al and Ca, which are in percent. N, not detected.

Var.	Minimum	Maximum	Mean	Standard Deviation	Valid	N
Al	8.000E-01	1.000E+00	9.000E-01	3.7796E-02	29	0
Ca	5.070E+01	5.960E+01	5.712E+01	2.0318E+00	29	0
Fe	7.500E+01	1.900E+03	2.274E+02	3.9409E+02	21	8
Mg	1.400E+02	3.300E+02	2.514E+02	5.3031E+01	29	0
K	4.500E+03	7.900E+03	5.500E+03	7.2111E+02	29	0
Mn	--	--	--	--	0	29
Na	1.200E+04	1.500E+04	1.376E+04	7.3946E+02	29	0
Ag	--	--	--	--	0	29
As	--	--	--	--	0	29
Ba	3.700E+01	3.800E+02	5.607E+01	6.2456E+01	29	0
Be	1.000E+00	4.400E+00	1.479E+00	7.0121E-01	29	0
Bi	--	--	--	--	0	29
Ce	5.200E+01	1.200E+02	8.600E+01	4.8083E+01	2	27
Co	--	--	--	--	0	29
Cr	5.000E+01	3.600E+02	1.320E+02	1.5209E+02	4	25
Cu	2.100E+00	1.500E+01	4.900E+00	4.2407E+00	12	17
La	8.000E+00	5.700E+01	1.986E+01	1.3416E+01	14	15
Li	3.200E+00	3.200E+00	3.200E+00	--	1	28
Mo	--	--	--	--	0	29
Ni	2.200E+01	1.900E+02	7.300E+01	7.9540E+01	4	25
P	--	--	--	--	0	29
Pb	5.300E+01	1.800E+02	9.500E+01	5.9872E+01	4	25
Sb	--	--	--	--	0	29
Sn	3.600E+01	3.600E+01	3.600E+01	--	1	28
Sr	2.000E+00	1.000E+02	6.389E+01	2.9811E+01	28	1
Ti	4.000E+00	5.900E+01	9.593E+00	1.0476E+01	29	0
V	--	--	--	--	0	29
W	--	--	--	--	0	29
Y	2.300E+00	7.700E+02	7.549E+01	1.4541E+02	27	2
Zn	2.800E+00	1.500E+01	6.467E+00	3.3875E+00	27	2
Zr	8.000E+00	2.000E+01	1.462E+01	2.6106E+00	29	0

Table 11.--Listing of elements infrequently detected by ICP-AES. Deposit type codes: 1, Au-Ag vein; 2, Ba-Pb vein; 3, "barren" vein; 4, W-Be skarn; 5, "questionable" deposit type. Detection limits in parenthesis.

SAMPLE	DEPOSIT TYPE	La (6)	Ce (30)	Cu (2)	Cr (8)	Ni (10)	Pb (50)	Sn (30)	Li (0.8)
SC007R1	4						53		
SC010R1	3	15							
SC014R6	1	19							
SC024R2	3			8.3					
SC028R4	3	11							
SC030R5	3	21							
SC030R9	3	26							
SC031R4	3	10							
SC047R1	2			2.2					
SC051R4	5			4.2					
SC056R3	3	10							
SC028R5	3	17		2.1					
SC046R1	2			15			53		
SC051R1	5	12		2.5					
SC052R1	3	8		3.6					
SC009R2	3	39	52	2.2					
SC054R1	5			2.9	55	24			
SC055R1	5			11	360	190		36	
SC005R	4	57	120				180		3.2
SC056R1	3	13		2.7	50	56			
SC030R1	3	20		2.1	63	22	94		

Sodium contents are rather high and vary only slightly in all 29 samples, ranging from 1.2% to 1.5%. Eighteen of the samples contained 1.4% and 6 samples contained 1.3%, further confining overall variation. No correlation was noted with deposit type.

Stoichiometrically, fluorite (CaF_2) should contain 51.3% Ca. Calcium ranged from 53.6% to 59.8% in the fluorites, except for 1 sample containing 50.7% Ca. The Ca contents are far above the normal ICP-AES working range and the excess Ca and the variation in content may be the result of excessive sample dilution. Caution must be used in interpretation of Ca content in the samples. No correlation between Ca content and deposit type was noted.

Potassium contents in the samples varied from 4500 to 7900 ppm, with a mean of 5500 ppm. Of the 4 samples with high K contents, 3 are from "barren" veins from the "Hanson" prospects area (SC009R2, 6900 ppm; SC010R1, 6700 ppm; SC028R5, 6700 ppm), and 1 sample is from Iron Mountain W-Be skarn (SC007R2, 7900 ppm). However, the high value for the skarn sample was not repeated in an analytical duplicate.

Barium was detected in all 29 samples in a narrow range from 37 to 50 ppm, except for 2 samples with 63 ppm (SC046R1) and 380 ppm (SC047R1). The two high Ba samples are derived from Ba-Pb veins in the Caballo Mountains. Barite inclusions were identified by XRD in other fluorite samples from the same area. No other correlations with deposit type were noted.

The remaining 5 elements determined by ICP-AES (Be, Ti, Y, and Sr) and ICP-MS (U) reveal interesting relationships when plotted against one another. Figure 9 is a plot of Ti versus Be. Titanium, detected in all 29 samples, ranges from 4 to 59 ppm. Beryllium was detected in all 29 samples, ranging from 1.0 to 4.4 ppm, with 22 samples having values below 1.5 ppm. While the range in Be values is rather narrow, some interesting features are evident. Two populations can be discerned in Figure 9. The majority of samples have relatively low Be and low Ti contents. This population contains all the Au-Ag vein samples and most of the "barren" vein samples. The second population contains 7 samples with Be values above 1.5 ppm and Ti content generally above 10 ppm. Two of the 7 samples are from W-Be endoskarn at Iron Mountain, 1 is from Ba-Pb veins, and 4 are from "barren" veins. A closer inspection of these 4 samples reveals that they are all from the "Hanson" prospects in the Sierra Cuchillo, several miles south of Iron Mountain. It is interesting to note that sample SC009R2 (Be, 4.4 ppm) contains nearly double the Be content in fluorite from W-Be skarn at Iron Mountain. Large variation in Ti concentration is found in the Iron Mountain W-Be skarn fluorites. The highest Ti content is found in fluorite from endoskarn, while very low Ti is found in fluorite from exoskarn. Heavy mineral concentrate sample SC045H contains an intermediate amount of Ti (14 ppm) and is derived from nearby endoskarn and distal exoskarn. Similarly, Be content is higher in W-Be endoskarn fluorite (above 2 ppm) compared to exoskarn fluorite (below 1.5 ppm), while the heavy mineral concentrate sample SC045H contains an intermediate amount.

Figure 10 is a plot of Y versus U. Yttrium was found in 27 samples, ranging in concentration from 2.3 to 770 ppm with a mean of 75 ppm. Low level U was found in all 29 samples in a very narrow range (0.1 to 1.1 ppb). Two general populations are found in Figure 10. The first population contains the majority of samples and is characterized by relatively low Y and low U content. Within this population, samples containing the lowest values for Y and U are from Au-Ag veins and from "barren" veins from the "Chavez" prospects. Fluorites from W-Be exoskarn also contain low Y and U content.

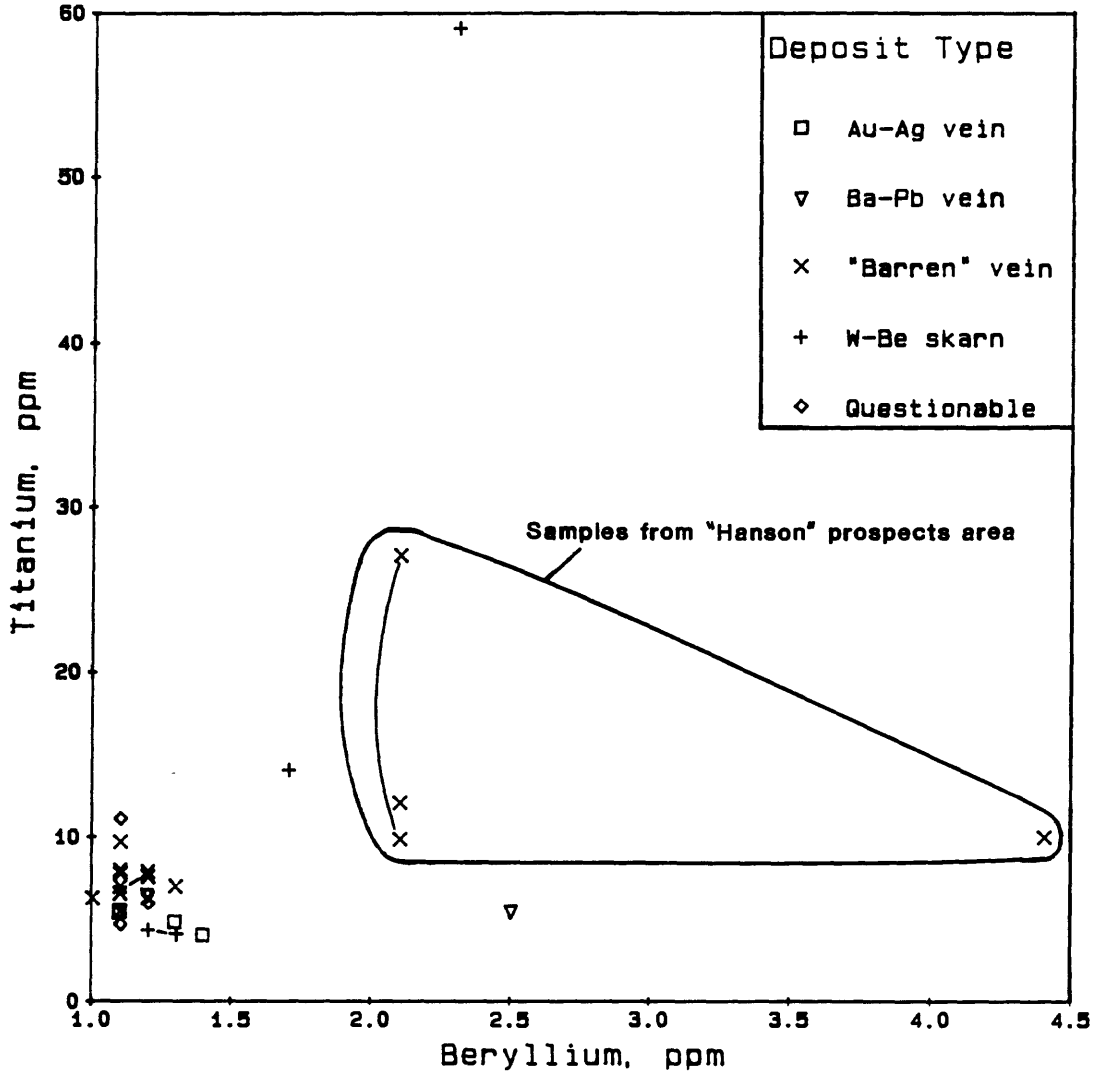

Figure 9.--Plot of Ti versus Be. Line segments link sample site duplicates. Samples analyzed by ICP-AES.

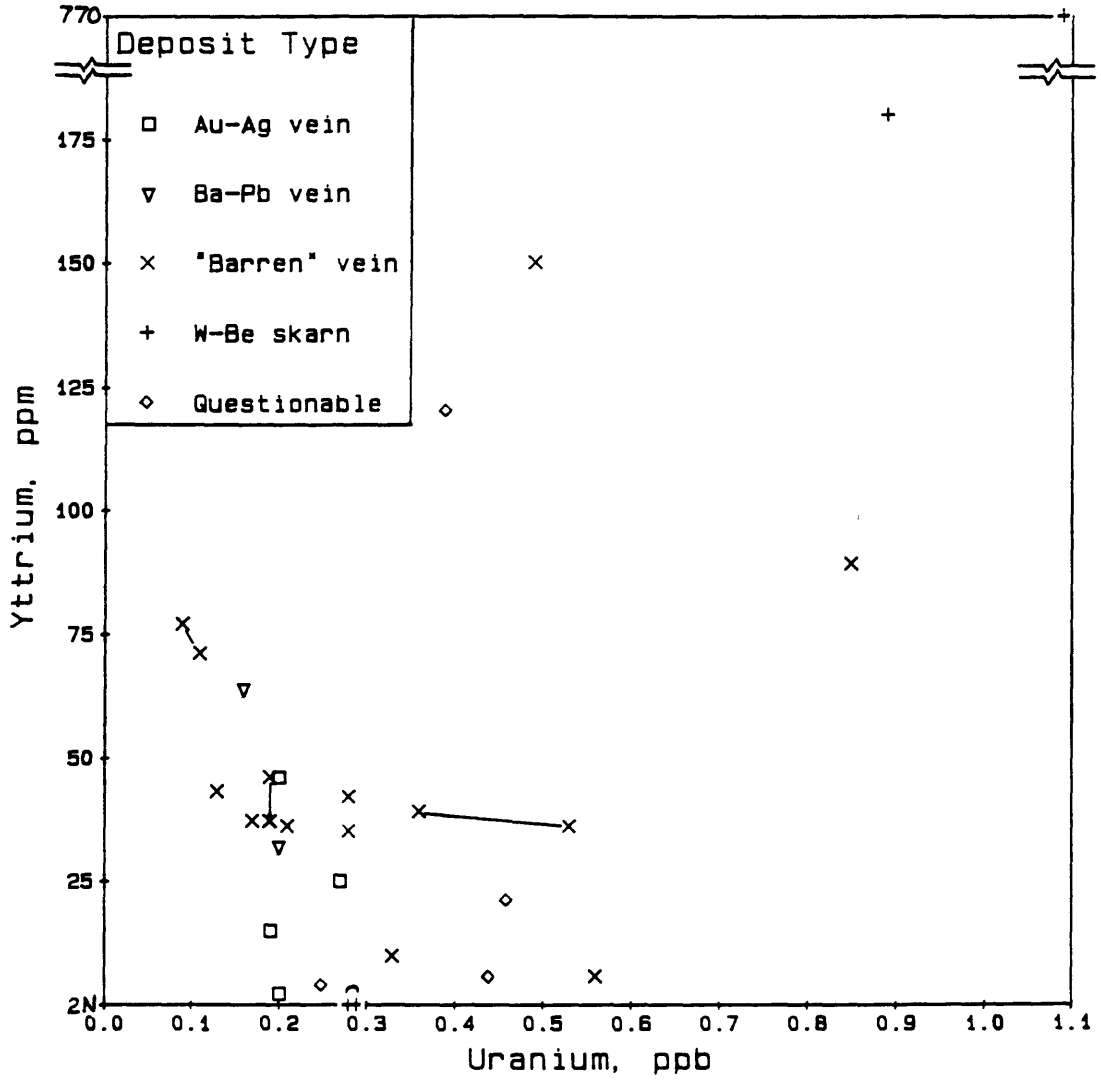

Figure 10.--Plot of Y versus U. Line segments link sample site duplicates. 2N = not detected at 2 ppm. Samples analyzed by ICP-AES (Y) and ICP-MS (U).

The second population contains 5 samples with higher contents of both Y and U. As seen in Figure 9, the second population contains two samples from W-Be endoskarn, and 2 samples are from "barren" veins from the "Hanson" prospects. The 5th sample in the second group is from a "questionable" deposit type. It is interesting that the 6 "barren" vein samples containing the most U (between 0.3 to 0.9 ppb) are all from the "Hanson" prospects. Similar to Ti and Be, extreme variation in Y content was found in W-Be skarn samples. The highest Y value was found in endoskarn (SC005R, 770 ppm). Yttrium was not detected (at 2 ppm) in exoskarn samples. Heavy mineral concentrate sample SC045H contained the second highest Y value (180 ppm). While not nearly as extreme, uranium exhibits the same relationship, with the highest U content in W-Be endoskarn and lower U content in exoskarn.

Strontium was detected in 28 samples, ranging in concentration from 2 to 100 ppm. Figure 11, a plot of Sr concentration, shows relatively low Sr values for the W-Be endo- and exoskarn fluorites and for Ba-Pb vein fluorites (not detected [at 0.2 ppm] to 34 ppm), compared to the "barren" vein and Au-Ag vein fluorites (33 to 100 ppm). "Questionable" deposit type fluorites are uniformly high in Sr (all above 80 ppm).

Results--Semiquantitative Emission Spectrography

Twenty of the 103 fluorite samples analyzed for 31 elements by SES are analytical duplicates discussed in the quality control section. The remaining 83 fluorite samples (60 from rock, 23 from heavy mineral concentrates) are discussed here. Standard 10 mg sample weights were used for all samples except SC020R3 (1 mg), SC021H (5 mg), SC022R1 (2.5 mg), SC036H (1 mg), and SC037H2 (5 mg). Since lower sample weights reduce precision in the SES method, data from these 5 samples, and particularly from the samples with weights less than 5 mg, are probably much less accurate than data from the rest of the samples.

Table 12 is a listing of univariate statistics for the 31 elements determined by SES. Twelve elements were not detected in any of the samples (Ag, As, Au, B, Bi, Cd, Co, Cr, Nb, Sb, Sn, and Th). Greater than 20% Ca was detected in all samples. Thirteen elements (Cu, Fe, Mo, Ni, Sc, W, Zn, Mn, Ba, Pb, Zr, Mg, and V) had 15% or less unqualified values. Five elements (Be, La, Sr, Ti, and Y) had unqualified values in 25% or more of the 83 samples.

Samples containing the 13 elements listed above are shown in Table 13. Seven of these elements (Cu, Fe, Mo, Ni, Sc, W, and Zn) were detected 5 times or less, at levels commonly near or below lower limits of determination. These two features severely limit usefulness of these elements. Scandium was detected in 5 samples, all below the lower determination limit. However, it is interesting that 4 of the 5 samples are from W-Be skarn. Three of 4 samples containing detectable zinc are derived from W-Be skarn, and the 4th sample is a concentrate draining "questionable" deposits. Iron detected in three samples probably is due to trace residual iron oxide stains on fluorite; most of the Fe was identified and removed during the binocular scan of the three samples.

Tungsten was detected in 1 concentrate sample (SC062H, 200 ppm). The same sample contained detectable Cu and Zn, and high concentrations of both Mo (700 ppm) and Pb (2000 ppm). Galena, sphalerite, and chalcopyrite were identified in the concentrate prior to removal of fluorite. Birefringent grains removed during the polarizing light scan of the fluorite separate were identified as mimetite (Pb arsenate). It is probable that fine-grained "clay" identified in cleavage recesses in the fluorite separate prior to analysis was misidentified and is responsible for the high metal values in sample SC062H.

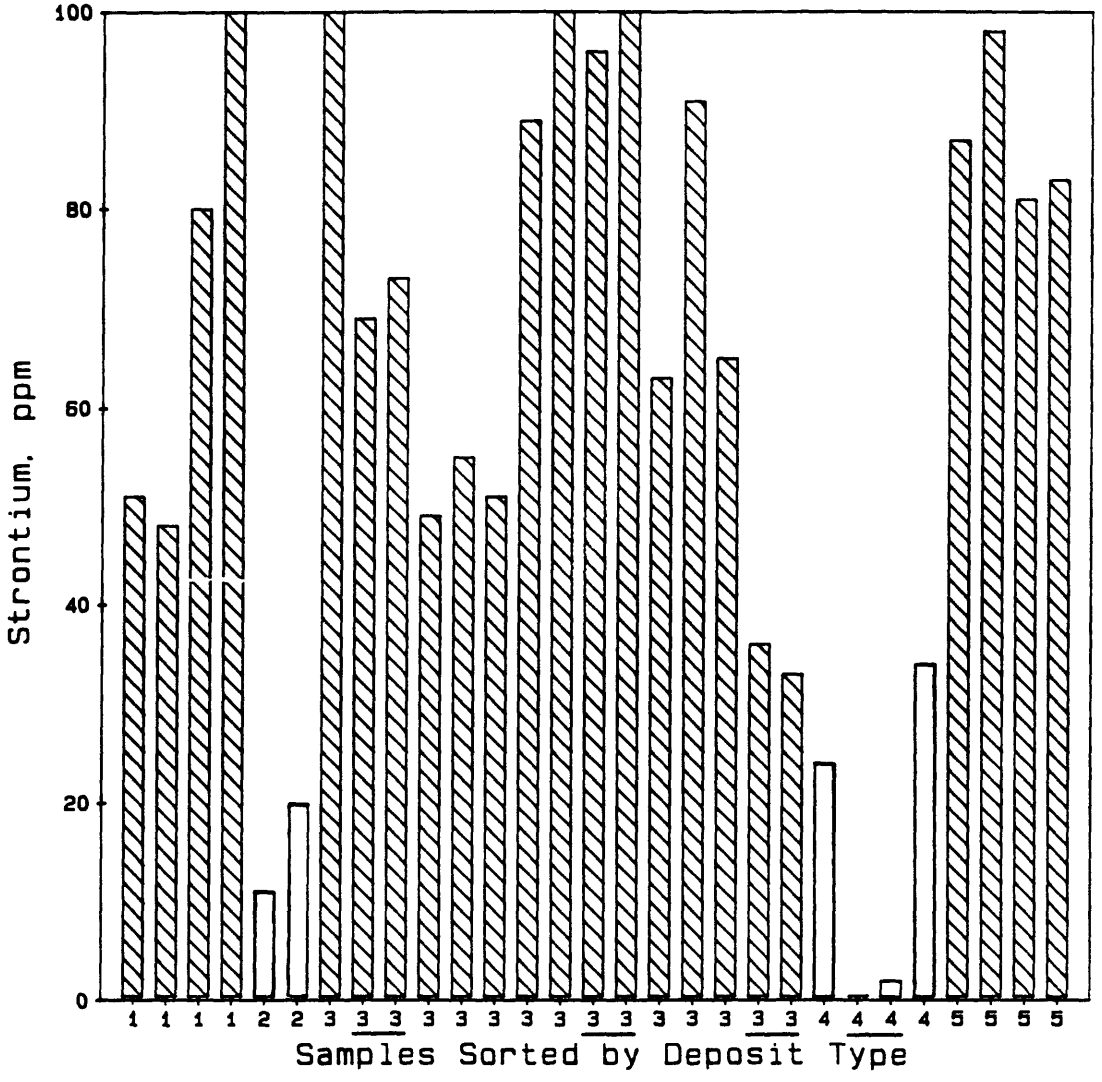

Figure 11.--Strontium concentration in fluorite samples analyzed by ICP-AES. Site duplicate samples are underlined. Deposit type code: 1, Au-Ag veins; 2, Ba-Pb veins; 3, "barren" veins; 4, W-Be skarn; 5, "questionable" deposit type.

Table 12.--Univariate statistics for trace elements determined by SES. Values are in ppm. N, not detected; L, detected, but below lower limit of determination.

Var.	Minimum	Maximum	Mean	Standard Deviation	Valid	L	N
Fe	7.000E+02	7.000E+02	7.000E+02	--	1	2	80
Mg	2.000E+02	2.000E+03	4.625E+02	6.3005E+02	8	45	30
Ti	3.000E+01	2.000E+02	7.890E+01	3.3185E+01	82	1	0
Mn	2.000E+01	7.000E+01	4.000E+01	2.7386E+01	5	4	74
Ag	--	--	--	--	0	0	83
As	--	--	--	--	0	0	83
Au	--	--	--	--	0	0	83
B	--	--	--	--	0	0	83
Ba	5.000E+01	1.500E+03	4.278E+02	4.9188E+02	9	1	73
Be	1.000E+00	1.500E+01	3.452E+00	3.2592E+00	21	7	55
Bi	--	--	--	--	0	0	83
Cd	--	--	--	--	0	0	83
Co	--	--	--	--	0	0	83
Cr	--	--	--	--	0	0	83
Cu	5.000E+00	5.000E+00	5.000E+00	--	1	3	79
La	5.000E+01	1.500E+02	6.905E+01	2.1681E+01	63	20	0
Mo	5.000E+00	7.000E+02	2.373E+02	4.0068E+02	3	1	79
Nb	--	--	--	--	0	0	83
Ni	--	--	--	--	0	1	82
Pb	1.000E+01	2.000E+03	2.440E+02	6.1984E+02	10	9	64
Sb	--	--	--	--	0	0	83
Sc	--	--	--	--	0	5	78
Sn	--	--	--	--	0	0	83
Sr	1.000E+02	2.000E+02	1.202E+02	2.6491E+01	57	23	3
V	1.000E+01	3.000E+01	1.192E+01	5.6045E+00	13	69	1
W	2.000E+02	2.000E+02	2.000E+02	--	1	0	82
Y	1.000E+01	1.000E+03	9.205E+01	1.3578E+02	78	1	4
Zn	2.000E+02	7.000E+02	3.667E+02	2.8868E+02	3	1	79
Zr	1.000E+01	5.000E+01	2.600E+01	1.0750E+01	10	13	60
Th	--	--	--	--	0	0	83

Table 13.--Listing of elements infrequently detected by SES. Deposit type codes: 1, Au-Ag vein; 2, Ba-Pb vein; 3, "barren" vein; 4, W-Be skarn; 5, "questionable" deposit type. L = detected, but below indicated lower determination limit.

Fluorite from Rock Samples

Sample	Sample Weight	Deposit Type	Ba	Cu	Fe	Mn	Mg	Mo	Ni	Pb	Sc	V	W	Zn	Zr
SC002R	10 mg	1								10L					10L
SC005R	10 mg	4	50			70					5L				20
SC007R1	10 mg	4				10L									
SC007R2	10 mg	4													
SC008R	10 mg	4			700	70	2000			10L				200	50
SC009R1	10 mg	3					200	7		20					
SC009R2	10 mg	3					200								
SC013R	10 mg	5										10			
SC014R5	10 mg	1								10L					
SC014R6	10 mg	1										10			
SC015R2	10 mg	1									5L	10			
SC017R1	10 mg	1										10			
SC020R3	1 mg	4				L	200				L	10		200	
SC022R1	2.5 mg	4									20L				50L
SC024R2	10 mg	3		5L			200								
SC026R2	10 mg	3										10			
SC027R2	10 mg	3										10			
SC027R3	10 mg	3										10			
SC028R5	10 mg	3				10L	200			15		10			
SC030R1	10 mg	3										10			
SC042R1	10 mg	1										10			
SC043R3	10 mg	1								10L					20
SC044R1	10 mg	1													10L
SC046R1	10 mg	2		5						30					
SC046R3	10 mg	2	1500					5L		30					
SC047R1	10 mg	2	300												10L
SC051R1	10 mg	5													30
SC051R4	10 mg	5								10L					
SC054R1	10 mg	5								10L					10L
SC055R1	10 mg	5													10L
SC058R1	10 mg	3													10L
SC061R1	10 mg	3													10L

Table 13 (continued).

Fluorite from Heavy Mineral Concentrate Samples

Sample	Sample Weight	Deposit Type	Ba	Cu	Fe	Mn	Mg	Mo	Ni	Pb	Sc	V	W	Zn	Zr
SC002H	10 mg	1													30
SC006H	10 mg	4				20				15					20
SC021H	5 mg	4		10L		20	500				10L			700	20L
SC029H	10 mg	3	20L				200			20					
SC035H1	10 mg	3													10L
SC035H2	10 mg	3													30
SC036H	1 mg	1							L						
SC037H1	10 mg	1	100		500L										
SC037H2	5 mg	1	1000												20L
SC038H2	10 mg	1	300		500L					10L					
SC039H	10 mg	1	100			10L				10					
SC041H	10 mg	1								10L					10L
SC045H	10 mg	4				20									
SC049H	10 mg	2	200												
SC053H	10 mg	5								100					20
SC057H1	10 mg	3													10
SC057H2	10 mg	3													10L
SC060H	10 mg	3								10L					
SC062H	10 mg	5	300	5L				700		2000		30	200	200L	
SC063H	10 mg	5						5		200		15			30

Manganese in fluorite from rock samples was detected 5 times ranging from less than 10 ppm to 70 ppm. Four of the manganese values are found in Iron Mountain W-Be skarn samples, and the 5th is from a "barren" vein from the "Hanson" prospects area. Manganese near the lower determination limit was found in three concentrates from streams draining W-Be skarn at Iron Mountain and in one concentrate from a stream draining Au-Ag veins in the Black Range. Manganite and pyrolusite were reported at Iron Mountain (Jahns, 1944) and it is likely that the Mn in the skarn fluorite samples is due to trace quantities of manganese oxide.

Barium was found in 3 samples of fluorite from rock. Two of the samples are from Ba-Pb veins (300 and 1500 ppm) and the third is from W-Be skarn. Barium was detected in 7 concentrates from streams draining Ba-Pb veins (1), "barren" veins (1), Au-Ag veins (4), and "questionable" deposits (1). The more common occurrence of Ba in concentrates compared to rocks probably reflects error in differentiating colorless anhedral barite and fluorite while selecting fluorite grains for analysis. Barite inclusions in fluorite are probable in rock samples from Ba-Pb veins.

Lead was found in 10 samples of fluorite from rock, ranging from less than 10 ppm to 30 ppm. Two samples from Ba-Pb veins contained the highest Pb values (both 30 ppm). Two samples from "barren" veins in the "Hanson" prospects area contained 15 and 20 ppm Pb. Less than 10 ppm Pb was detected in 3 samples from Au-Ag veins, in 1 sample from W-Be skarn, and in 2 samples from "questionable" deposits. Much more variablity in Pb was found in fluorite from concentrates, with values ranging from less than 10 ppm to 200 ppm, with 1 sample having 2000 ppm. The three concentrates with the highest Pb values (SC053H, 100; SC063H, 200; SC062H, 2000 ppm) are from fluorites from "questionable" sites. However, these 3 samples are from sites in drainages downstream from known galena deposits. Thus, it is possible that the higher Pb content in these fluorite samples is due to supergene secondary Pb minerals coating fluorite grains.

Zirconium was detected in 23 samples; 13 of these had Zr contents below the lower limit of determination. Zr values above that limit ranged from 10 to 50 ppm. Zirconium distribution was not observed to correlate with deposit type, sample type, or relative abundance of anisotropic inclusions in fluorite.

Magnesium was detected at less than 200 ppm in 45 samples, at 200 ppm in 6 samples, and at 500 ppm and 2000 ppm in 1 sample each. All 8 unqualified Mg values are from either W-Be skarn (3 samples) or from "barren" veins in the "Hanson" prospects area (5 samples).

Vanadium was detected in 80 samples at or below the determination limit (10 ppm) and in two samples at 30 and 15 ppm (SC062H and SC063H, respectively). The slightly higher V content in these two samples may be due to other mineral contaminants on fluorite, as described earlier for these samples.

The elements Be, La, Sr, Ti, and Y were detected more frequently and provide more information than the previous 13 elements. Histograms presented in the following discussion of these 5 elements do not include analyses for the samples with sample weights less than 10 mg, since data for these samples have different detection limits and are generally more qualitative than the data for the 10 mg samples.

Beryllium was detected in 28 samples ranging from less than 1 ppm (7 samples) to 15 ppm. Histograms for Be in fluorite from rocks and concentrates are shown in Figure 12. In agreement with the ICP-AES results, the highest Be values are from "barren" veins. All of the unqualified Be values in fluorite from rock from "barren" veins are derived from samples from the "Hanson" prospects area. "Hanson" prospect concentrate samples account for two of the

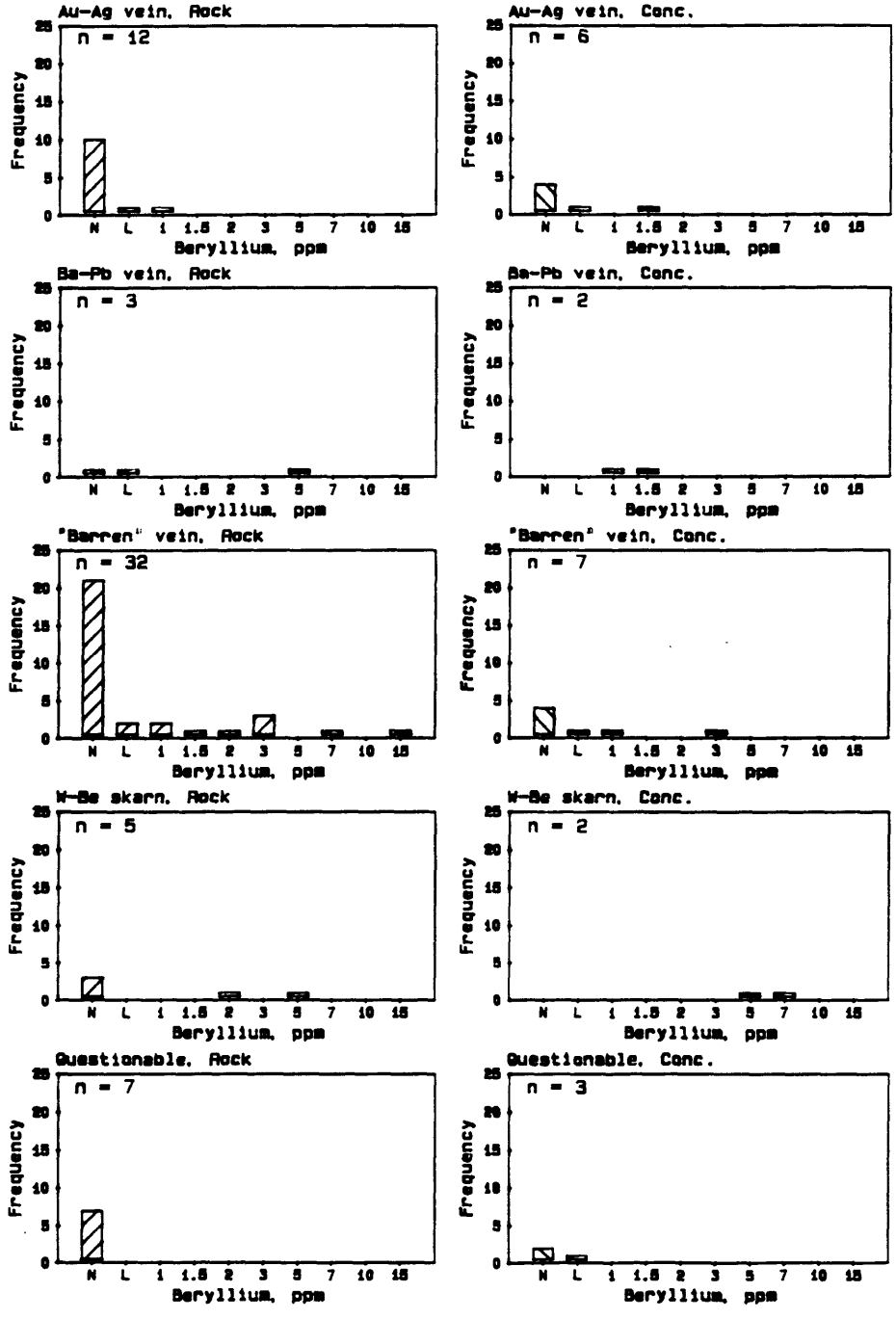

Figure 12.--Histograms for Be in fluorite from rocks and concentrates. N = not detected, L = detected, but less than lower limit of determination. Samples analyzed by SES.

three Be values detected in fluorite from "barren" vein concentrates. Four of the 7 rock and concentrate samples from W-Be skarn at Iron Mountain contain Be ranging from 2 to 7 ppm. Beryllium was detected in endoskarn samples, but not in exoskarn samples. Beryllium also was detected in 4 of 5 rock and concentrate samples from Ba-Pb veins, although all but 1 sample had values at or near the detection limit. Four of 18 rock and concentrate samples from Au-Ag veins contained Be near the detection limit.

Lanthanum was detected in all 79 samples ranging from less than 20 ppm to 150 ppm. Histograms for La (Figure 13) reveal relatively higher La content in fluorites from Au-Ag vein, "barren" vein, and "questionable" deposit types compared to fluorites from Ba-Pb veins. Fluorites from W-Be skarn rock samples generally are low in La, except for one endoskarn sample (SC005R). High La concentration in sample SC005R agrees with ICP-MS results which indicated that the same sample contained the highest total REE contents. Intermediate La concentrations were found in fluorite from concentrates derived from sites near endoskarn, but with exoskarn occurring further upstream.

Strontium was found in all but 3 samples in a fairly narrow range of less than 100 ppm to 150 ppm. This narrow range represents only 3 step intervals for SES. However, histograms for Sr (Figure 14) reveal an overall trend of lower Sr values for Ba-Pb veins and W-Be skarn, and higher Sr values for Au-Ag veins, "barren" veins, and "questionable" deposits. While validity of this trend is hampered by the low sample populations for all but the "barren" vein rock fluorites, the trend agrees with a similar trend found for Sr determined by ICP-AES.

Titanium was found in all 79 samples ranging from less than 20 ppm to 150 ppm. Histograms for Ti are shown in Figure 15. "Barren" vein samples exhibit a normal distribution with a mean of about 70 ppm. Samples from other deposit types generally tend to cluster around 70 ppm as well, and the mean for all 79 samples is 79 ppm (Table 12). Titanium distributions in fluorite from concentrates do not appear to vary from those in fluorite from rocks. No correlation with deposit type was found.

Yttrium was found in all but 3 samples, ranging from less than 10 ppm to 1000 ppm (Figure 16). A fairly normal distribution was found for "barren" vein samples; the 3 highest Y values are all from samples from the "Hanson" prospects. As found with the ICP-AES results, Y was most variable in samples from W-Be skarn. The highest Y values were found in fluorite from W-Be endoskarn, while Y was not detected in W-Be exoskarn samples. Fluorite from concentrates collected below W-Be skarn had values intermediate between the two extremes. Clear relationships between Y and other deposit types were not observed.

Summary of Analytical Results

The results of analyses of fluorite are summarized here by respective analytical method.

ICP-MS

(1) Three parameters--slope, (La/Yb)n; europium behavior, (Eu/Eu*)n; and cerium behavior, (Ce/Ce*)n--are useful in discerning overall variation in the chondrite-normalized REE patterns with respect to deposit type. Slope alone probably is the least effective in distinguishing fluorites from different deposit types.

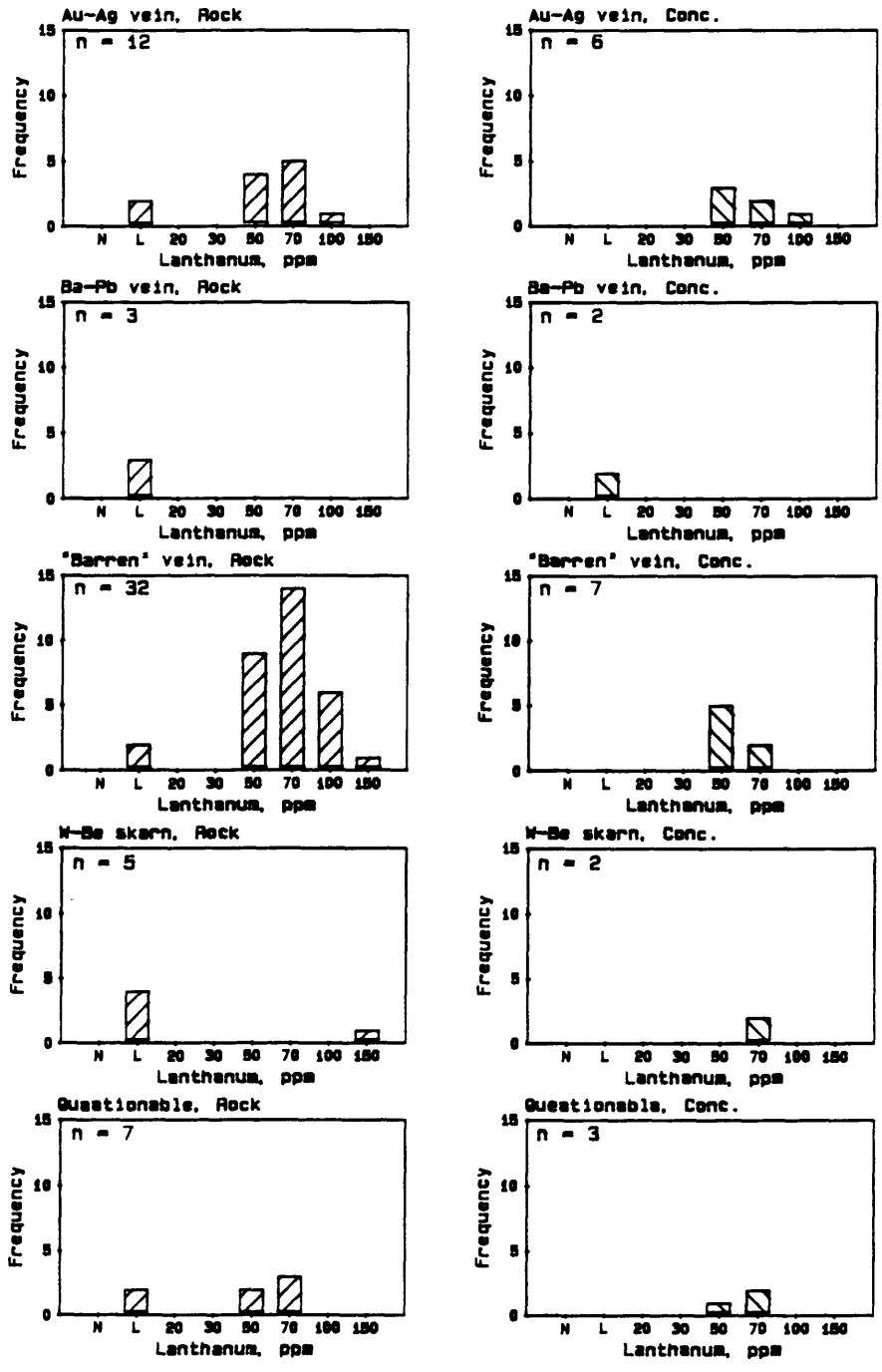

Figure 13.--Histograms for La in fluorite from rocks and concentrates. N = not detected, L = detected, but less than lower limit of determination. Samples analyzed by SES.

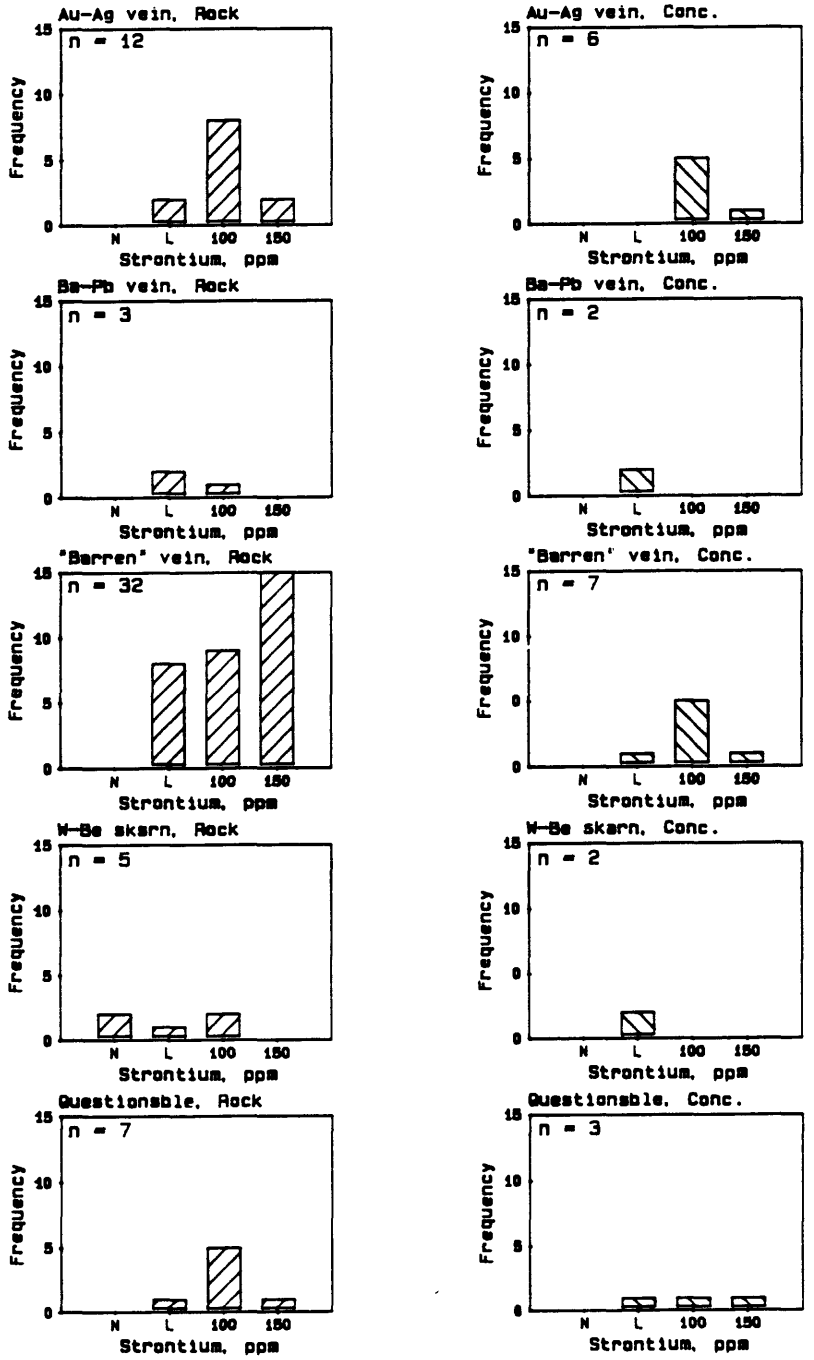

Figure 14.--Histograms for Sr in fluorite from rocks and concentrates. N = not detected, L = detected, but less than lower limit of determination. Samples analyzed by SES.

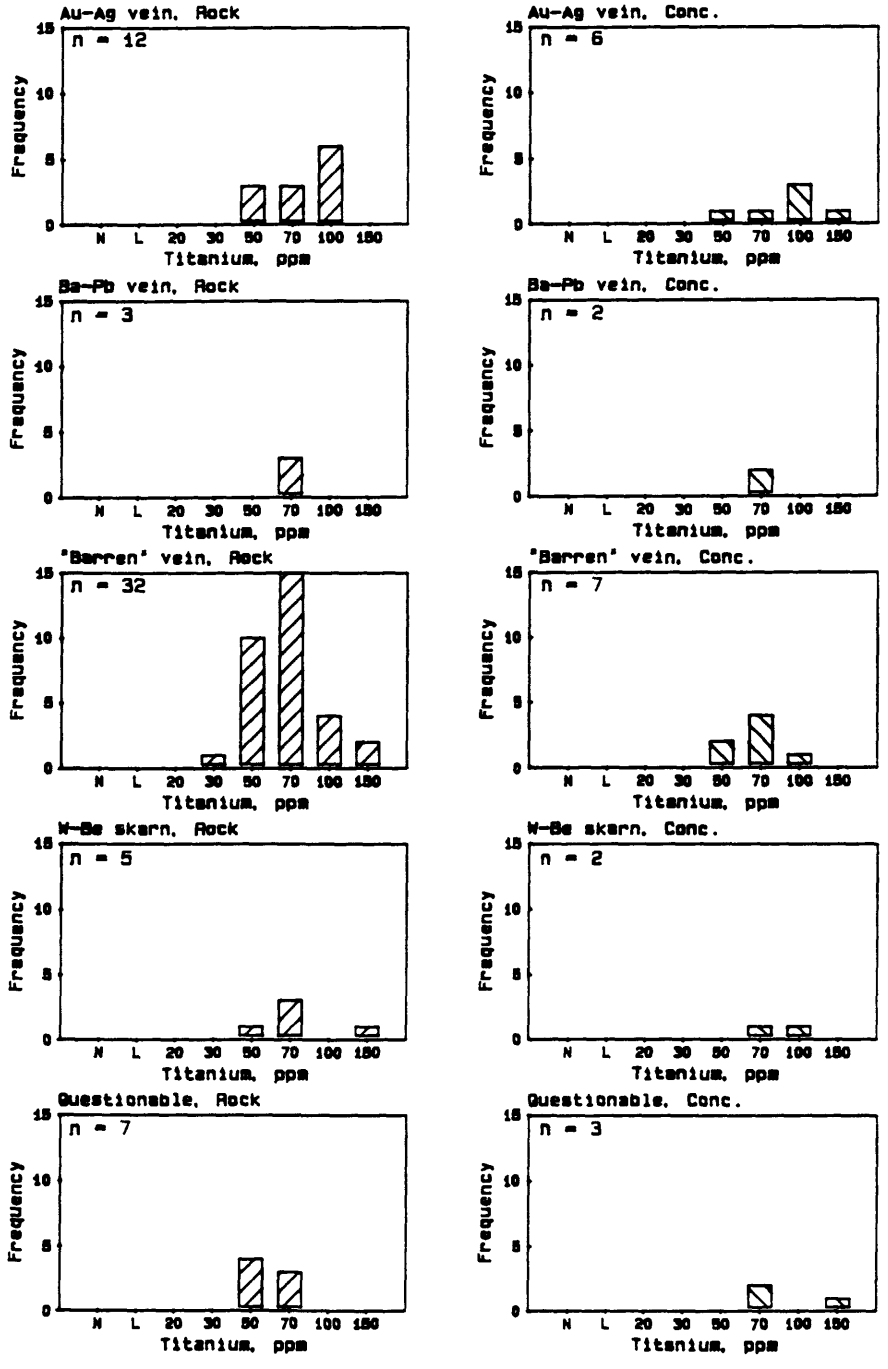

Figure 15.--Histograms for Ti in fluorite from rocks and concentrates. N = not detected, L = detected, but less than lower limit of determination. Samples analyzed by SES.

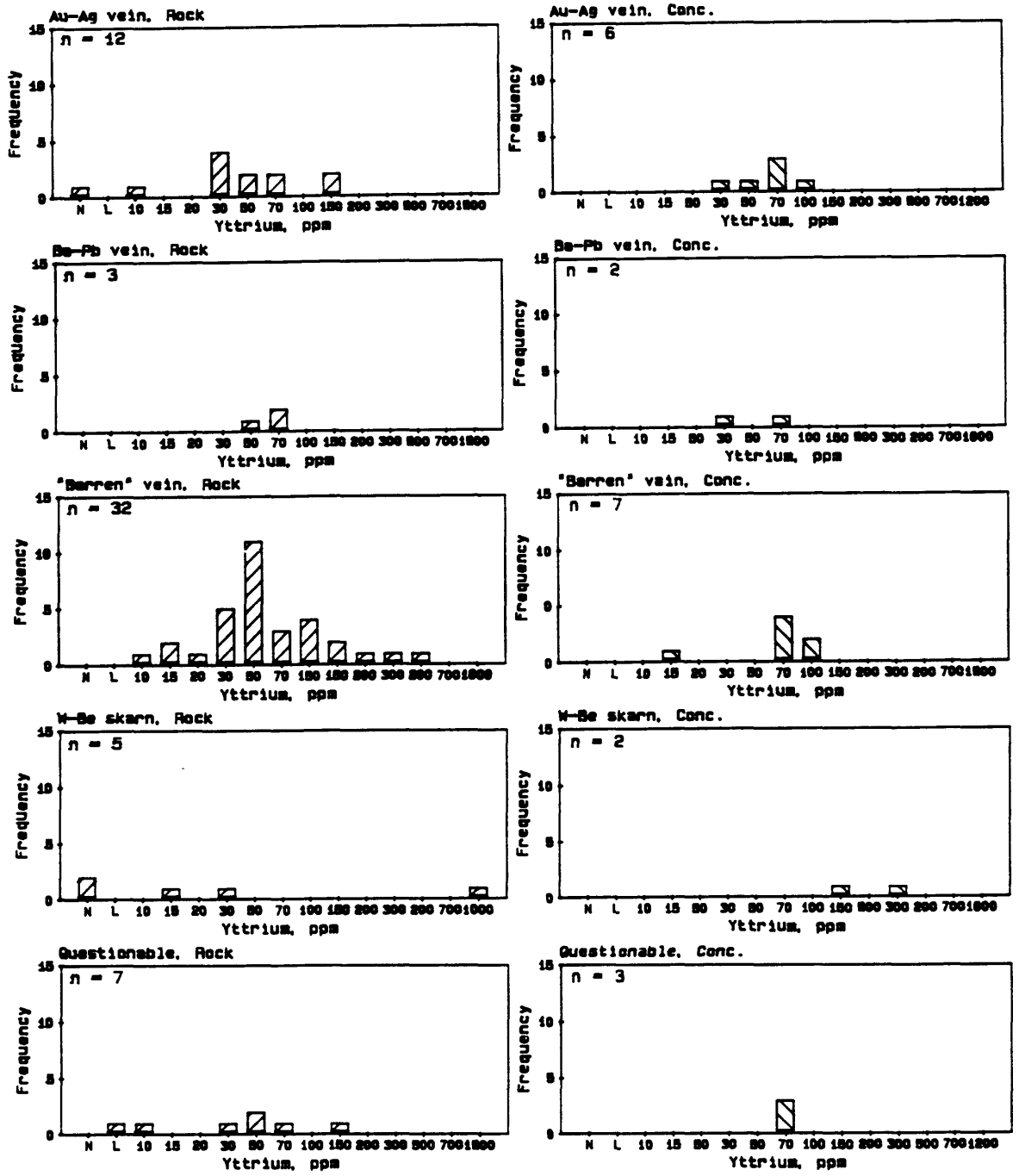

Figure 16.--Histograms for Y in fluorite from rocks and concentrates. N = not detected, L = detected, but less than lower limit of determination. Samples analyzed by SES.

(2) REE enrichment (relative to chondrites) is variable, although light REE enrichment overall is most common.
(3) The Ba-Pb vein fluorites appear to cluster with the W-Be skarn fluorites, particularly in the plot of slope versus europium behavior. However, Ba-Pb vein fluorites differ by exhibiting middle REE enrichment, not reflected by the slope parameter.
(4) Behavior of europium successfully differentiates W-Be skarn and Ba-Pb vein fluorites from Au-Ag vein fluorites.
(5) "Barren" vein fluorites exhibit wide variation in all three parameters.
(6) Fluorites from "questionable" deposits generally occupy the same fields as "barren" fluorites.
(7) A group of 5 "barren" vein fluorites from the "Chavez" prospects behaves sympathetically to Au-Ag vein fluorites with respect to all three parameters.
(8) The W-Be skarn fluorites from exoskarn and endoskarn are easily distinguishable with the cerium behavior parameter, and to a lesser degree with europium behavior and slope.

ICP-AES

(1) Ten elements were not detected by ICP-AES: Ag, As, Bi, Co, Mn, Mo, P, Sb, V, and W.
(2) Six elements were detected in a small number of samples and are of limited use: Li and Sn (1 observation each); Ce (2 observations); Pb, Cr, and Ni (4 observations each).
(3) Two elements, Cu and La, were detected in less than half of the samples.
(4) No correlation with deposit type was noted for the above 8 elements.
(5) Seven elements (Al, Fe, Mg, Zn, Zr, Na, and Ca) were detected in all or most of the samples, but generally correlations of these with different deposit types were not found. Use of these elements is hindered by problems such as contamination during sample preparation (Al), poor analytical resolution possibly due to very narrow ranges in concentration (Zn, Zr, Na, Ca), large analytical and/or site duplicate variation (Fe, Mg, Zn, Zr), and possibly sample dilution error (Ca).
(6) Four samples containing high K values were found in "barren" vein fluorites from the "Hanson" prospects. No other correlations with deposit type were found.
(7) Generally, Ba was found in a narrow range in concentration, limiting its usefulness. However, the two highest Ba values are from Ba-Pb vein fluorites in the Caballo Mountains. Barite inclusions were identified in fluorite from the same area.
(8) The Au-Ag vein fluorites contain relatively low Ti, Be, Y, and U, while these elements in W-Be endoskarn fluorites are relatively high. "Barren" vein, Ba-Pb vein, and "questionable" fluorites generally contain intermediate concentrations in these elements. One group of "barren" vein fluorite samples, all from the "Hanson" prospects area, contains relatively high contents of these 4 elements. "Barren" vein fluorites from the "Chavez" prospects behave similarly to Au-Ag vein fluorites with respect to Y and U.
(9) Large variation is found for Ti and Y between W-Be endoskarn (high values) and exoskarn (low values). The same relationship is repeated for Be and U, although differences are not as extreme. A heavy mineral concentrate sample from a site draining nearby endoskarn and distal exoskarn contains intermediate values for these elements.
(10) Strontium content is high in Au-Ag vein, "barren" vein, and "questionable" fluorites. Relatively low Sr values are found for W-Be endoskarn and exoskarn and for Ba-Pb vein fluorites.

SES

(1) Twelve elements were not detected (Ag, As, Au, B, Bi, Cd, Co, Cr, Nb, Sb, Sn, and Th).
(2) Greater than 20% Ca was detected in all samples.
(3) Seven elements (Cu, Fe, Mo, Ni, Sc, W, and Zn) were detected 5 times or less, at levels commonly near or below lower limits of determination. Four of the 5 samples containing Sc and 3 of the 4 samples containing Zn are from W-Be skarn. Iron, detected in three samples, probably is due to trace residual iron oxide stains on fluorite. High values for W, Mo and Pb in concentrate sample SC062H probably are due to analysis of an impure fluorite separate, with foreign mineral matter residing in cleavage recesses in the fluorite.
(4) Manganese was detected 5 times in fluorite from rock; 4 of the samples are from W-Be skarn and the 5th is from a "barren" vein from the "Hanson" prospects area. Manganese was found in three of 4 fluorite samples from concentrates derived from W-Be skarn. It is likely that Mn in the skarn fluorite samples is due to trace quantities of manganese oxide.
(5) Two of 3 Ba values found in fluorite from rock are from Ba-Pb veins and the 3rd is from W-Be skarn. Barium was detected in 7 concentrates. The more common occurrence of Ba in concentrates compared to rocks probably reflects error in differentiating colorless anhedral barite and fluorite while selecting fluorite grains for analysis.
(6) Two samples from Ba-Pb veins contained the highest Pb values. Three fluorites from concentrates with high Pb values are from "questionable" sites downstream from known galena deposits. Thus, the Pb may be due to supergene secondary Pb minerals coating fluorite.
(7) All 8 unqualified Mg values are from either W-Be skarn (3 samples) or from "barren" veins in the "Hanson" prospects area (5 samples).
(8) In agreement with ICP-AES results, the highest Be values are from "barren" veins from the "Hanson" prospects area. High Be content also is found in fluorite from W-Be endoskarn, but none was found in exoskarn samples. Relatively high Be content also was detected in a Ba-Pb vein sample.
(9) Lanthanum content was relatively high in fluorites from Au-Ag vein, "barren" vein, and "questionable" deposit types compared to fluorites from Ba-Pb veins. Fluorites from W-Be skarn rock samples generally are low in La, except for one sample from endoskarn. Intermediate La concentrations were found in fluorite from concentrates derived from sites near endoskarn, but with exoskarn occurring further upstream.
(10) Strontium values revealed an overall trend of lower Sr values for Ba-Pb veins and W-Be skarn, and higher Sr values for Au-Ag veins, "barren" veins, and "questionable" deposit types. However, validity of this trend is hampered by low sample populations for all but "barren" vein rock fluorites. The trend agrees with a similar one found for Sr determined by ICP-AES.
(11) Titanium was not found to correlate with deposit type.
(12) The highest Y values in "barren" veins are all from samples from the "Hanson" prospects. The highest Y values were found in fluorite from W-Be endoskarn, while Y was not detected in W-Be exoskarn samples, similar to results for Y determined by ICP-AES. Fluorite from concentrates below W-Be skarn had values intermediate between the two extremes. No other relationships for Y were observed.

Results--X-Ray Diffraction Studies

Mineral identification by XRD was undertaken to identify inclusions in fluorite samples prior to chemical analysis and to identify insoluble residues resulting from fluorite dissolution procedures for the ICP-MS and ICP-AES analytical methods. Single fluorite grain mounts and a Gandolfi camera were used for identification. However, both inclusions and insoluble residues commonly were too small for XRD identification.

Quartz was the most commonly identified inclusion in fluorite. This agrees with common observations of very small birefringent prismatic (locally hexagonal) inclusions in fluorite. Prismatic inclusions and quartz inclusions were observed only in fluorite samples from Au-Ag veins and "barren" veins. Other inclusions identified in fluorite include barite from a Ba-Pb vein sample (SC046R3), phlogopite from a W-Be skarn sample (SC005R), calcite from W-Be skarn samples (SC006H, SC008R, and SC021H), hematite from two "barren" vein samples (SC026R1, SC027R2), and sphalerite from a concentrate from a "questionable" site (SC053H).

Extremely small insoluble residues resulted from dissolution of 31 samples analyzed by ICP methods. Four samples of residue were selected for analysis by XRD. Results generally were inconclusive because of small sample size, but a single vague line in a film from one sample is in the correct position for one of the stronger lines for quartz.

DISCUSSION OF RESULTS

Slope and Ce Behavior in Chondrite-Normalized REE Plots

Fluorites exhibited large variation in the slope, (La/Yb)n, of chondrite normalized REE patterns. Fleischer (1969) found that heavy REE were found in fluorites from granitic pegmatites, and that light REE were concentrated in fluorites from alkalic rocks. Ganzeev and Sotskov (1976) briefly mention that high La content in fluorite may serve as an indicator of "heightened alkalinity of the medium." Thus, fluorites with high (La/Yb)n ratios (light REE enrichment) may reflect alkalic source rocks. Alkalic rocks are found spatially associated with fluorite within the study area: syenites were mapped by Huskinson (1975) in the Chise fluorspar area, and Lamarre and others (1974) believed that nepheline monzodiorite may have been the source of fluorine in fluorspar deposits in the Salado Mountains (just east of the southern Sierra Cuchillo). However, fluorite samples from the Chise fluorspar area analyzed in this study were only slightly enriched in light REE (Table 9, samples SC056R1 and SC056R3). A universal simple association of alkalic rocks and light REE enrichment in fluorite seems unlikely. Thus, origin and significance of the variety of slopes in the REE patterns are largely unknown.

Slight to fairly strong negative Ce anomalies were found in all fluorites analyzed for REE, indicating fluorite precipitation from Ce-deficient solutions. Understanding the reason for this behavior is difficult because of the scant literature on Ce behavior in hydrothermal systems, and particularly in fluorite. Möller and Morteani (1983) note that, in the presence of high oxygen fugacities, trivalent Ce can be oxidized readily and adsorbed subsequently by oxyhydrates. Thus, Ce^{4+} may not migrate like trivalent REE and may be left behind. If oxidation/reduction is responsible for Ce behavior in samples analyzed in this study, then similar oxidation/reduction conditions may have occurred for both the "barren" vein samples from the "Chavez" prospects and Au-Ag vein samples clustered together in Figure 8. Conversely,

more variable oxidation/reduction conditions are suggested for W-Be endoskarn and exoskarn samples (Figure 8). Whatever the origin for Ce behavior, hydrothermal fluids which precipitated fluorite were similarly depleted in Ce in both Au-Ag veins and in "barren" veins at the "Chavez" prospects. However, fluorite from W-Be skarn at Iron Mountain precipitated from fluids with much more variable Ce content.

Sr and Eu Behavior

Figure 17 is a plot of Sr versus Eu behavior. These two parameters clearly differentiate W-Be skarn and Ba-Pb vein fluorites from Au-Ag vein, "questionable," and "barren" vein fluorites. Fluorites with positive Eu anomalies and relatively high Sr content include all Au-Ag vein samples and all "barren" vein samples from the "Chavez" prospects area. Relatively strong negative Eu anomalies and low Sr content are found for all W-Be skarn and Ba-Pb vein fluorites.

Feldspars from rhyolitic and dacitic rocks have high distribution coefficients for both Sr and Eu (Hanson, 1978). Thus, as feldspars in a magma crystallize, the remaining melt becomes progressively depleted in Sr and Eu. Conversely, wallrock alteration of feldspar would release both Sr and Eu, enriching the hydrothermal fluid. Intermediate to rhyolitic volcanic rocks, containing abundant plagioclase and variable K-feldspar, are common in the study area.

Robertson (1986) found that aplitic rhyolite intrusive rocks related to W-Be-F skarn at Iron Mountain were depleted in Eu and Sr. He concluded that this was due to feldspar fractionation and that the intrusive rhyolitic rocks were highly differentiated. Davis (1986) found similar geochemical evidence for possible feldspar fractionation in porphyritic rhyolite intrusive rocks near Iron Mountain. Relatively low Sr values and negative Eu anomalies in fluorites from W-Be skarn at Iron Mountain suggest precipitation from highly evolved hydrothermal solutions.

Relatively high Sr content and positive Eu anomalies in fluorites from Au-Ag vein and "barren" veins from the "Chavez" prospects may be due to more intense wallrock alteration of feldspar. Hydrothermal alteration (silicification, kaolinitization, and alunitization) is common in and around rhyolite flow-domes complexes in the Chloride Au-Ag vein district (Harrison, 1986). Wallrock in the Black Range Au-Ag vein areas and at the "Chavez" site commonly is composed of locally plagioclase-rich volcanics which range up to several hundred feet thick. Wallrock alteration of feldspar was believed by Grappin and others (1979) to be the cause of positive Eu anomalies in fluorite at Rossignol, France. Möller and Morteani (1983) state that positive Eu anomalies in Ca minerals are mostly the result of decomposition of feldspar.

It is possible that most "barren" vein fluorites in the center of the Sr versus (Eu/Eu*)n diagram (Figure 17) may reflect varying degrees of wallrock feldspar alteration.

The Ba-Pb vein fluorites in the Caballo Mountains exhibit similarities to W-Be skarn fluorites in the behavior of Sr and Eu. This association is problematic. No igneous rocks crop out in the vicinity of veins in the Caballo Mountains. One could speculate that the veins may be related to a highly differentiated igneous system at depth. However, the Ba-Pb veins are rather distal from the rest of the sample sites and are separated from them by a major gravel-filled graben related to the Rio Grande rift. Thus, it is possible that the Ba-Pb veins are related to a separate fluorine-rich province different from the Sierra Cuchillo/Black Range fluorine-rich province. If

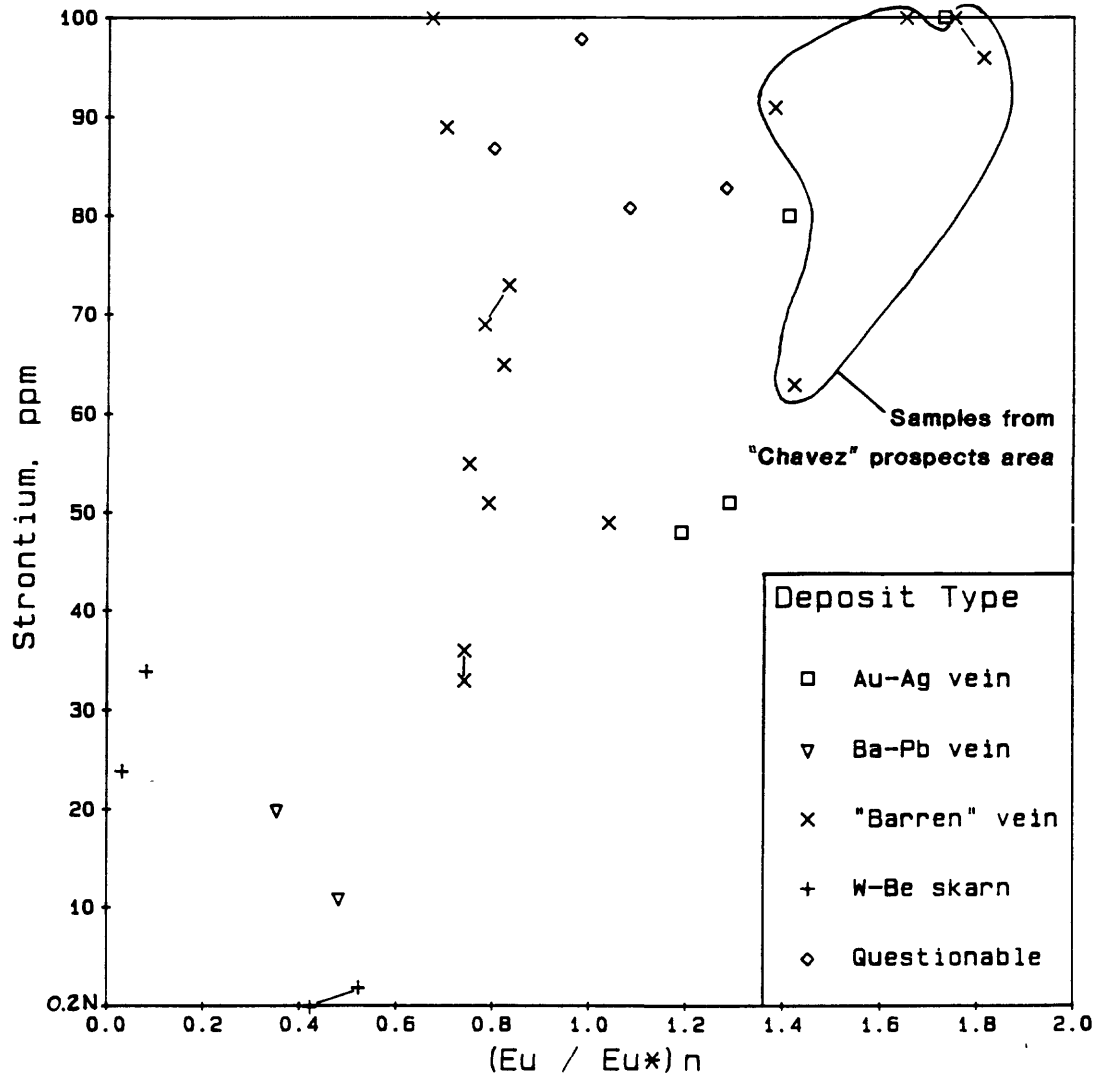

Figure 17.--Plot of Sr versus europium behavior, (Eu/Eu*)n. Line segments link sample site duplicates. 0.2N = not detected at 0.2 ppm. Samples analyzed by ICP-AES (Sr) and ICP-MS (Eu).

this were the case, differences in trace element behavior in fluorite from the two provinces could arise.

Interestingly, an igneous connection for the Caballo Mountain Ba-Pb veins also was concluded recently by North and Tuff (1986). They undertook a fluid inclusion and trace element study of fluorites from several areas in south-central New Mexico. Initially, they believed that fluorites from Ba-Pb veins in the Caballo Mountains were of a sedimentary-hydrothermal origin. However, the fluorites had quite low salinities, a characteristic of the igneous-related fluorites they studied. Thus, North and Tuff (1986) concluded that Ba-Pb veins in the Caballo Mountains appear to be igneous-related, although the area shows no evidence of igneous activity at the surface.

Other Trace Elements

Relatively high contents of Be, Ti, U, and Y were found in fluorites from W-Be skarn and from "barren" veins in the "Hanson" prospects area. Robertson (1986) concluded that W-Be skarn was related to aplitic rhyolite intrusives. Davis (1986) found skarn developed at Reilly Peak, a couple of miles south of Iron Mountain, along contacts of Paleozoic limestone with andesite and porphyritic rhyolite dikes. "Barren" veins at the Hanson prospects intrude Paleozoic limestones, but porphyritic and aplitic felsic dikes were observed in drainages below the prospects. Approximately 2 miles south of "Hanson" prospects, "barren" veins were observed cutting across mineralized skarn at a high angle. It is possible that the high contents of these 4 elements in fluorites from the "Hanson" prospects area may be due to younger "barren" veins cutting through concealed mineralized skarn and remobilizing these elements. With this model in mind, the "Hanson" prospects area was revisited during a late stage of this study. A prospected pipe-like patch of skarn about 12 ft in diameter was found about 1/4 mile north of and essentially on strike with the sampled "barren" veins, supporting the model.

Fluorites from "Questionable" Deposits

Trace and REE from fluorite samples of "questionable" deposit type generally were found to behave similarly to those of "barren" vein fluorites. In most cases, this relationship was suspected prior to chemical analysis. To illustrate this point, two fluorite samples (SC051R1 and SC051R4) were collected from dump material at the Vindicator Mine, an adit in mineralized skarn developed along a nearly horizontal contact of monzonite and overlying limestone. The two samples were considered "questionable" because of their silica-calcite gangue mineralogy, which resembled "barren" veins and was unlike the calc-silicate minerals typical of most of the dump material. A near-vertical thin "barren" vein was found in outcrop approximately 100 ft stratigraphically above the skarn contact in unaltered limestone. A projection of this vein down through the skarn zone coincided roughly with a thin silica-calcite-fluorite vein in the mine adit cutting skarn at a high angle. Generally, these two "questionable" samples exhibited trace element behavior similar to that of the "barren" vein fluorite sample (SC052R1).

Endoskarn/Exoskarn Fluorites at Iron Mountain

Extreme variation was found in REE concentrations in fluorites from W-Be endoskarn and exoskarn at Iron Mountain. Chondrite-normalized REE plots ranged from nearly 500 times chondrite abundances in endoskarn to less than

chondrite abundances in exoskarn (Figure 18). Plots for all other fluorite samples analyzed fell between these two extremes. Variation in cerium behavior ([Ce/Ce*]n) and in slope ([La/Yb]n) also were found for endoskarn and exoskarn samples (Table 9). Endoskarn and exoskarn fluorite samples were most similar in behavior of Eu ([Eu/Eu*]n).

Figure 18 also shows chondrite-normalized REE plots for aplitic rhyolite and porphyritic rhyolite intrusives from the Iron Mountain district. Rare earth element analyses for two aplitic rhyolite intrusives were given by Robertson (1986). Rare earth element analyses for 5 porphyritic rhyolite intrusive samples were given by Robertson (1986, 2 samples) and Davis (1986, 3 samples). Analyses for intrusive samples were averaged in constructing chondrite-normalized plots shown in Figure 18.

Robertson (1986) concluded from field relations and geochemical data that the aplitic rhyolites are associated with W-Be-F skarn at Iron Mountain. Although Robertson (1986) determined just 6 REE, his averaged aplitic rhyolite pattern is still quite similar to the pattern for endoskarn fluorite from Iron Mountain: both patterns overall are fairly flat, exhibit strong negative Eu anomalies, a slight depletion between Dy and Ho, and slight heavy REE enrichment. In contrast to endoskarn fluorite, porphyritic rhyolite samples are more enriched in light REE, have less intense negative Eu anomalies, and exhibit flat heavy REE patterns. Thus, endoskarn fluorite patterns more closely approximate aplitic rhyolite patterns, lending support to Robertson's (1986) conclusion.

Endoskarn fluorite is much richer in REE than aplitic rhyolite (Figure 18). Robertson (1986) reports that the aplitic rhyolite contains accessory apatite and fluorite, both of which can contain up to several weight percent REE (Clark, 1984). If these minerals were the major hosts for REE in the aplitic rhyolite, then dilution of REE concentration would be expected in analyzing the whole rock. Thus, differences in REE abundance between the aplitic rhyolite (about 100 times chondrite abundances) and endoskarn fluorite (nearly 500 times chondrite abundances) likely are due to dilution effects in analyzing the whole rock.

A chondrite-normalized REE plot for a typical limestone also is shown in Figure 18. Data for limestone is from Haskin and others (1966), averaged from analyses of 9 limestones. Overall, the pattern is fairly similar to that for averaged exoskarn fluorite from Iron Mountain: both patterns exhibit negative slopes, slight negative Eu anomalies, and a positive hump in the middle REE. The two patterns differ in relative magnitude; exoskarn fluorite REE concentrations generally are about 0.5 times chondrite abundances, while average limestone reported in Haskin and others (1966) has concentrations in the range of about 10 times chondrite abundances. However, carbonate rocks with REE concentrations below chondrite abundances have been reported elsewhere, such as in Hein and Schneider (1983). Möller and Morteani (1983) show typical "fluorites from limestone" with REE concentrations of about 0.5 times chondrite abundances. The "fluorites from limestone" exhibit chondrite-normalized REE patterns similar to the Iron Mountain exoskarn fluorite pattern. Clearly, REE analyses of limestone at Iron Mountain are needed to elucidate this problem.

Two points can be drawn from the above discussion. First, similarities in REE patterns between the mineralizing intrusive and endoskarn fluorite suggest a magmatic source for REE in endoskarn fluorite. Second, similarities in REE patterns between average limestone and exoskarn fluorite may reflect a limestone source for REE in exoskarn.

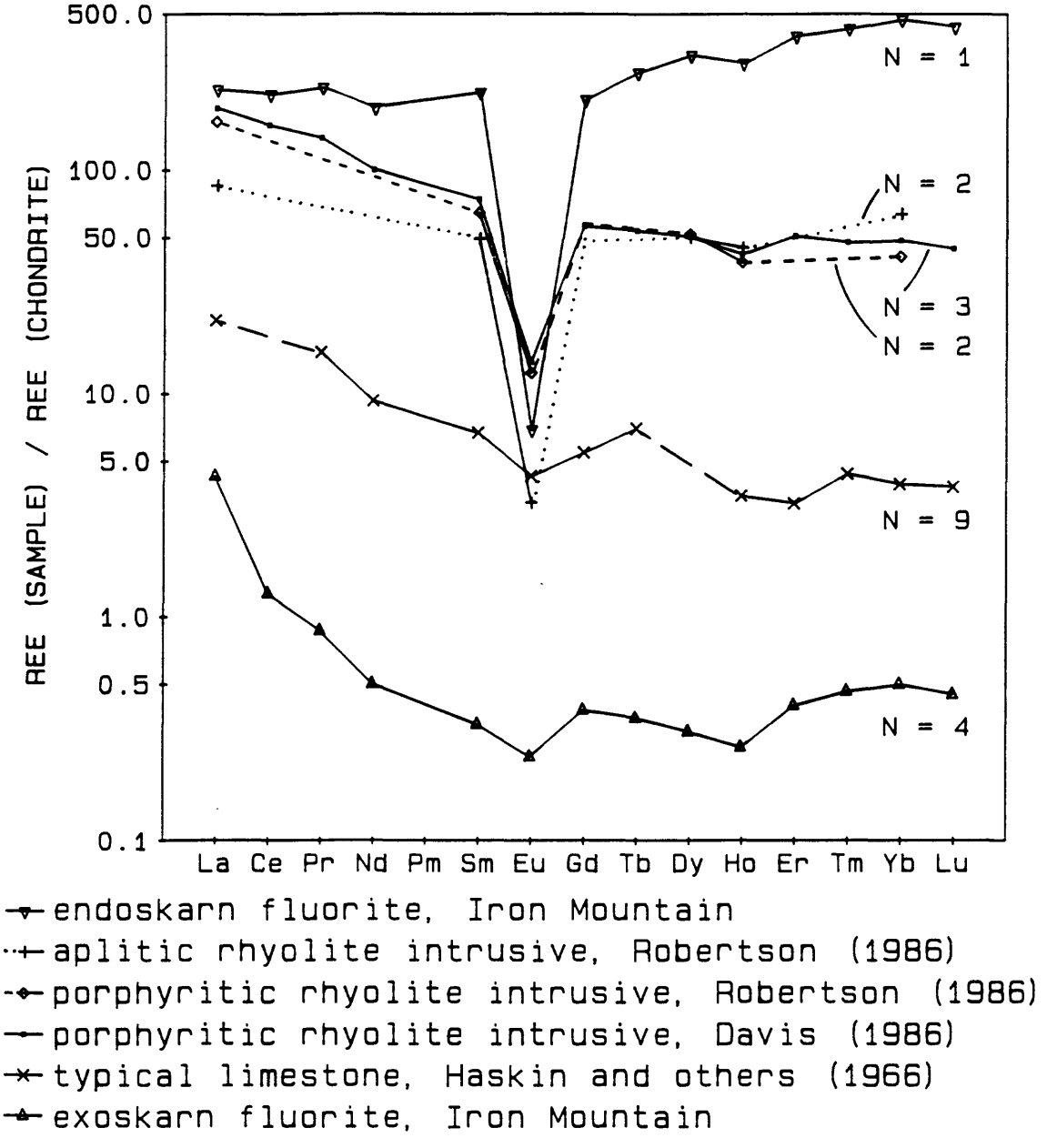

Figure 18.--Averaged chondrite-normalized REE plots for samples from Iron Mountain and vicinity, and from typical limestones. N indicates number of samples from which pattern is averaged.

The behavior of cerium, (Ce/Ce*)n, may support the latter conclusion. Exoskarn fluorite is low in Ce, relative to endoskarn fluorite (Table 9). Cerium content is low in seawater relative to other REE, possibly due to oxidation of Ce and subsequent adsorption to hydrous Mn oxide (Clark, 1984; Fleet, 1984). It seems logical that limestone precipitating from seawater with low Ce content also might have low Ce content. Thus, the more negative Ce anomalies in the exoskarn fluorite may reflect a limestone source for the REE.

Yttrium and Ti contents also are higher in endoskarn fluorite relative to exoskarn fluorite. The behavior of Y probably is related to the relative abundances of REE, being higher in endoskarn than in exoskarn fluorite. Titanium is more problematic. Robertson (1986) analyzed various mineralized rocks from Iron Mountain and found erratic Ti values ranging from 100 to 6400 ppm, suggesting irregular Ti distribution throughout the mineralized area. A simple model of limestone and magmatic sources for Ti in exoskarn and endoskarn fluorites, respectively, is unlikely.

The problematic behavior of REE and trace elements in fluorites from Iron Mountain probably reflect the complex nature of the mineralizing system there. Certainly, more detailed work involving mineral paragenetic studies and wallrock chemical analyses are needed to understand the processes responsible for the unusual element behavior discovered in this study.

Rare Earth Elements, Uranium, and Color of Fluorite

Fluorites from the study area were generally colorless or light to dark green (Appendix E). Purple fluorite was found locally. No association between color in fluorite and deposit type was found. Contents of REE and U were compared with color observed in fluorite. No relation with color was found in heavy REE (Gd, Tb, Dy, Ho, Er, Tm, Yb, and Lu) (Figure 19). However, light REE (La, Ce, Pr, and Nd) were found in relatively high concentration in all colored fluorites (Figure 20). Specific colors in fluorite were not found to be associated with any particular REE.

Low content of light REE was found in all but 2 colorless fluorites. One of the colorless fluorites (containing approximately 75 ppm combined light REE) was a sample collected from a prospect exposed to sunlight. All exposed fluorite was colorless at this site; however, colored fluorite was found in buried cobbles. Thus, color in the fluorite may have been bleached by sunlight (uV light?). In addition, sunlight-exposed fluorite would have been subject to fairly high summertime temperatures (110° F and higher) which may have bleached the fluorite colorless. In laboratory studies by Berman (1957) color was bleached from fluorite by heating, but at much higher temperatures. Whatever the cause of the bleaching, the sample still contains elevated light REE values.

The single colorless sample that contradicts the association of color and high light REE content is W-Be skarn sample SC005R, with approximately 425 ppm combined light REE. This sample, collected from a sunlight-exposed dump, contained the highest concentration of total REE (nearly 900 ppm) of any of the samples studied. However, no colored fluorite was found at sample site SC005.

The association of color in fluorite and light REE content found in this study contradicts a recent study on coloration in fluorite by Naldrett and others (1987). They found no relation between REE and color. Naldrett and others (1987) report that ionizing radiations from incorporated radioactive elements produce divalent REE ions which account for purple color in fluorite. In this study, U content in fluorite was found to be below 1 ppb; no relation was found between purple fluorite and U content (Figure 21).

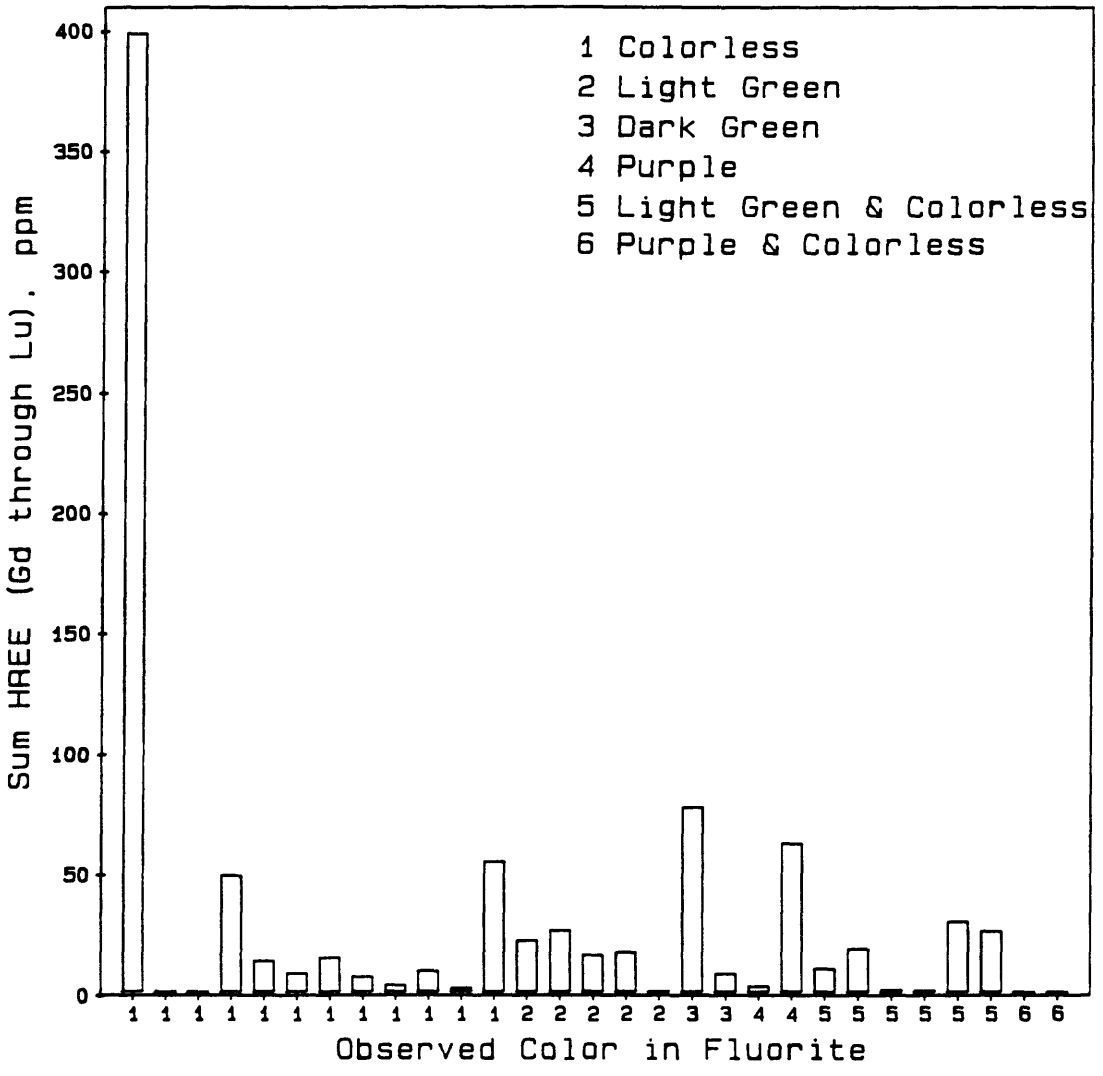

Figure 19.--Sum of heavy REE sorted by observed color in fluorite.

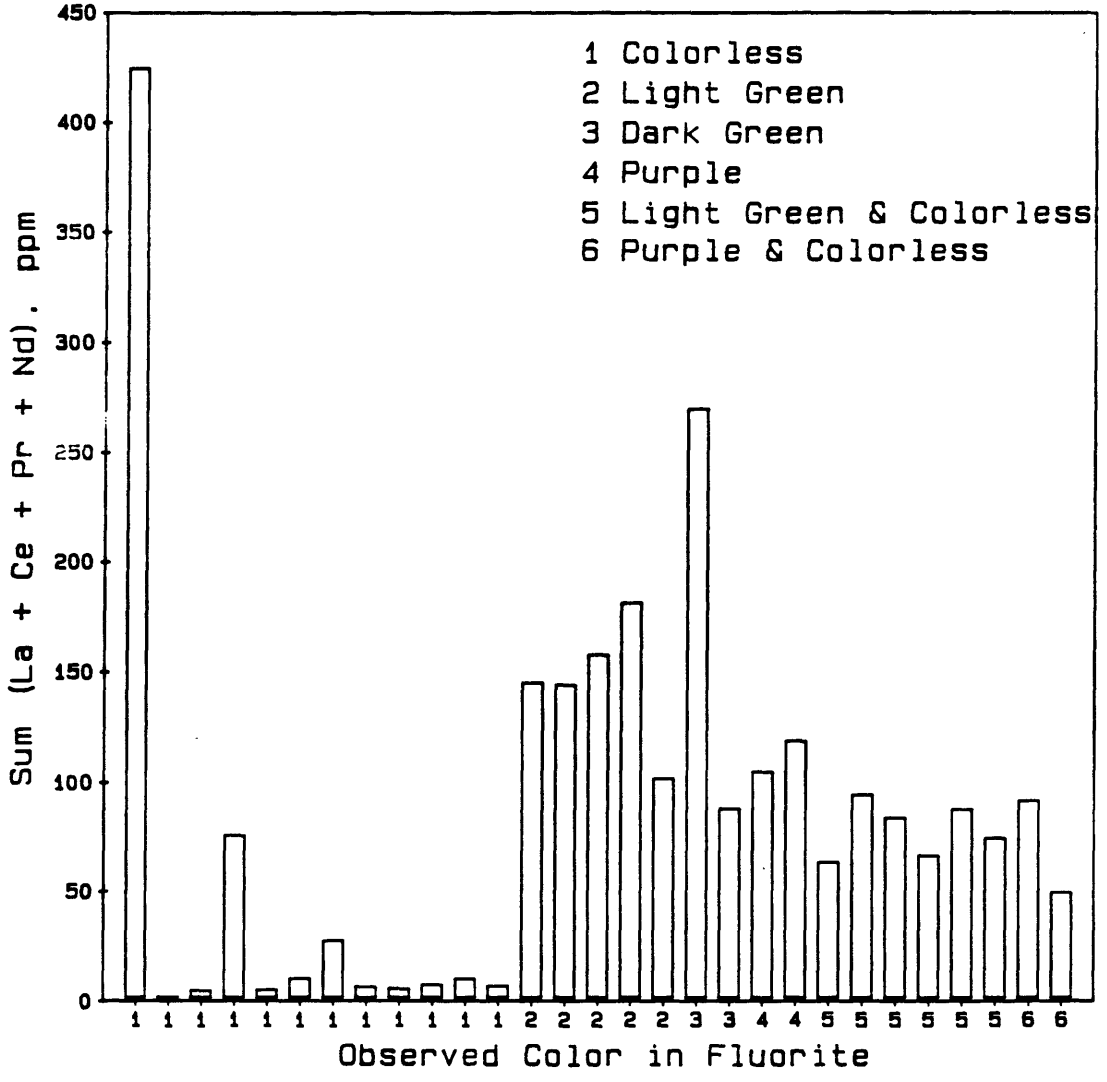

Figure 20.--Sum of light REE sorted by observed color in fluorite.

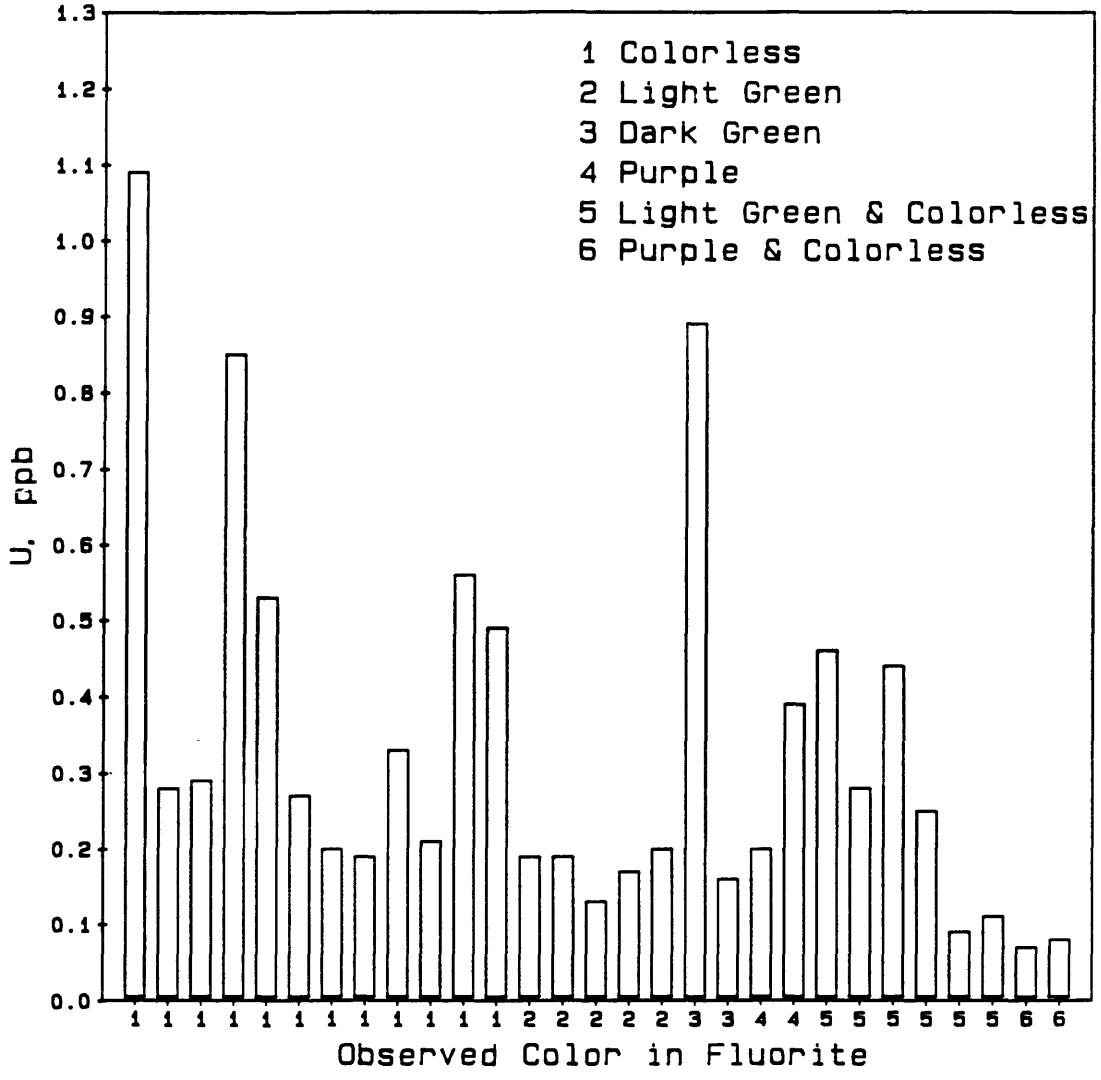

Figure 21.--Uranium concentration sorted by observed color in fluorite.

Green was by far the most common color of the colored fluorites. Bill and others (1967) and Bill and Calas (1978) found that divalent Sm was responsible for green color in fluorite. In this study, Sm (valancy undetermined) and green color show a weak association, although all green fluorites are not rich in Sm (Figure 22). Numerous colorless fluorites also have relatively high Sm content; however, the possiblity of bleaching by sunlight exists for these samples.

Fluorescence in fluorite was compared against REE and trace elements, but no strong relationships were found. Dull purple was by far the most common fluorescing color. A subtle association was found between higher total REE content and fluorescence other than dull purple. However, there were several exceptions to this association. The two samples containing the highest REE content (SC005R and SC045R) were unique in fluorescing bright orange. Phosphorescence was not observed in any samples.

Quantitative versus Semiquantitative Analytical Methods

Quantitative ICP-MS was used for REE analyses. Trace elements were determined by both quantitatitve (ICP-AES) and semiquantitative (SES) methods. This section addresses whether the more cost-efficient expedient semiquantitative method alone could have successfully differentiated the different deposit types.

Quantitative analyses of fluorite samples by ICP-AES revealed that the following trace elements were most useful in differentiating deposit types: Ba, Be, Sr, Ti, U, and Y. Rare earth elements determined by ICP-MS revealed that the behavior of Eu, (Eu/Eu*)n, was the most useful parameter for differentiating deposit types. Behavior of these elements in fluorite from the different deposit types is summarized in Table 14. Fluorites from Au-Ag veins had higher Sr content and exhibited positive Eu anomalies, while fluorites from W-Be skarn and Ba-Pb veins contained less Sr and exhibited negative Eu anomalies. Fluorites from W-Be skarn commonly contained higher Be, Ti, U, and Y compared to Au-Ag vein fluorites. "Barren" vein fluorites exhibited variable behavior for the above elements. Within "barren" vein fluorites, fluorites from the "Hanson" prospects area exhibited strong similarities in trace element behavior to W-Be skarn fluorites, while fluorites from the "Chavez" prospects were more similar to Au-Ag vein fluorites. Fluorites from Ba-Pb veins were higher in Ba and Pb compared to other fluorites. In general, fluorite from "questionable" deposit types behaved similarly to "barren" vein fluorites.

Europium and U were not determined by SES, so a comparison using these elements cannot be made. Strontium was determined, but the very narrow range in concentration (only 3 step intervals) limited its effectiveness. A weak trend in semiquantitative Sr analyses (Figure 14) was found to parallel the trend described above found in quantitative Sr analyses. However, this trend likely would not have been discerned using semiquantitative data alone. Titanium analyses by SES (Figure 15) were not found to correlate with deposit type, while Ti analyses by ICP-AES (Figure 9) were moderately useful.

Beryllium determined by SES closely paralleled the behavior of Be determined by ICP-AES. Fluorites from "barren" veins at the "Hanson" prospects were highest, variable Be content was found in W-Be skarn and Ba-Pb vein fluorites, and low Be was found in fluorites from Au-Ag veins and "barren" veins from the "Chavez" prospects.

Yttrium determined by SES was found in highest concentrations in W-Be skarn and "barren" vein fluorites from the "Hanson" prospects, identical to

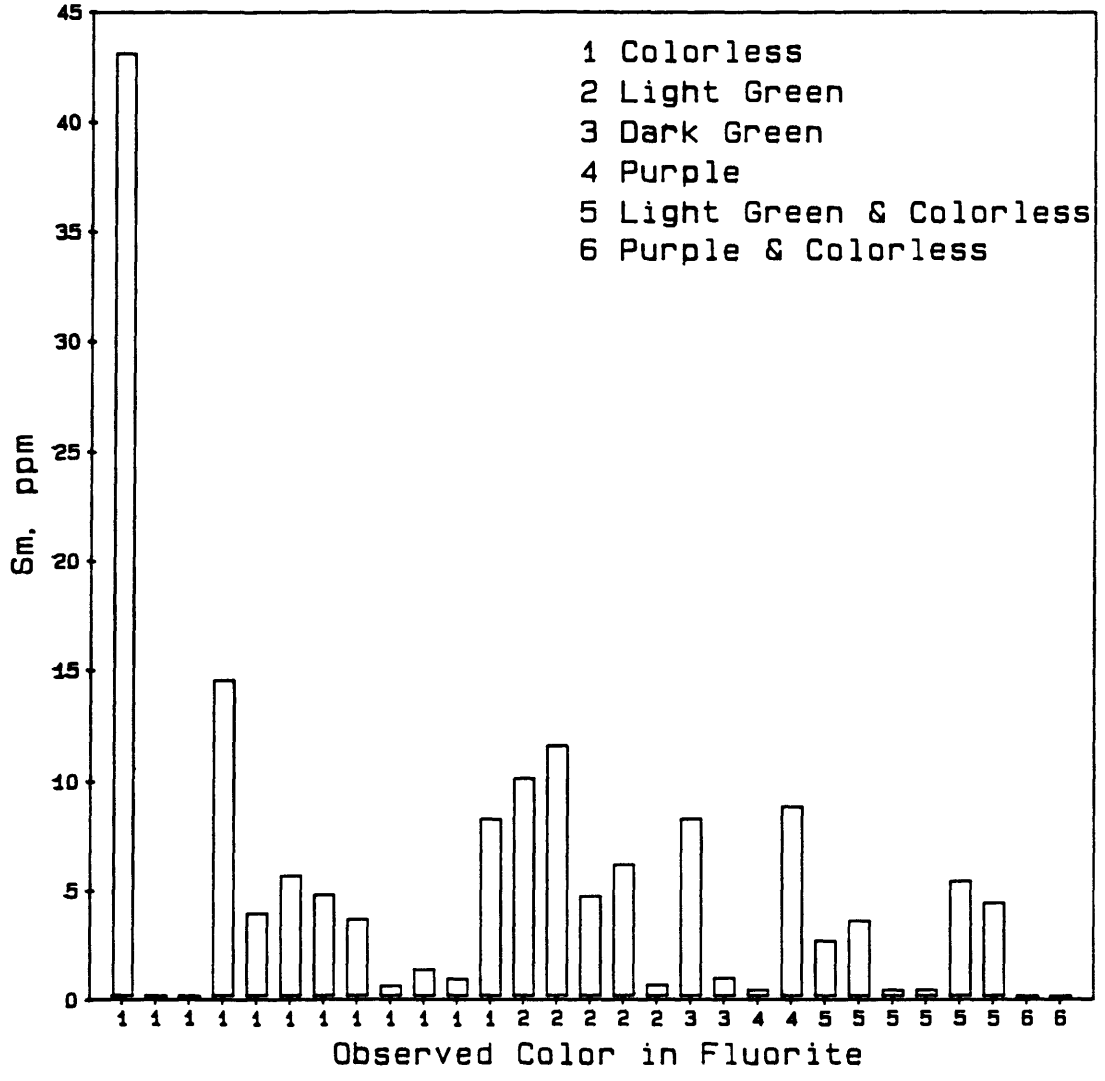

Figure 22.--Samarium concentration sorted by observed color in fluorite.

Table 14.--Summary of elements in fluorite found useful in differentiating the different deposit types. Upper case letters = quantitative analyses (ICP-MS, ICP-AES); lower case letters = semiquantitative analyses (SES). Relative abundance: H = high; L = low; N = not detected; D = rarely detected; (+) = positive Eu anomaly; (-) = negative Eu anomaly; V = variable (combination of H, L, N, D; + or -). Deposit type code: 1 = Au-Ag vein; 2 = Ba-Pb vein; 3 = "barren" vein; 4 = W-Be skarn; 5 = "questionable" deposit type.

ELEMENT	DEPOSIT TYPE						
	1	2	3a Other areas	3b "Chavez" prospects area	3c "Hanson" prospects area	4	5
Eu[1]	(+)	(-)	V	(+)	(-)	(-)	V
Sr[2]	H/v	L/v	H/v	H/v	H/v	L/v	H/v
Be	L/l	V/v	V/l	L/l	H/h	V/v	L/l
Ba[3]	L/v	H/h	L/n	L/n	L/d	L/d	L/d
Pb[4]	N/d	D/h	D/n	D/n	D/d	D/d	N/v
Ti	L/v	V/v	V/v	L/v	H/v	V/v	L/v
U[1]	L	L	V	L	H	V	V
Y	L/l	V/l	V/l	L/l	H/h	V/v	V/l
La	V/h	N/l	V/h	V/h	V/h	V/v	V/v
Mg[5]	V/d	V/d	V/d	V/d	V/h	V/h	V/d
Mn[6]	N/n	N/n	N/n	N/n	N/d	N/h	N/n

Footnotes:

[1]Not determined by SES.
[2]Sr analyzed by SES has low variablity (3 step intervals).
[3]Variable Ba in Au-Ag vein samples analyzed by SES is likely due to impure samples.
[4]Variable Pb in "questionable" deposit type samples analyzed by SES is likely due to impure samples.
[5]High variablility in sample site and analytical duplicates analyzed by ICP-AES limits usefulness of Mg.
[6]High Mn in W-Be skarn samples may be due to trace MnO_2 contamination.

the highest Y values determined by ICP-AES. Similarly, Ba determined by both SES and ICP-AES was found in highest concentrations in fluorites from Ba-Pb veins.

Detectable Mn and unqualified Mg determined by SES were found only in fluorites from W-Be skarn and "barren" veins from the "Hanson" prospects. Manganese was not detected by ICP-AES, which has a higher detection limit than SES (80 ppm and 10 ppm, respectively). Magnesium determined by ICP-AES, hindered by large analytical variation, was not found to correlate with deposit type.

Lanthanum determined by SES was moderately effective, differentiating fluorites from Au-Ag veins and "barren" veins (high) from Ba-Pb veins (low). Fluorites from W-Be skarn exhibited variable behavior.

To summarize the above information, analysis of fluorite samples by SES alone would have successfully differentiated Ba-Pb vein fluorites and W-Be fluorites from the rest of the samples. The SES method would not have been as successful in differentiating fluorites of Au-Ag vein, "barren" vein, and "questionable" affinities. The association between fluorites from "barren" veins at the "Hanson" prospects and those from W-Be skarn would have been evident. However, the potentially more significant association between fluorites from "barren" veins at the "Chavez" prospects and those from Au-Ag veins would not have been discovered.

Fluorite Samples from Stream Sediment Concentrates

Fluorite samples were collected from stream sediment concentrates from drainages below sampled fluorite-bearing outcrop. This section discusses problems encountered with fluorites from concentrates which generally were not encountered with fluorites from rocks. The 26 fluorites from concentrates analyzed by SES are discussed here.

Higher sample site and analytical variabilities were found for fluorites from concentrates (Table 7). The higher variablity probably is due to the fact that fluorite grains in the sample probably are not derived from a single source upstream, as are the rock samples.

Separation of clean fluorite grains from the concentrates was very time-consuming and apparently not entirely successful. Barium best illustrates this problem, being detected much more frequently in fluorite from concentrates than from rocks. This probably was due to grain misidentification. Fluorite and barite in concentrates commonly were anhedral and colorless. Occasionally cleavage planes were not discernable, leading to misidentification of barite grains as fluorite grains. In most cases, misidentified barite grains were removed during the scan of the samples with a petrographic microscope. However, more frequent detection of Ba in fluorite from concentrates suggests that a trace of barite remained in the sample. Perhaps trace barite was adhered to the fluorite grains.

Lead exhibited higher overall variablity in fluorites from concentrates than in fluorites from rocks. The higher variability was largely due to 3 fluorite samples with values 1 to 2 orders of magnitude above the rest. "Clay" was observed in cleavage recesses in a few samples, including the 3 samples discussed here. Most, but probably not all, "clay" was removed prior to analysis during the ultrasonic cleaning process. The "clay" was possibly a supergene Pb mineral, as the 3 samples were collected from drainages with known galena deposits upstream of the sample sites. One of the high Pb samples also contained high W and Mo, which possibly resided in the "clay."

The above problems were largely avoided with fluorite samples collected from rock. A major reason for this was the relative ease of fluorite identification in rock containing relatively large fluorite crystals which had undergone minimal mechanical weathering. Secondly, fluorite grains from rock were not acted upon by hydromorphic processes, as were grains in the stream sediments.

POTENTIAL MINERAL RESOURCES IN THE STUDY AREA

Results from fluorite analyses in this study indicate 2 areas in which concealed deposits may exist. These areas include "barren" veins at the "Hanson" prospects and the "Chavez" prospects areas.

"Hanson" Prospects Area

The "Hanson" prospects area contains numerous quartz-calcite-fluorite veins oriented sub-parallel to range front faults in the Sierra Cuchillo. These veins generally have been prospected only for fluorspar. However, fluorite from the veins exhibit trace element content very similar to, but commonly higher than fluorites from the Iron Mountain W-Be skarn. Total Be content in fluorites from throughout the study area was highest in fluorites from the "Hanson" prospects area, even higher than Be in fluorites collected from an area of high-grade W-Be skarn at Iron Mountain.

The veins at the "Hanson" prospects area are hosted in Paleozoic limestone. Porphyritic and aplitic felsic dikes were observed below the "Hanson" prospects in a drainage which cuts through the limestone. As demonstrated in this study and in studies by Robertson (1986) and Davis (1986) intrusives of similar composition are likely responsible for W-Be skarn in the vicinity of Iron Mountain. "Barren" quartz-calcite-fluorite veins found throughout the Sierra Cuchillo probably are much younger than the skarn deposits (Allen Heyl, U. S. Geological Survey, personal communication, 1987).

It is possible that "barren" veins at the "Hanson" prospects area have cut through underlying Be-bearing skarn, remobilizing certain elements such as Be, Ti, U, and Y. An isolated pipe of skarn near the "Hanson" prospects area suggests that any concealed skarn probably is shallow.

"Chavez" Prospects Area

"Barren" vein fluorites from the "Chavez" prospects area east of the Sierra Cuchillo appear to have been prospected only for fluorspar. These fluorites exhibit strong similarities in trace and REE behavior to Au-Ag vein fluorites of the Chloride mining district in the Black Range.

The steeply dipping Au-Ag veins in the Chloride mining district are commonly hosted in mid-Tertiary intermediate volcanic and volcaniclastic rocks and are spatially associated with rhyolite flow-dome complexes. The epithermal vein deposits appear to have formed from hydrothermal convection cells generated by intrusion of rhyolitic magma associated with the flow-dome complexes (Harrison, 1986). Some veins are found in radial and tangential fractures produced during arching of country rocks by the flow-dome complexes. Higher grade mineral deposits commonly are associated with the exotic limestone blocks, which behaved brittlely during intrusion of the domes and thus provided structurally favorable sites for open-space filling.

An isolated rhyolite flow-dome complex was mapped a few miles to the southeast of the "Chavez" prospects (Allen Heyl, U.S. Geological Survey,

unpub. mapping). The veins in the "Chavez" prospects area are steeply dipping, arranged in a sub-parallel fashion, and appear to be oriented radially to the rhyolite flow-dome center. Bedrock at the Chavez site includes a thick sequence of intermediate to rhyolitic volcanic and volcaniclastic rocks, and small exposures of Paleozoic limestone. The veins at the "Chavez" prospects area exhibit a vertical chemical zonation, reflected by mineral assemblages within the vein. Over a vertical distance of about 200 ft, banded calcite is predominant in the highest vein exposures; druzy quartz, calcite, and fluorite are found in vuggy intermediate exposures; and massive fluorite is predominant in the lowest exposures.

It is possible that quartz-calcite-fluorite veins in the "Chavez" prospects area are related to the nearby rhyolite flow-dome complex. If this is the case, then the area may contain concealed precious metal deposits as do similar veins in the Chloride mining district to the west.

CONCLUSIONS

Several conclusions can be drawn from this study:

(1) Fluorites from four different deposit types were distinguished on the basis of their trace and REE contents. The differences are summarized below.

(a) Au-Ag vein fluorites:
- positive Eu anomalies
- high Sr content
- low Be, Ba, Ti, U, Y content.

(b) Ba-Pb vein fluorites:
- negative Eu anomalies
- high Ba, Pb content
- low Sr, U content.

(c) W-Be skarn fluorites:
- negative Eu anomalies
- high Be, Ti, U, Y, Mn, Mg content
- low Sr, Ba content.

(d) "Barren" vein fluorites:
- variable Eu anomalies
- high Sr content
- variable Be, Ti, U, Y, La, Mg
- low Ba content.

(2) Trace and REE in fluorites collected from "questionable" deposit types were most similar to those of "barren" vein fluorites. Fluorites of "questionable" origin are most likely derived from "barren" veins.

(3) "Barren" vein fluorites from the "Hanson" prospects area were similar in REE and trace element behavior to W-Be skarn fluorites at Iron Mountain. Geochemical similarities in the fluorites and geological similarities between the two areas are favorable for shallow concealed mineralized skarn through which the younger "barren" veins have cut.

(4) "Barren" vein fluorites from the "Chavez" prospects area were similar in REE and trace element behavior to Au-Ag vein fluorites in the Black Range. This, coupled with the overall geologic setting at the "Chavez" prospects area make it favorable for precious metal deposits similar to those in the Black Range.

(5) Trace and REE similarities were found in fluorites from Ba-Pb veins in the Caballo Mountains and from W-Be skarn at Iron Mountain. These similarities may indicate a highly differentiated igneous source for the Ba-Pb veins.

(6) The variable behavior of Eu and Sr in the fluorites studied may reflect varying degrees of wallrock feldspar alteration.

(7) Color in fluorite shows a positive correlation with light REE enrichment (compared to chondrites). The following REE correlate most strongly with color in fluorite: La, Ce, Pr, and Nd. Relatively high content of these REE are found in dark green, light green, and purple fluorites. Colorless fluorites generally contain less light REE. Colored fluorites which have been bleached colorless by sunlight exposure still contain relatively high amounts of light REE. Samarium was weakly correlated with green fluorite. No correlation was found between purple fluorite and U content.
(8) Fluorites collected from stream sediment heavy-mineral concentrates generally exhibited higher variability for certain elements than fluorites collected from rocks. Also, certain elements were detected more frequently in fluorites from concentrates than in fluorites from rocks. These problems probably are caused by trace contaminant minerals coating the fluorite grains or residing in cleavage recesses, and to a lesser extent by anhedral fluorite grain misidentification.
(9) Semiquantitative emission spectrographic analysis alone would have differentiated Ba-Pb vein fluorites and W-Be fluorites from the rest of the samples. Fluorites from Au-Ag veins, "barren" veins, and "questionable" deposit types would not have been differentiated. The W-Be skarn/"Hanson" prospects association would have been evident, but the Au-Ag vein/"Chavez" vein connection would not have been discernable.
(10) Rare earth element patterns in fluorites from endoskarn at Iron Mountain are most similar to those of aplitic rhyolite intrusives.
(11) Variations in REE in fluorites from endoskarn and exoskarn at Iron Mountain may reflect a magmatic source for REE in endoskarn and a sedimentary source for REE in exoskarn. More work is needed to document this relationship.
(12) Fluorite mineral separates geochemistry delineated potential concealed mineral deposits. These results indicate that fluorite mineral separates geochemistry could be a useful tool elsewhere in mineral exploration for concealed deposits.

SUGGESTIONS FOR FURTHER STUDY

This study was successful in differentiating fluorites from several mineral deposit types and in delineating two areas with potential for concealed mineral deposits. Numerous questions were raised during the study, and further work is warranted.

This study was conducted largely without regard to mineral paragenesis within specific deposits. Paragenetic studies at individual deposits would help to elucidate problems such as the large chemical variation found in skarn fluorites at Iron Mountain. Fluid inclusion work on fluorite or associated minerals, with good paragenetic control, might help identify fluid chemistry and physical conditions during mineralization.

Isotopic work may help to reveal sources of fluids. The relatively high Sr values in fluorite suggest that Sr might be a viable isotope for this work. Similar isotopic compositions between fluorites from Au-Ag veins and the "Chavez" veins would solidify the tie between these deposits suggested in this study.

Studies of REE in hydrothermal systems are sparse and all are relatively recent. The lack of published work on this topic hinders interpretations of REE behavior in hydrothermal minerals such as fluorite. Europium behavior in hydrothermal systems has been investigated most commonly, while published research on Ce behavior in hydrothermal systems is almost nonexistent. These two REE commonly exhibit valency states other than 3+, and they may provide clues to oxidation/reduction conditions in hydrothermal systems.

There is abundant literature on trace and REE in fluorite. Most of the research has been centered around crystal chemistry, metallurgy, and laser research. Little has been applied to mineral exploration problems. There is also abundant literature on associations of trace and REE with color in fluorite. However, results have not been conclusive, and further work is needed to better understand this relationship.

This study was conducted in an area with a unique geologic time/space setting. Several types of fluorite deposits are found within one large fluorine-rich province, and mineralization occurred within a rather narrow time frame. Similar studies need to be conducted to test whether this method will work elsewhere.

REFERENCES

Abitz, R. J., 1984, Volcanic geology and geochemistry of the northeastern Black Range Primitive Area and vicinity, Sierra County, New Mexico: Albuquerque, N. M., University of New Mexico, M. S. thesis, 121 p.

Al-Hashimi, A. R. K. and Brownlow, A. H., 1970, Copper content of biotites from the Boulder Batholith, Montana: Ecomonic Geology, v. 65, p. 985-992.

Allen, R. D., 1952, Variations in chemical and physical properties of fluorite: American Mineralogist, v. 37, p. 910-930.

Alminas, H. V., Watts, K. C., and Siems, D. F., 1972a, Lead distribution in the Winston and Chise quadrangles and the west part of the Priest Tank quadrangle, Sierra County, New Mexico: U. S. Geological Survey Misc. Field Studies Map MF 398.

_____1972b, Molybdenum distribution in the Winston and Chise quadrangles and the west part of the Priest Tank quadrangle, Sierra County, New Mexico: U. S. Geological Survey Misc. Field Studies Map MF 399.

_____1972c, Silver and gold distribution in the Winston and Chise quadrangles and the west part of the Priest Tank quadrangle, Sierra County, New Mexico: U. S. Geological Survey Misc. Field Studies Map MF 400.

_____1972d, Tungsten distribution in the Winston and Chise quadrangles and the west part of the Priest Tank quadrangle, Sierra County, New Mexico: U. S. Geological Survey Misc. Field Studies Map MF 401.

_____1972e, Fluorite distribution in the Winston and Chise quadrangles and the west part of the Priest Tank quadrangle, Sierra County, New Mexico: U. S. Geological Survey Misc. Field Studies Map MF 402.

Alminas, H. V., Watts, K. C., Griffitts, W. R., Siems, D. L., Kraxberger, V. E., and Curry, K. J., 1975a, Map showing anomalous distribution of tungsten, fluorite, and silver in stream-sediment concentrates from the Sierra Cuchillo-Animas uplifts and adjacent areas, southwestern New Mexico: U. S. Geological Survey Misc. Investigation Series Map I-880.

_____1975b, Map showing anomalous distribution of lead, tin, and bismuth in stream-sediment concentrates from the Sierra Cuchillo-Animas uplifts and adjacent areas, southwestern New Mexico: U. S. Geological Survey Misc. Investigation Series Map I-881.

_____1975c, Map showing anomalous distribution of molybdenum, copper, and zinc in stream-sediment concentrates from the Sierra Cuchillo-Animas uplifts and adjacent areas, southwestern New Mexico: U. S. Geological Survey Misc. Investigation Series Map I-882.

Auger, P. R., 1941, Zoning and district variations of the minor elements in pyrite of Canadian gold deposits: Economic Geology, v. 36, p. 401-423.

Baldridge, W. S., Olsen, K. H., and Callender, J. F., 1984, Rio Grande rift: problems and perspectives: New Mexico Geological Society, Guidebook, 35th Field Conference, Rio Grande rift, northern New Mexico, p. 1-12.

Berman, R., 1957, Some physical properties of naturally irradiated fluorite: American Mineralogist, v. 42, p. 191-203.
Bill, H., Sierro, J., and Lacroix, R., 1967, Origin of coloration in some fluorites: American Mineralogist, v. 52, p. 1003-1008.
Bill, H., and Calas, G., 1978, Color centers, associated rare-earth ions and the origin of coloration in natural fluorites: Physics and Chemistry of Minerals, v. 3, p. 117-131.
Birk, R. H., 1980, The petrology, petrography, and geochemistry of the Black Jack breccia pipe, Silver Star Plutonic Complex, Skamania County, Washington: Western Washington University, M. S. thesis, 107 p.
Brown, C. E. and Ayuso, R. A., 1985, Significance of tourmaline-rich rocks in the Grenville Province of St. Lawrence County, New York: U. S. Geological Survey, Bulletin 1626-C, 33 p.
Chapin, C. E., 1979, Evolution of the Rio Grande rift--a summary: in Riecker, R. E. (editor), Rio Grande rift: tectonics and magmatism: Washington, D. C., American Geophysical Union, p. 1-5.
Chapin, C. E. and Seager, W. R., 1975, Evolution of the Rio Grande rift in the Socorro and Las Cruces areas: New Mexico Geological Society, Guidebook, 26th Field Conference, Guidebook of the Las Cruces country, p. 297-321.
Chapin, C. E., Siemers, W. T., and Osburn G. R.. 1975, Summary of radiometric ages of New Mexico rocks: New Mexico Bureau of Mines and Mineral Resources, Open-file Report 60.
Chapin, C. E., Jahns, R. H., Chamberlin, R. M., and Osburn, G. R., 1978, First-day road log from Socorro to Truth or Consequences via Magdalena and Winston: in Chapin, C.E., and Elston, W. E. (editors), Field guide to selected cauldrons and mining districts of the Datil-Mogollon volcanic field, New Mexico Geological Society, Special Publication 7. p. 1-31.
Church, S. E., 1981, Multi-element analysis of fifty-four geochemical reference samples using inductively coupled plasma-atomic emission spectrometry: Geostandards Newsletter, v. 5, no. 2, p 133-160.
Clark, A. M., 1984, Mineralogy of the rare earth elements: in Henderson, P. (ed.), Rare earth element geochemistry, Elsevier Science Publishers, Amsterdam, p. 33-61.
Clemons, R. E. and Osburn, G. R., 1986, Geology of the Truth or Consequences area: New Mexico Geological Society, Guidebook, 37th Field Conference, Truth or Consequences Region, p. 69-81.
Correa, B. P., 1980, Fluorine and lithophile element mineralization in the Black Range and Sierra Cuchillo, New Mexico: in Burt, D. M. and Sheridan, M. F. (eds.), Uranium mineralization in fluorine-enriched volcanic rocks: U. S. Department of Energy, Report GJBX-225-80, p. 459-494.
Cox, D. P., and Singer, D. A. (eds.), 1986, Mineral deposit models: U. S. Geological Survey, Bulletin 1693, 379 p.
Dane, C. H. and Bachman, G. O., 1965, Geologic map of New Mexico: U. S. Geological Survey, scale 1:500,000.
Darling, R., 1971, Prelimiary study of the distribution of minor and trace elements in biotite from quartz monzonite associated with contact-metasomatic tungsten-molybdenum-copper ore, California, U.S.A.: in Boyle, R. W. and McGerrigle, J. I. (eds.), Geochemical Exploration 1970, Can. Inst. Min. Metall., spec. vol. 11, p. 315-322.
Davis, L. L., 1986, Petrology and geochemistry of the intrusive rocks and associated iron-rich polymetallic skarn at Reilly Peak, New Mexico: Athens, Georgia, University of Georgia, M. S. thesis, 108 p.

Deer, W. A., Howie, R. A., and Zussman, J., 1962, Rock-forming minerals, non-silicates, v. 5, John Wiley and Sons, New York, p. 347-356.
deGrys, A., 1970, Copper and zinc in alluvial magnetites from central Ecuador: Economic Geology, v. 65, p. 714-717.
Ethier, V. G. and Campbell, F. A., 1977, Tourmaline concentrations in Proterozoic sediments of the southern Cordillera of Canada and their economic significance: Can. Jour. Earth Sci., v. 14, p. 2348-2363.
Feigl, Fritz, 1958, Spot tests in inorganic analysis (5th ed.): Amsterdam, Elsevier Publishing Co., 600 p.
Fleet, A. J., 1984, Aqueous and sedimentary geochemistry of the rare earth elements: in Henderson, P. (editor), Rare earth element geochemistry, Elsevier Science Publishers, Amsterdam, p. 343-373.
Fleischer, M., 1969, The lanthanide elements in fluorite: The Indian Mineralogist, v. 10, p. 36-39.
Ford, W. E., 1926, A textbook of mineralogy with an extended treatise on crystallography and physical mineralogy, John Wiley and Sons, New York, 720 p.
Freeman, P. S., and Harrison, R. W., 1984, Geology and development of the St. Cloud silver deposit, Sierra County, New Mexico: Arizona Geological Society Digest, v. 15, p. 231-233.
Ganzeev, A. A., and Sotskov, Y. P., 1976, Rare earth elements in fluorite of different genesis: Geokhimia, no. 3, p. 390-395.
Glines, P. G., 1982, Sierra County, the argonauts of yesterday: published by the author, P. O. Box 394, Hillsboro, New Mexico, 79 p.
Grappin, C., Treuil, M, Yamen, S., and Touray, J. C., 1979, Le spectre des terres rares de la fluorine en tant que marqueur des proprietes du milieu de depot et des interactions entre solutions mineralisantes et roches sources. Exemple pris dans le district de la Marche Occidentale, France: Mineralium Deposita, v. 14, p. 297-309.
Graybeal, F. T., 1973, Copper, manganese, and zinc in coexisting mafic minerals from Laramide intrusive rocks in Arizona: Economic Geology, v. 68, p. 785-798.
Greenwood, N. N., 1968, Ionic crystals, lattice defects, and nonstoichiometry, Butterworths and Co., London.
Grimes, D. J. and Marranzino, A. P., 1968, Direct-current arc and alternating-current spark emission spectrographic field methods for the semiquantitative analysis of geologic materials: U. S. Geological Survey, Circular 591, 6 p.
Hamil, B. M. and Nackowski, M. P., 1971, Trace element distribution in accessory magnetite from quartz monzonite intrusives and its relation to sulphide mineralization in the Basin and Range Province of Utah and Nevada-a preliminary report: in Boyle, R. W. and McGerrigle, J. I. (eds.), Geochemical Exploration 1970, Can. Inst. Min. Metall., spec. vol. 11, p. 331-333.
Hanson, G. N., 1978, The application of trace elements to the petrogenesis of igneous rocks of granitic composition: Earth and Planetary Science Letters, v. 38, p. 26-43.
Harley, G. T., 1934, The geology and ore deposits of Sierra County, New Mexico: New Mexico Bureau of Mines and Mineral Resources, Bulletin 10, 220 p.
Harrison, R. W., 1986, General geology of the Chloride mining district, Sierra and Catron Counties, New Mexico: New Mexico Geological Society, Guide-book, 37th Field Conference, Truth or Consequences Region, p. 265-272.

Haskin, L. A., Wildeman, T. R., Frey, F. A., Collins, K. A., Keedy, C. R., and Haskin, M. A, 1966, Rare earths in sediments: Journal of Geophysical Research, v. 71, p. 6091-6105.

Hawley, J. E. and Nichol, I., 1961, Trace elements in pyrite, pyrrhotite, and chalcopyrite of different ores: Economic Geology, v. 56, p. 467-487.

Hein, W. F., and Schneider, H. J., 1983, Fluorine anomalies accompanying the Alpine Pb-Zn deposits compared to the geochemistry of their fluorites: in Schneider, H. J. (ed.), Mineral deposits of the Alps and of the Alpine Epoch in Europe, Springer-Verlag, Berlin, p. 198-212.

Heinrich, E. W., 1962, Geochemical prospecting for beryl and columbite: Economic Geology, v. 57, p. 616-619.

Heyl, A. V., Maxwell, C. H., and Davis, L. L., 1983, Geology and mineral deposits of the Priest Tank quadrangle, Socorro County, New Mexico: U. S. Geological Survey, Misc. Field Studies Map 1665, scale 1:24,000.

Huskinson, E. J., 1975, Geology and fluorspar deposits of the Chise Fluorspar District, Sierra County, New Mexico: El Paso, Texas, University of Texas at El Paso, M. S. thesis, 74 p.

Jacobs, D. C. and Parry, W. T., 1976, A comparison of the geochemistry of biotite from some Basin and Range stocks: Economic Geology, v. 71, p. 1029-1035.

Jahns, R. H., 1944, Beryllium and tungsten deposits of the Iron Mountain district, Sierra and Socorro Counties, New Mexico: U. S. Geological Survey, Bulletin 945-C, p. 45-79.

_____1955, Geology of the Sierra Cuchillo, New Mexico: New Mexico Geological Society, Guidebook, 6th Field Conference, Guidebook of south-central New Mexico, p. 158-174.

Jahns, R. H., Kottlowski, F. E., and Kuellmer, F. J., 1955, Volcanic rocks of south-central New Mexico: New Mexico Geological Society, Guidebook, 6th Field Conference, Guidebook of south-central New Mexico, p. 92-95.

Jahns, R. H., McMillan, D. K., O'Brient, J. D., and Fisher, D. L., 1978, Geologic section in the Sierra Cuchillo and flanking areas, Sierra and Socorro Counties, New Mexico: in Chapin, C. E. and Elston, W. E. (eds.), Field guide to selected cauldrons and mining districts of the Datil-Mogollon volcanic field, New Mexico, New Mexico Geological Society, Special Publication 7, p. 131-138.

Johnson, A. E., 1972, Origin of Cyprus pyrite deposits: Int. Geol. Congress, 24th, Montreal, Sec. 4, p. 291-298.

Kelley, V. C., 1955a, Regional tectonics of south-central New Mexico: New Mexico Geological Society, Guidebook, 6th Field Conference, Guidebook of south-central New Mexico, p. 96-104.

_____1955b, Geologic map of the Sierra County region, New Mexico: New Mexico Geological Society, Guidebook, 6th Field Conference, Guidebook of south-central New Mexico, in pocket.

Kelley, V. C. and Silver, C., 1952, Geology of the Caballo Mountains: University of New Mexico publications in geology no. 4, University of New Mexico Press, Albuquerque, 286 p.

Kunkel, K. E., 1984, Temperature and precipitation summaries for selected New Mexico localities: New Mexico Department of Agriculture, 190 p.

Lamarre, A. L., 1974, Fluorite in jasperoid of the Salado Mountains, Sierra County, New Mexico: significance to metallogeny of the western United States: London, Canada, Univ. of Western Ontario, M. S. thesis, 134 p.

Lamarre, A. L., Perry, A. J., and Jonson, D. C., 1974, The Salado fluorspar deposit, Sierra County, New Mexico: Symposium on base metal and fluorspar districts of New Mexico, New Mexico Geological Society, May 22-25, 1974, abstract.

Lichte, F. E., Meier, A. L., and Crock, J. G., 1987, Determination of the rare earth elements in geological materials by inductively coupled plasma mass spectrometry: Analytical Chemistry, v.59, no.8, p.1150-1157.

Loftus-Hills, G. and Solomon, M., 1967, cobalt, nickel, and selenium in sulphides as indicators of ore genesis: Mineralium Deposita, v. 2, p. 228-242.

Lovering, T. G., Cooper, J. R., Drewes, H. and Cone, G. C., 1970, Copper in biotites from igneous rocks in southern Arizona as an ore indicator: U.S. Geological Survey, Professional Paper 700-B, p. 1-8.

Lovering, T. G., and Hedal, J. A., 1987, Trace elements in magnetic concentrates from stream sediments in southwestern New Mexico--a potential tool for reconnaissance geochemical exploration in arid lands: U. S. Geological Survey, Bulletin 1566, 31 p.

Lozinsky, R. P., 1986, Geology and Late Cenozoic history of the Elephant Butte area, Sierra County, New Mexico: New Mexico Bureau of Mines and Mineral Resources, Circular 187, 40 p.

Mantei, E. J. and Brownlow, A. H., 1967, Variation in gold content of minerals of the Marysville quartz diorite stock, Montana: Geochimica et Cosmochimica Acta, v. 31, p. 225-235.

Mason, D. R., 1978, Compositional variations in ferromagnesian minerals from porphyry copper-generating and barren intrusions of the Western Highlands, Papua, New Guinea: Economic Geology, v. 73, p. 878-890.

_____1979, Chemical variations in ferromagnesian minerals: a new exploration tool to distinguish between mineralized and barren stocks in porphyry copper provinces: in Theobald, P. K. and Watterson, J. R. (eds.), Geochemical Exploration 1978, proceedings of the 7th international geochemical exploration symposium, p. 243-249.

Maxwell, C. H. and Heyl, A. V., 1976, Preliminary geologic map of the Winston quadrangle, Sierra County, New Mexico: U. S. Geological Survey, Open-file Report 76-858, 1 sheet.

Maxwell, C. H. and Oakman, M. R., 1986, Geologic map and sections of the Cuchillo quadrangle, Sierra County, New Mexico: U. S. Geological Survey, Open-file Report 86-0279, scale 1:24,000.

McAnulty, W. N., 1978, Fluorspar in New Mexico: New Mexico Bureau of Mines and Mineral Resources, Memoir 34, 64 p.

Möller P., and Morteani, G., 1983, On the geochemical fractionation of rare earth elements during the formation of Ca-minerals and its application to problems of the genesis of ore deposits: in Augustuthis, S. S. (ed.), The significance of trace elements in solving petrogeneitc problems and controversies, Theophrastus Publications, Athens, p. 747-791.

Motooka, J. N. and Grimes, D. J., 1976, Analytical precision of one-sixth order semiquantitative spectrographic analyses: U.S. Geological Survey, Circular 738, 25 p.

Mueller, J. E., 1986 Climate of Truth or Consequences: New Mexico Geological Society, Guidebook, 37th Field Conference, Truth or Consequences Region, p. 4.

Naldrett, D. L., Lachaine, A., and Naldrett, S. N., 1987, Rare earth elements, thermal history and the colour of natural fluorites Canadian Journal of Earth Science, v. 24, no. 10, p. 2082-2088.

New Mexico Geological Society, 1986, Guidebook, 37th Field Conference, Truth or Consequences Region, 317 p.

North, R. M., and Tuff, M. A., 1986, Fluid-inclusion and trace-element analyses of some barite-fluorite deposits in south-central New Mexico: New Mexico Geological Society, Guidebook, 37th Field Conference, Truth or Consequences Region, p. 301-306.

Palache, C., Berman, H., and Frondel, C., 1951, Dana's system of mineralogy, v. 2, 7th ed., John Wiley and Sons, New York, 1124 p.
Power, G. M., 1968, Chemical variation in tourmaline from south-west England: Min. Mag. & Jour. Min. Soc. London, v. 36, no. 284, p. 1078-1089.
Robertson, D. E., 1986, Skarn mineralization at Iron Mountain, New Mexico: Tempe, Arizona, Arizona State University, M. S. thesis, 76 p.
Ryall, W. R., 1977, Anomalous trace elements in pyrite in the vicinity of mineralized zones at Woodlawn, N. S. W., Australia: Jour. Geochem. Explor, v. 8, p. 73-84.
Seager, W. R., Shafiquallah, M., Hawley, J. W., and Marvin, R. F., 1984, New K-Ar dates from basalts and the evolution of the southern Rio Grande rift: Geological Society of America, Bulletin 95, p. 87-99.
Shawe, D., R., 1976, Geology and resources of fluorine in the United States: U.S. Geological Survey, Professional Paper 933, 99 p.
Silliman, B., 1882, The mineral regions of southern New Mexico: American Institute of Mining Engineering, Transactions, v. 10, p. 440-443.
Smith, S. M., Closs, L. G., and Theobald, P. K., 1987, Trace-element variation in hydrothermal tourmalines associated with mineralization: El Correo, Sonora, Mexico: in Elliott, I. L. and Smee, B. W. (eds.), Geoexpo/86, Exploration in the North American Cordillera, proceedings, Assoc. Expl. Geochem., Rexdale, Ontario, Canada, p. 109-125.
Taylor, B. E. and Slack, J. F., 1984, Tourmalines from Appalachian Caledonian massive sulfide deposits: textural, chemical, and isotopic relationships: Economic Geology, v. 79, p. 1703-1726.
Tsusue, A., Nedachi, M., and Hashimoto, K., 1981, Geochemistry of apatites in the granitic rocks of the molybdenum, tungsten, and barren provinces of southwest Japan: in Rose, A. W. and Gundlach, H. (eds.), Geochemical Exploration 1980, J. Geochem. Explor., v. 15, p. 285-294.
Theobald, P. K. and Havens, R. G., 1960, Base metals in biotite, magnetite, and their alteration products in a hydrothermally altered quartz monzonite porphyry sill, Summit County, Colorado: Geol. Soc. Amer., proceedings, p. 223.
Theobald, P. K. and Thompson, C. E., 1962, Zinc in magnetite from alluvium and igneous rocks associated with ore deposits: U.S. Geological Survey, Professional Paper 450-C, p. C72-C73.
Theobald, P. K., Overstreet. W. C., and Thompson, C. E., 1967, Minor elements in alluvial magnetite from the Inner Piedmont Belt, North and South Carolina: U.S. Geological Survey, Professional Paper 554-A, 34 p.
Wakita, H. Rey, P. and Schmitt, R. A., 1971, Abundances of the 14 rare-earth elements and 12 other trace-elements in Apollo 12 samples: five igneous and one breccia rocks and four soils: Proceedings 2nd Lunar Sci. Conf., p. 1319-1329.
Williams, F. E., 1966, Fluorspar deposits of New Mexico: U. S. Bureau of Mines, Inf. Circular 8307, 143 p.
Williams, S. A. and Cesbron, F. P., 1977, Rutile and apatite-useful prospecting guides for porphyry copper deposits: Mineral. Mag., v.41, no. 318, p. 288-292.
Woodard, T. W., 1982, Geology of the Lookout Mountain area, Black Range, Sierra County, New Mexico: Albuquerque, N. M., University of New Mexico, M. S. thesis, 95 p.

Appendix A.--Procedure used for fluorite dissolution.

This appendix outlines the fluorite dissolution procedure used in this study for the analysis of the rare earth elements (REE) by inductively coupled plasma mass spectrometry (ICP-MS). This procedure is a modification of a brief description of the topic by Feigl (1958, p. 270-271), where it is mentioned that "in the presence of small amounts of acid, precipitated or native calcium fluoride is readily soluble in warm aqueous solutions of salts that form complex fluorides." Salts mentioned include those of aluminum, beryllium, boron, chromium, and iron.

In this study, chloride salts and HCl were avoided, since chlorine complexes with REE (Al Meier, U. S. Geological Survey, personal communication, 1986). Instead, a 5000 ppm boron standard and nitric acid were used.

The mechanism for fluorite dissolution is relatively simple: the salt disassociates in the acid, aqueous solution and the salt cation (in this study, B^{+++}) forms a complex ion with fluorine (in this study, the fluoroborate ion, BF_4^-). Since the complex ion is more stable than fluorite in the acid, aqueous solution, fluorite goes into solution. Warming the solution speeds up the reaction.

Qualitatively, the reaction is shown below:

$$2CaF_2 + B^{+++} \text{ ---- } 2Ca^{++} + BF_4^-$$

Since the REE substitute for Ca in fluorite, the above reaction puts the REE into solution for analysis.

The following procedure was used for fluorite dissolution:

(1) weigh .100 ± .001 g CaF_2 powder
(2) add .5 ml concentrated HNO_3
(3) add 1 ml 5000 ppm B standard (as H_3BO_3 in water)
(4) heat to 90° C for 10 minutes
(5) let cool to room temperature; let sit for 24 hours (capped)
(6) add 1 ml 5000 ppm B standard
(7) heat to 90° C for about 4 hours
(8) let cool to room temperature
(9) add 1 ml 5 ppm Th and 5 ppm Cd standards
(10) bring solution up to 10 ml with demineralized water
(11) cap/agitate
(12) analyze solution.

The Th and Cd standards are used as internal standards for correction of both sensitivity changes and of changes in metal to metal oxide ion ratios (Lichte and others, 1987).

The dilution factor is 1:100, as shown below:

(.1 g CaF_2)/(10 ml solution) = 1/100.

Appendix B.--Rare earth element and uranium data determined by ICP-MS.
Analyst: A. Meier, U.S. Geological Survey.

	SAMPLE	LATITUDE	LONGITUDE	La ppm	Ce ppm	Pr ppm	Nd ppm	Eu ppm	Sm ppm
1	SC005R	33,28,13	107,38,28	77.58	198.05	28.26	120.77	.50	43.09
2	SC007R1	33,28,17	107,38,22	.64	.69	.09	.34	.01	.09
3	SC007R2	33,28,17	107,38,22	2.55	1.81	.14	.38	.01	.06
4	SC009R2	33,23,41	107,36,39	55.98	132.42	15.98	65.56	3.04	14.55
5	SC010R1	33,24,04	107,36,43	29.41	46.30	6.16	23.17	.99	3.94
6	SC014R6	33,29,02	107,45,32	34.63	67.86	8.56	34.16	2.04	5.69
7	SC015R2	33,28,45	107,45,28	16.50	32.67	4.62	22.07	1.94	4.82
8	SC018R1	33,30,10	107,44,31	16.03	26.80	3.68	17.16	1.61	3.67
9	SC024R2	33,23,15	107,36,30	1.21	1.93	.34	1.84	.26	.62
10	SC027R2	33,23,19	107,36,37	1.77	4.25	.69	3.71	.44	1.36
11	SC027R3	33,23,19	107,36,37	8.29	12.80	1.47	5.04	.23	.94
12	SC028R4	33,24,04	107,36,43	25.02	29.95	5.83	27.26	2.16	8.28
13	SC028R5	33,24,04	107,36,43	31.53	53.67	7.03	26.79	1.20	4.52
14	SC030R1	33,21,50	107,32,17	34.41	65.13	8.51	36.14	4.15	8.04
15	SC030R5	33,21,50	170,32,17	36.85	69.04	9.58	42.34	5.67	10.12
16	SC030R9	33,21,50	107,32,17	41.49	79.69	11.10	48.97	6.23	11.60
17	SC031R4	33,21,43	107,32,18	23.18	43.04	5.33	22.97	2.24	4.74
18	SC032R2	33,21,41	107,32,20	18.37	36.09	5.15	24.30	2.78	6.20
19	SC040R5	33,28,26	107,44,40	1.38	2.50	.39	2.43	.41	.66
20	SC045H	33,28,17	107,38,35	16.83	43.03	6.26	25.66	.24	8.29
21	SC046R1	33,05,35	107,13,47	.90	2.27	.37	2.28	.23	.98
22	SC047R1	33,05,01	107,13,39	1.55	3.08	.46	2.55	.09	.45
23	SC051R1	33,21,51	107,36,07	26.13	40.02	6.37	29.31	2.59	8.84
24	SC051R4	33,21,51	107,36,07	14.16	21.23	2.98	11.39	.85	2.69
25	SC052R1	33,21,52	107,36,05	20.35	25.93	4.00	16.38	1.01	3.62
26	SC054R1	33,21,12	107,35,49	3.49	3.84	.60	2.41	.16	.44
27	SC055R1	33,21,10	107,35,47	2.06	2.64	.43	1.96	.23	.45
28	SC056R1	33,16,29	107,34,39	26.23	33.21	5.50	22.88	1.40	5.45
29	SC056R3	33,16,29	107,34,39	22.61	27.44	4.68	19.89	1.19	4.45
30	SC107R1	33,28,17	107,38,22	.35	.45	.05	.22	.03	.06
31	SC107R2	33,28,17	107,38,22	2.22	1.61	.13	.33	.02	.05

Appendix B (continued).

	SAMPLE	Gd ppm	Tb ppm	Dy ppm	Ho ppm	Er ppm	Tm ppm	Yb ppm	Lu ppm	U ppb
1	SC005R	53.46	12.81	97.97	23.35	79.56	13.70	103.32	14.83	1.09
2	SC007R1	.13	.02	.15	.04	.14	.02	.18	.03	.28
3	SC007R2	.10	.02	.07	.01	.06	.01	.08	.01	.29
4	SC009R2	12.80	2.30	14.31	2.95	8.08	1.13	7.10	1.00	.85
5	SC010R1	3.81	.69	4.42	.89	2.37	.30	1.70	.24	.53
6	SC014R6	3.71	.55	3.01	.51	1.05	.10	.40	.02	.27
7	SC015R2	5.16	.85	5.22	.96	2.17	.23	1.08	.10	.20
8	SC018R1	3.21	.44	2.29	.40	.84	.10	.54	.06	.19
9	SC024R2	.96	.18	1.19	.27	.77	.11	.77	.11	.33
10	SC027R2	2.38	.53	3.60	.77	1.82	.19	1.01	.10	.21
11	SC027R3	.80	.17	1.01	.20	.50	.07	.38	.05	.56
12	SC028R4	11.02	2.20	15.92	3.78	11.10	1.49	8.81	1.14	.49
13	SC028R5	4.28	.79	5.26	1.08	2.99	.38	2.20	.33	.36
14	SC030R1	7.26	1.09	5.39	.97	2.14	.25	1.32	.14	.28
15	SC030R5	8.81	1.32	7.00	1.16	2.64	.28	1.51	.18	.19
16	SC030R9	9.93	1.53	8.41	1.40	3.23	.36	1.98	.23	.19
17	SC031R4	4.90	.89	5.54	1.07	2.53	.27	1.48	.17	.13
18	SC032R2	6.07	1.00	5.87	1.04	2.31	.26	1.32	.15	.17
19	SC040R5	.81	.10	.46	.07	.14	.02	.12	.01	.20
20	SC045H	9.96	2.43	19.20	4.53	15.73	2.63	20.67	2.98	.89
21	SC046R1	2.05	.42	2.97	.68	1.81	.18	.86	.10	.16
22	SC047R1	1.32	.15	1.01	.26	.68	.08	.36	.05	.20
23	SC051R1	11.16	2.41	18.51	4.27	12.84	1.74	10.85	1.41	.39
24	SC051R4	2.60	.53	3.50	.70	1.86	.25	1.58	.21	.46
25	SC052R1	3.99	.81	5.87	1.31	3.65	.46	3.01	.40	.28
26	SC054R1	.50	.09	.69	.16	.48	.07	.50	.08	.44
27	SC055R1	.66	.09	.56	.11	.32	.05	.36	.06	.25
28	SC056R1	6.29	1.28	9.40	2.09	5.92	.73	4.41	.57	.09
29	SC056R3	5.59	1.17	8.22	1.87	5.14	.64	3.75	.49	.11
30	SC107R1	.10	.01	.09	.02	.08	.01	.10	.01	.07
31	SC107R2	.07	.02	.05	.01	.04	.01	.08	.01	.08

Appendix C.--Trace element data determined by ICP-AES. N, not detected at indicated limit.
Analyst: J. Motooka, U. S. Geological Survey.

	SAMPLE	Latitude	Longitude	Al %	Ca %	Fe ppm	Mg ppm	K ppm	Mn ppm
1	SC005R	33,28,13	107,38,28	.90	55.3	70N	250	5200	80N
2	SC007R1	33,28,17	107,38,22	.90	54.2	70N	150	5400	80N
3	SC007R2	33,28,17	107,38,22	1.00	58.3	70N	280	7900	80N
4	SC009R2	33,23,41	107,36,39	.90	57.6	70N	210	6900	80N
5	SC010R1	33,24,04	107,36,43	.90	58.3	70N	150	6700	80N
6	SC014R6	33,29,02	107,45,32	.90	57.3	70N	140	6000	80N
7	SC015R2	33,28,45	107,45,28	.90	58.8	70N	140	5900	80N
8	SC018R1	33,30,10	107,44,31	.90	55.3	90	250	5200	80N
9	SC024R2	33,23,15	107,36,30	.90	58.4	140	300	5300	80N
10	SC027R2	33,23,19	107,36,37	.90	57.9	130	280	5100	80N
11	SC027R3	33,23,19	107,36,37	.90	57.6	86	270	5300	80N
12	SC028R4	33,24,04	107,36,43	.90	59.1	140	280	5000	80N
13	SC028R5	33,24,04	107,36,43	1.00	58.9	190	330	6700	80N
14	SC030R1	33,21,50	107,32,17	.80	50.7	70N	150	4500	80N
15	SC030R5	33,21,50	170,32,17	.90	54.7	82	270	4900	80N
16	SC030R9	33,21,50	107,32,17	.90	57.2	130	290	5000	80N
17	SC031R4	33,21,43	107,32,18	.90	56.5	120	290	5200	80N
18	SC032R2	33,21,41	107,32,20	.90	58.3	120	280	5200	80N
19	SC040R5	33,28,26	107,44,40	.90	58.7	100	270	5300	80N
20	SC045H	33,28,17	107,38,35	.90	56.0	140	290	5300	80N
21	SC046R1	33,05,35	107,13,47	.90	58.3	93	280	5500	80N
22	SC047R1	33,05,01	107,13,39	.90	57.1	100	260	5300	80N
23	SC051R1	33,21,51	107,36,07	.90	57.3	110	270	5100	80N
24	SC051R4	33,21,51	107,36,07	.90	59.4	110	280	5300	80N
25	SC052R1	33,21,52	107,36,05	.90	59.4	110	280	5600	80N
26	SC054R1	33,21,12	107,35,49	.90	59.6	360	280	5600	80N
27	SC055R1	33,21,10	107,35,47	.80	57.0	1900	250	4800	80N
28	SC056R1	33,16,29	107,34,39	.90	55.7	450	270	5200	80N
29	SC056R3	33,16,29	107,34,39	.90	53.6	75	250	5100	80N
30	SC107R1	33,28,17	107,38,22	1.00	59.5	350	280	5600	80N
31	SC107R2	33,28,17	107,38,22	.90	55.8	130	270	5100	80N

Appendix C (continued).

	SAMPLE	Na ppm	Ag ppm	As ppm	Ba ppm	Be ppm	Bi ppm	Ce ppm.	Co ppm	Cr ppm	Cu ppm
1	SC005R	14000	6N	30N	42	2.3	80N	120	8N	8N	2N
2	SC007R1	14000	6N	30N	44	1.3	80N	30N	8N	8N	2N
3	SC007R2	15000	6N	30N	46	1.2	80N	30N	8N	8N	2N
4	SC009R2	14000	6N	30N	44	4.4	80N	52	8N	8N	2.2
5	SC010R1	14000	6N	30N	44	2.1	80N	30N	8N	8N	2N
6	SC014R6	14000	6N	30N	43	1.4	80N	30N	8N	8N	2N
7	SC015R2	14000	6N	30N	42	1.3	80N	30N	8N	8N	2N
8	SC018R1	13000	6N	30N	41	1.1	80N	30N	8N	8N	2N
9	SC024R2	14000	6N	30N	44	1.1	80N	30N	8N	8N	8.3
10	SC027R2	14000	6N	30N	46	1.3	80N	30N	8N	8N	2N
11	SC027R3	14000	6N	30N	44	1.2	80N	30N	8N	8N	2N
12	SC028R4	14000	6N	30N	43	2.1	80N	30N	8N	8N	2N
13	SC028R5	14000	6N	30N	49	2.1	80N	30N	8N	8N	2.1
14	SC030R1	12000	6N	30N	37	1.1	80N	30N	8N	63	2.1
15	SC030R5	14000	6N	30N	43	1.1	80N	30N	8N	8N	2N
16	SC030R9	14000	6N	30N	45	1.2	80N	30N	8N	8N	2N
17	SC031R4	13000	6N	30N	44	1.0	80N	30N	8N	8N	2N
18	SC032R2	13000	6N	30N	43	1.1	80N	30N	8N	8N	2N
19	SC040R5	14000	6N	30N	43	1.1	80N	30N	8N	8N	2N
20	SC045H	14000	6N	30N	43	1.7	80N	30N	8N	8N	2N
21	SC046R1	15000	6N	30N	63	1.2	80N	30N	8N	8N	15
22	SC047R1	14000	6N	30N	380	2.5	80N	30N	8N	8N	2.2
23	SC051R1	13000	6N	30N	48	1.1	80N	30N	8N	8N	2.5
24	SC051R4	14000	6N	30N	50	1.2	80N	30N	8N	8N	4.2
25	SC052R1	14000	6N	30N	46	1.2	80N	30N	8N	8N	3.6
26	SC054R1	15000	6N	30N	45	1.2	80N	30N	8N	55	2.9
27	SC055R1	12000	6N	30N	40	1.1	80N	30N	8N	360	11.0
28	SC056R1	13000	6N	30N	42	1.1	80N	30N	8N	50	2.7
29	SC056R3	13000	6N	30N	42	1.1	80N	30N	8N	8N	2N
30	SC107R1	15000	6N	30N	45	1.2	80N	30N	8N	54	3.2
31	SC107R2	13000	6N	30N	42	1.1	80N	30N	8N	8N	2N

Appendix C (continued).

	SAMPLE	La ppm	Li ppm	Mo ppm	Ni ppm	P ppm	Pb ppm	Sb ppm	Sn ppm	Sr ppm	Ti ppm
1	SC005R	57	3.2	7N	10N	100N	180	50N	30N	24.0	59.0
2	SC007R1	6N	.8N	7N	10N	100N	53	50N	30N	.2N	4.0
3	SC007R2	6N	.8N	7N	10N	100N	50N	50N	30N	2.0	4.3
4	SC009R2	39	.8N	7N	10N	100N	50N	50N	30N	100.0	9.9
5	SC010R1	15	.8N	7N	10N	100N	50N	50N	30N	69.0	9.8
6	SC014R6	19	.8N	7N	10N	100N	50N	50N	30N	51.0	4.0
7	SC015R2	6N	.8N	7N	10N	100N	50N	50N	30N	48.0	4.8
8	SC018R1	6N	.8N	7N	10N	100N	50N	50N	30N	80.0	5.5
9	SC024R2	6N	.8N	7N	10N	100N	50N	50N	30N	49.0	9.6
10	SC027R2	6N	.8N	7N	10N	100N	50N	50N	30N	55.0	6.9
11	SC027R3	6N	.8N	7N	10N	100N	50N	50N	30N	51.0	6.2
12	SC028R4	11	.8N	7N	10N	100N	50N	50N	30N	89.0	12.0
13	SC028R5	17	.8N	7N	10N	100N	50N	50N	30N	73.0	27.0
14	SC030R1	20	.8N	7N	22	100N	94	50N	30N	100.0	5.4
15	SC030R5	21	.8N	7N	10N	100N	50N	50N	30N	96.0	6.9
16	SC030R9	26	.8N	7N	10N	100N	50N	50N	30N	100.0	7.8
17	SC031R4	10	.8N	7N	10N	100N	50N	50N	30N	63.0	6.2
18	SC032R2	6N	.8N	7N	10N	100N	50N	50N	30N	91.0	6.5
19	SC040R5	6N	.8N	7N	10N	100N	50N	50N	30N	100.0	5.4
20	SC045H	6N	.8N	7N	10N	100N	50N	50N	30N	34.0	14.0
21	SC046R1	6N	.8N	7N	10N	100N	53	50N	30N	11.0	6.5
22	SC047R1	6N	.8N	7N	10N	100N	50N	50N	30N	20.0	5.5
23	SC051R1	12	.8N	7N	10N	100N	50N	50N	30N	87.0	11.0
24	SC051R4	6N	.8N	7N	10N	100N	50N	50N	30N	98.0	6.4
25	SC052R1	8	.8N	7N	10N	100N	50N	50N	30N	65.0	7.5
26	SC054R1	6N	.8N	7N	24	100N	50N	50N	30N	81.0	5.9
27	SC055R1	6N	.8N	7N	192	100N	50N	50N	36	83.0	4.6
28	SC056R1	13	.8N	7N	56	100N	50N	50N	30N	36.0	7.9
29	SC056R3	10	.8N	7N	10N	100N	50N	50N	30N	33.0	7.7
30	SC107R1	6N	.8N	7N	68	100N	50N	50N	30N	.9	5.7
31	SC107R2	6N	.8N	7N	10N	100N	50N	50N	30N	2.3	5.4

Appendix C (continued).

	SAMPLE	V ppm	W ppm	Y ppm	Zn ppm	Zr ppm
1	SC005R	3N	30N	770.0	6.0	19
2	SC007R1	3N	30N	2.0N	9.9	19
3	SC007R2	3N	30N	2.0N	15.0	20
4	SC009R2	3N	30N	89.0	4.1	16
5	SC010R1	3N	30N	36.0	2.0N	16
6	SC014R6	3N	30N	25.0	4.5	12
7	SC015R2	3N	30N	46.0	15.0	13
8	SC018R1	3N	30N	15.0	6.3	13
9	SC024R2	3N	30N	9.8	9.7	14
10	SC027R2	3N	30N	36.0	5.5	15
11	SC027R3	3N	30N	5.7	4.4	16
12	SC028R4	3N	30N	150.0	4.5	13
13	SC028R5	3N	30N	39.0	5.3	12
14	SC030R1	3N	30N	35.0	12.0	13
15	SC030R5	3N	30N	37.0	2.8	17
16	SC030R9	3N	30N	46.0	3.7	17
17	SC031R4	3N	30N	43.0	3.6	12
18	SC032R2	3N	30N	37.0	3.7	14
19	SC040R5	3N	30N	2.3	4.0	12
20	SC045H	3N	30N	180.0	6.1	14
21	SC046R1	3N	30N	64.0	3.6	17
22	SC047R1	3N	30N	32.0	4.5	14
23	SC051R1	3N	30N	120.0	8.7	12
24	SC051R4	3N	30N	21.0	8.1	13
25	SC052R1	3N	30N	42.0	3.4	16
26	SC054R1	3N	30N	5.5	5.4	15
27	SC055R1	3N	30N	3.9	5.9	8
28	SC056R1	3N	30N	77.0	8.9	15
29	SC056R3	3N	30N	71.0	2.0N	17
30	SC107R1	3N	30N	2.0N	7.4	15
31	SC107R2	3N	30N	2.0N	8.9	14

Appendix D.--Trace elements determined by SES. N, not detected at indicated lower determination limit; L, detected, but below indicated determination limit.
Analyst: B. Adrian, U. S. Geological Survey.

	SAMPLE	Latitude	Longitude	Sample weight	Fe ppm	Mg ppm	Ti ppm	Mn ppm	Ag ppm	As ppm	Au ppm	B ppm
1	SC002H	33,29,02	107,45,06	10 mg	500N	200N	70	10N	.5N	200N	10N	10N
2	SC002R	33,29,35	170,45,06	10 mg	500N	200N	50	10N	.5N	200N	10N	10N
3	SC005R	33,28,13	107,38,28	10 mg	500N	200L	50	70	.5N	200N	10N	10N
4	SC006H	33,28,17	107,38,40	10 mg	500N	200L	100	20	.5N	200N	10N	10N
5	SC007R1	33,28,17	107,38,22	10 mg	500N	200N	70	10L	.5N	200N	10N	10N
6	SC007R2	33,28,17	107,38,22	10 mg	500N	200N	70	10N	.5N	200N	10N	10N
7	SC008R	33,27,22	107,38,31	10 mg	700	2000	150	70	.5N	200N	10N	10N
8	SC009R1	33,23,41	107,36,39	10 mg	500N	200	50	10N	.5N	200N	10N	10N
9	SC009R2	33,23,41	107,36,39	10 mg	500N	200	100	10N	.5N	200N	10N	10N
10	SC010R1	33,24,04	107,36,43	10 mg	500N	200L	100	10N	.5N	200N	10N	10N
11	SC010R2	33,24,04	107,36,43	10 mg	500N	200L	50	10N	.5N	200N	10N	10N
12	SC010R4	33,24,04	107,36,43	10 mg	500N	200L	50	10N	.5N	200N	10N	10N
13	SC010R5	33,24,04	107,36,43	10 mg	500N	200L	100	10N	.5N	200N	10N	10N
14	SC011H	33,23,55	107,36,50	10 mg	500N	200L	50	10N	.5N	200N	10N	10N
15	SC012R	33,22,12	107,36,17	10 mg	500N	200N	50	10N	.5N	200N	10N	10N
16	SC013R	33,21,51	107,36,07	10 mg	500N	200N	50	10N	.5N	200N	10N	10N
17	SC014R5	33,29,02	107,45,32	10 mg	500N	200L	100	10N	.5N	200N	10N	10N
18	SC014R6	33,29,02	107,45,32	10 mg	500N	200N	50	10N	.5N	200N	10N	10N
19	SC015R2	33,28,45	107,45,28	10 mg	500N	200N	100	10N	.5N	200N	10N	10N
20	SC017R1	33,29,35	107,45,06	10 mg	500N	200L	100	10N	.5N	200N	10N	10N
21	SC017H	33,29,35	107,45,06	10 mg	500N	200L	50	10N	.5N	200N	10N	10N
22	SC018R1	33,30,10	107,44,31	10 mg	500N	200L	50	10N	.5N	200N	10N	10N
23	SC019R1	33,27,22	107,38,31	10 mg	500N	200L	70	10N	.5N	200N	10N	10N
24	SC024R2	33,23,15	107,36,30	10 mg	500N	200	50	10N	.5N	200N	10N	10N
25	SC026R1	33,23,10	107,36,34	10 mg	500N	200L	30	10N	.5N	200N	10N	10N
26	SC026R2	33,23,10	107,36,34	10 mg	500N	200L	50	10N	.5N	200N	10N	10N
27	SC027R2	33,23,19	107,36,37	10 mg	500N	200L	50	10N	.5N	200N	10N	10N
28	SC027R3	33,23,19	107,36,37	10 mg	500N	200L	50	10N	.5N	200N	10N	10N
29	SC028R4	33,24,04	107,36,43	10 mg	500N	200L	50	10N	.5N	200N	10N	10N
30	SC028R5	33,24,04	107,36,43	10 mg	500N	200	150	10L	.5N	200N	10N	10N
31	SC029H	33,23,37	107,36,44	10 mg	500N	200	100	10N	.5N	200N	10N	10N
32	SC030R1	33,21,50	107,32,17	10 mg	500N	200L	70	10N	.5N	200N	10N	10N
33	SC030R3	33,21,50	107,32,17	10 mg	500N	200L	70	10N	.5N	200N	10N	10N
34	SC030R5	33,21,50	107,32,17	10 mg	500N	200N	70	10N	.5N	200N	10N	10N
35	SC030R7	33,21,50	107,32,17	10 mg	500N	200L	70	10N	.5N	200N	10N	10N
36	SC030R8	33,21,50	107,32,17	10 mg	500N	200L	100	10N	.5N	200N	10N	10N
37	SC030R9	33,21,50	107,32,17	10 mg	500N	200N	70	10N	.5N	200N	10N	10N
38	SC031R4	33,21,43	107,32,18	10 mg	500N	200N	70	10N	.5N	200N	10N	10N
39	SC032R2	33,21,41	107,32,20	10 mg	500N	200L	70	10N	.5N	200N	10N	10N
40	SC034R1	33,21,45	107,32,31	10 mg	500N	200L	70	10N	.5N	200N	10N	10N

Appendix D (continued).

	SAMPLE	Latitude	Longitude	Sample weight	Fe ppm	Mg ppm	Ti ppm	Mn ppm	Ag ppm	As ppm	Au ppm	B ppm
41	SC034R2	33,21,45	107,32,31	10 mg	500N	200L	150	10N	.5N	200N	10N	10N
42	SC034R3	33,21,45	107,32,31	10 mg	500N	200L	70	10N	.5N	200N	10N	10N
43	SC035H1	33,21,50	107,32,20	10 mg	500N	200N	70	10N	.5N	200N	10N	10N
44	SC035H2	33,21,50	107,32,20	10 mg	500N	200L	70	10N	.5N	200N	10N	10N
45	SC037H1	33,28,54	107,45,21	10 mg	500L	200N	150	10N	.5N	200N	10N	10N
46	SC038H2	33,28,46	107,45,24	10 mg	500L	200L	100	10N	.5N	200N	10N	10N
47	SC039H	33,30,11	107,44,33	10 mg	500N	200L	100	10L	.5N	200N	10N	10N
48	SC040R2	33,28,26	107,44,40	10 mg	500N	200L	70	10N	.5N	200N	10N	10N
49	SC040R5	33,28,26	107,44,40	10 mg	500N	200N	70	10N	.5N	200N	10N	10N
50	SC041H	33,28,28	107,44,36	10 mg	500N	200L	100	10N	.5N	200N	10N	10N
51	SC042R1	33,28,33	107,44,43	10 mg	500N	200N	100	10N	.5N	200N	10N	10N
52	SC043R3	33,28,51	107,44,57	10 mg	500N	200L	100	10N	.5N	200N	10N	10N
53	SC044R1	33,28,45	107,44,53	10 mg	500N	200N	70	10N	.5N	200N	10N	10N
54	SC045H	33,28,17	107,38,35	10 mg	500N	200L	70	20	.5N	200N	10N	10N
55	SC046R1	33,05,35	107,13,47	10 mg	500N	200N	70	10N	.5N	200N	10N	10N
56	SC046R3	33,05,35	107,13,47	10 mg	500N	200L	70	10N	.5N	200N	10N	10N
57	SC047R1	33,05,01	107,13,39	10 mg	500N	200N	70	10N	.5N	200N	10N	10N
58	SC048H	33,05,02	107,13,44	10 mg	500N	200N	70	10N	.5N	200N	10N	10N
59	SC049H	33,05,32	107,13,57	10 mg	500N	200L	70	10N	.5N	200N	10N	10N
60	SC050R1	33,22,12	107,36,17	10 mg	500N	200N	70	10N	.5N	200N	10N	10N
61	SC051R1	33,21,51	107,36,07	10 mg	500N	200N	70	10N	.5N	200N	10N	10N
62	SC051R4	33,21,51	107,36,07	10 mg	500N	200N	50	10N	.5N	200N	10N	10N
63	SC052R1	33,21,52	107,36,05	10 mg	500N	200N	70	10N	.5N	200N	10N	10N
64	SC053H	33,21,48	107,36,14	10 mg	500N	200L	70	10N	.5N	200N	10N	10N
65	SC054R1	33,21,12	107,35,49	10 mg	500N	200L	50	10N	.5N	200N	10N	10N
66	SC055R1	33,21,10	107,35,47	10 mg	500N	200L	70	10N	.5N	200N	10N	10N
67	SC056R1	33,16,29	107,34,39	10 mg	500N	200N	50	10N	.5N	200N	10N	10N
68	SC056R3	33,16,29	107,34,39	10 mg	500N	200N	50	10N	.5N	200N	10N	10N
69	SC057H1	33,16,30	107,34,45	10 mg	500N	200N	50	10N	.5N	200N	10N	10N
70	SC057H2	33,16,30	107,34,45	10 mg	500N	200N	70	10N	.5N	200N	10N	10N
71	SC058R1	33,16,12	107,34,34	10 mg	500N	200L	70	10N	.5N	200N	10N	10N
72	SC059R1	33,15,37	107,34,07	10 mg	500N	200L	70	10N	.5N	200N	10N	10N
73	SC059R3	33,15,37	107,34,07	10 mg	500N	200L	70	10N	.5N	200N	10N	10N
74	SC060H	33,15,40	107,34,07	10 mg	500N	200L	70	10N	.5N	200N	10N	10N
75	SC061R1	33,16,15	107,34,17	10 mg	500N	200N	70	10N	.5N	200N	10N	10N
76	SC062H	33,20,20	107,34,36	10 mg	500N	200N	70	10N	.5N	200N	10N	10N
77	SC063H	33,21,16	107,35,23	10 mg	500N	200L	150	10N	.5N	200N	10N	10N
78	SC064R1	33,21,16	107,35,24	10 mg	500N	200L	70	10N	.5N	200N	10N	10N
79	SC107R1	33,28,17	107,38,22	10 mg	500N	200N	50	10L	.5N	200N	10N	10N
80	SC107R2	33,28,17	107,38,22	10 mg	500N	200N	70	10N	.5N	200N	10N	10N

Appendix D (continued).

	SAMPLE	Latitude	Longitude	Sample weight	Fe ppm	Mg ppm	Ti ppm	Mn ppm	Ag ppm	As ppm	Au ppm	B ppm
81	SC126R1	33,23,10	107,36,34	10 mg	500N	200L	70	10N	.5N	200N	10N	10N
82	SC126R2	33,23,10	107,36,34	10 mg	500N	200L	70	10N	.5N	200N	10N	10N
83	SC128R4	33,24,04	107,36,43	10 mg	500N	200L	50	10N	.5N	200N	10N	10N
84	SC110R2	33,24,04	107,36,43	10 mg	500N	200N	50	10N	.5N	200N	10N	10N
85	SC128R5	33,24,04	107,36,43	10 mg	500N	200	100	10	.5N	200N	10N	10N
86	SC110R1	33,24,04	107,36,43	10 mg	500N	200L	100	10N	.5N	200N	10N	10N
87	SC130R1	33,21,50	107,32,17	10 mg	500N	200L	100	10N	.5N	200N	10N	10N
88	SC130R7	33,21,50	107,32,17	10 mg	500N	200L	70	10N	.5N	200N	10N	10N
89	SC130R3	33,21,50	107,32,17	10 mg	500N	200L	70	10N	.5N	200N	10N	10N
90	SC130R8	33,21,50	107,32,17	10 mg	500N	200L	70	10N	.5N	200N	10N	10N
91	SC130R5	33,21,50	107,32,17	10 mg	500N	200L	50	10N	.5N	200N	10N	10N
92	SC130R9	33,21,50	107,32,17	10 mg	500N	200N	50	10N	.5N	200N	10N	10N
93	SC135H1	33,21,50	107,32,20	10 mg	500N	200L	50	10N	.5N	200N	10N	10N
94	SC135H2	33,21,50	107,32,20	10 mg	500N	200L	70	10N	.5N	200N	10N	10N
95	SC156R1	33,16,29	107,34,39	10 mg	500N	200N	50	10N	.5N	200N	10N	10N
96	SC156R3	33,16,29	107,34,39	10 mg	500N	200N	50	10N	.5N	200N	10N	10N
97	SC157H1	33,16,30	107,34,45	10 mg	500N	200L	50	10N	.5N	200N	10N	10N
98	SC157H2	33,16,30	107,34,45	10 mg	500N	200L	70	10N	.5N	200N	10N	10N
99	SC020R3	33,27,24	107,38,31	1 mg	N	200	200	L	N	N	N	N
100	SC021H	33,27,22	107,38,33	5 mg	1000N	500	150	20	N	500N	20N	20N
101	SC022R1	33,26,32	107,38,06	2.5 mg	2000N	1000L	200	50N	N	1000N	50N	50N
102	SC036H	33,28,52	107,45,30	1 mg	N	N	L	N	N	N	N	N
103	SC037H2	33,28,54	107,45,21	5 mg	1000N	500L	100	20N	N	500N	20N	20N

Appendix D (continued).

	SAMPLE	Ba ppm	Be ppm	Bi ppm	Cd ppm	Co ppm	Cr ppm	Cu ppm	La ppm	Mo ppm	Nb ppm
1	SC002H	20N	1N	10N	20N	5N	10N	5N	50	5N	20N
2	SC002R	20N	1N	10N	20N	5N	10N	5N	70	5N	20N
3	SC005R	50	5	10N	20N	5N	10N	5N	150	5N	20N
4	SC006H	20N	5	10N	20N	5N	10N	5N	70	5N	20N
5	SC007R1	20N	1N	10N	20N	5N	10N	5N	20L	5N	20N
6	SC007R2	20N	1N	10N	20N	5N	10N	5N	20L	5N	20N
7	SC008R	20N	2	10N	20N	5N	10N	5N	20L	5N	20N
8	SC009R1	20N	7	10N	20N	5N	10N	5N	100	7	20N
9	SC009R2	20N	15	10N	20N	5N	10N	5N	150	5N	20N
10	SC010R1	20N	3	10N	20N	5N	10N	5N	70	5N	20N
11	SC010R2	20N	2	10N	20N	5N	10N	5N	70	5N	20N
12	SC010R4	20N	1	10N	20N	5N	10N	5N	50	5N	20N
13	SC010R5	20N	1.5	10N	20N	5N	10N	5N	100	5N	20N
14	SC011H	20N	1	10N	20N	5N	10N	5N	50	5N	20N
15	SC012R	20N	1N	10N	20N	5N	10N	5N	70	5N	20N
16	SC013R	20N	1N	10N	20N	5N	10N	5N	50	5N	20N
17	SC014R5	20N	1L	10N	20N	5N	10N	5N	100	5N	20N
18	SC014R6	20N	1	10N	20N	5N	10N	5N	70	5N	20N
19	SC015R2	20N	1N	10N	20N	5N	10N	5N	50	5N	20N
20	SC017R1	20N	1N	10N	20N	5N	10N	5N	70	5N	20N
21	SC017H	20N	1N	10N	20N	5N	10N	5N	70	5N	20N
22	SC018R1	20N	1N	10N	20N	5N	10N	5N	50	5N	20N
23	SC019R1	20N	1N	10N	20N	5N	10N	5N	20L	5N	20N
24	SC024R2	20N	1N	10N	20N	5N	10N	5L	20L	5N	20N
25	SC026R1	20N	1N	10N	20N	5N	10N	5N	50	5N	20N
26	SC026R2	20N	1N	10N	20N	5N	10N	5N	50	5N	20N
27	SC027R2	20N	1	10N	20N	5N	10N	5N	20L	5N	20N
28	SC027R3	20N	1L	10N	20N	5N	10N	5N	50	5N	20N
29	SC028R4	20N	3	10N	20N	5N	10N	5N	70	5N	20N
30	SC028R5	20N	3	10N	20N	5N	10N	5N	100	5N	20N
31	SC029H	20L	3	10N	20N	5N	10N	5N	50	5N	20N
32	SC030R1	20N	1N	10N	20N	5N	10N	5N	70	5N	20N
33	SC030R3	20N	1N	10N	20N	5N	10N	5N	70	5N	20N
34	SC030R5	20N	1N	10N	20N	5N	10N	5N	70	5N	20N
35	SC030R7	20N	1N	10N	20N	5N	10N	5N	70	5N	20N
36	SC030R8	20N	1N	10N	20N	5N	10N	5N	100	5N	20N
37	SC030R9	20N	1N	10N	20N	5N	10N	5N	100	5N	20N
38	SC031R4	20N	1N	10N	20N	5N	10N	5N	50	5N	20N
39	SC032R2	20N	1N	10N	20N	5N	10N	5N	50	5N	20N
40	SC034R1	20N	1N	10N	20N	5N	10N	5N	70	5N	20N

Appendix D (continued).

	SAMPLE	Ba ppm	Be ppm	Bi ppm	Cd ppm	Co ppm	Cr ppm	Cu ppm	La ppm	Mo ppm	Nb ppm
41	SC034R2	20N	1N	10N	20N	5N	10N	5N	70	5N	20N
42	SC034R3	20N	1N	10N	20N	5N	10N	5N	70	5N	20N
43	SC035H1	20N	1N	10N	20N	5N	10N	5N	70	5N	20N
44	SC035H2	20N	1N	10N	20N	5N	10N	5N	70	5N	20N
45	SC037H1	100	1.5	10N	20N	5N	10N	5N	50	5N	20N
46	SC038H2	300	1L	10N	20N	5N	10N	5N	100	5N	20N
47	SC039H	100	1N	10N	20N	5N	10N	5N	70	5N	20N
48	SC040R2	20N	1N	10N	20N	5N	10N	5N	20L	5N	20N
49	SC040R5	20N	1N	10N	20N	5N	10N	5N	20L	5N	20N
50	SC041H	20N	1N	10N	20N	5N	10N	5N	50	5N	20N
51	SC042R1	20N	1N	10N	20N	5N	10N	5N	50	5N	20N
52	SC043R3	20N	1N	10N	20N	5N	10N	5N	70	5N	20N
53	SC044R1	20N	1N	10N	20N	5N	10N	5N	70	5N	20N
54	SC045H	20N	7	10N	20N	5N	10N	5N	70	5N	20N
55	SC046R1	20N	1N	10N	20N	5N	10N	5	20L	5N	20N
56	SC046R3	1500	1L	10N	20N	5N	10N	5N	20L	5L	20N
57	SC047R1	300	5	10N	20N	5N	10N	5N	20L	5N	20N
58	SC048H	20N	1.5	10N	20N	5N	10N	5N	20L	5N	20N
59	SC049H	200	1	10N	20N	5N	10N	5N	20L	5N	20N
60	SC050R1	20N	1N	10N	20N	5N	10N	5N	70	5N	20N
61	SC051R1	20N	1N	10N	20N	5N	10N	5N	70	5N	20N
62	SC051R4	20N	1N	10N	20N	5N	10N	5N	50	5N	20N
63	SC052R1	20N	1N	10N	20N	5N	10N	5N	50	5N	20N
64	SC053H	20N	1N	10N	20N	5N	10N	5N	70	5N	20N
65	SC054R1	20N	1N	10N	20N	5N	10N	5N	20L	5N	20N
66	SC055R1	20N	1N	10N	20N	5N	10N	5N	20L	5N	20N
67	SC056R1	20N	1N	10N	20N	5N	10N	5N	70	5N	20N
68	SC056R3	20N	1N	10N	20N	5N	10N	5N	70	5N	20N
69	SC057H1	20N	1N	10N	20N	5N	10N	5N	50	5N	20N
70	SC057H2	20N	1L	10N	20N	5N	10N	5N	50	5N	20N
71	SC058R1	20N	1N	10N	20N	5N	10N	5N	70	5N	20N
72	SC059R1	20N	1N	10N	20N	5N	10N	5N	100	5N	20N
73	SC059R3	20N	1N	10N	20N	5N	10N	5N	50	5N	20N
74	SC060H	20N	1N	10N	20N	5N	10N	5N	50	5N	20N
75	SC061R1	20N	1N	10N	20N	5N	10N	5N	70	5N	20N
76	SC062H	300	1L	10N	20N	5N	10N	5L	50	700	20N
77	SC063H	20N	1N	10N	20N	5N	10N	5N	70	5	20N
78	SC064R1	20N	1L	10N	20N	5N	10N	5N	50	5N	20N
79	SC107R1	20N	1.5	10N	20N	5N	10N	5N	20L	5N	20N
80	SC107R2	20	1N	10N	20N	5N	10N	5N	20L	5N	20N

Appendix D (continued).

	SAMPLE	Ba ppm	Be ppm	Bi ppm	Cd ppm	Co ppm	Cr ppm	Cu ppm	La ppm	Mo ppm	Nb ppm
81	SC126R1	20N	1N	10N	20N	5N	10N	5N	70	5N	20N
82	SC126R2	20N	1N	10N	20N	5N	10N	5N	70	5N	20N
83	SC128R4	20N	5	10N	20N	5N	10N	5N	70	5N	20N
84	SC110R2	20N	3	10N	20N	5N	10N	5N	70	5N	20N
85	SC128R5	20N	1.5	10N	20N	5N	10N	5N	100	5N	20N
86	SC110R1	20N	3	10N	20N	5N	10N	5N	70	5N	20N
87	SC130R1	20N	1N	10N	20N	5N	10N	5N	100	5N	20N
88	SC130R7	20N	1N	10N	20N	5N	10N	5N	70	5N	20N
89	SC130R3	20N	1N	10N	20N	5N	10N	5N	70	5N	20N
90	SC130R8	20N	1N	10N	20N	5N	10N	5N	70	5N	20N
91	SC130R5	20N	1N	10N	20N	5N	10N	5N	70	5N	20N
92	SC130R9	20N	1N	10N	20N	5N	10N	5N	100	5N	20N
93	SC135H1	20N	1N	10N	20N	5N	10N	5N	70	5N	20N
94	SC135H2	20N	1N	10N	20N	5N	10N	5N	70	5N	20N
95	SC156R1	20N	1N	10N	20N	5N	10N	5N	70	5N	20N
96	SC156R3	20N	1N	10N	20N	5N	10N	5N	70	5N	20N
97	SC157H1	20N	1N	10N	20N	5N	10N	5N	50	5N	20N
98	SC157H2	20N	1N	10N	20N	5N	10N	5N	70	5N	20N
99	SC020R3	N	N	N	N	N	N	N	L	N	N
100	SC021H	50N	2N	20N	50N	10N	20N	10L	50L	10N	50N
101	SC022R1	100N	5N	50N	100N	20	50N	20N	100L	20N	100N
102	SC036H	N	N	N	N	N	N	N	L	N	N
103	SC037H2	1000	3	20N	50N	10N	20N	10N	50L	10N	50N

Appendix D (continued).

	SAMPLE	Ni ppm	Pb ppm	Sb ppm	Sc ppm	Sn ppm	Sr ppm	V ppm	W ppm	Y ppm	Zn ppm	Zr ppm	Th ppm
1	SC002H	5N	10N	100N	5N	10N	100	10L	50N	50	200N	30	100N
2	SC002R	5N	10L	100N	5N	10N	100	10L	50N	50	200N	10L	100N
3	SC005R	5N	10N	100N	5L	10N	100N	10L	50N	1000	200N	20	100N
4	SC006H	5N	15	100N	5N	10N	100L	10l	50N	150	200N	20	100N
5	SC007R1	5N	10N	100N	5N	10N	100N	10L	50N	10N	200N	10N	100N
6	SC007R2	5N	10N	100N	5N	10N	100L	10L	50N	10N	200N	10N	100N
7	SC008R	5N	10L	100N	5N	10N	100	10L	50N	30	200	50	100N
8	SC009R1	5N	20	100N	5N	10N	150	10L	50N	150	200N	10N	100N
9	SC009R2	5N	10N	100N	5N	10N	150	10L	50N	100	200N	10N	100N
10	SC010R1	5N	10N	100N	5N	10N	150	10L	50N	50	200N	10N	100N
11	SC010R2	5N	10N	100N	5N	10N	100	10L	50N	300	200N	10N	100N
12	SC010R4	5N	10N	100N	5N	10N	100	10L	50N	50	200N	10N	100N
13	SC010R5	5N	10N	100N	5N	10N	100	10L	50N	500	200N	10N	100N
14	SC011H	5N	10N	100N	5N	10N	100	10L	50N	100	200N	10N	100N
15	SC012R	5N	10N	100N	5N	10N	100L	10L	50N	50	200N	10N	100N
16	SC013R	5N	10N	100N	5N	10N	100	10	50N	70	200N	10N	100N
17	SC014R5	5N	10L	100N	5N	10N	100	10L	50N	50	200N	10N	100N
18	SC014R6	5N	10N	100N	5N	10N	100L	10	50N	30	200N	10N	100N
19	SC015R2	5N	10N	100N	5L	10N	100	10	50N	70	200N	10N	100N
20	SC017R1	5N	10N	100N	5N	10N	100	10	50N	70	200N	10N	100N
21	SC017H	5N	10N	100N	5N	10N	100	10L	50N	70	200N	10N	100N
22	SC018R1	5N	10N	100N	5N	10N	100	10L	50N	30	200N	10N	100N
23	SC019R1	5N	10N	100N	5N	10N	100	10L	50N	15	200N	10N	100N
24	SC024R2	5N	10N	100N	5N	10N	100L	10L	50N	15	200N	10N	100N
25	SC026R1	5N	10N	100N	5N	10N	100L	10L	50N	30	200N	10N	100N
26	SC026R2	5N	10N	100N	5N	10N	100L	10	50N	50	200N	10N	100N
27	SC027R2	5N	10N	100N	5N	10N	100L	10	50N	50	200N	10N	100N
28	SC027R3	5N	10N	100N	5N	10N	100L	10	50N	10	200N	10N	100N
29	SC028R4	5N	10N	100N	5N	10N	100	10L	50N	200	200N	10N	100N
30	SC028R5	5N	15	100N	5N	10N	100	10	50N	50	200N	10N	100N
31	SC029H	5N	20	100N	5N	10N	100	10L	50N	70	200N	10N	100N
32	SC030R1	5N	10N	100N	5N	10N	150	10	50N	50	200N	10N	100N
33	SC030R3	5N	10N	100N	5N	10N	150	10L	50N	30	200N	10N	100N
34	SC030R5	5N	10N	100N	5N	10N	150	10L	50N	50	200N	10N	100N
35	SC030R7	5N	10N	100N	5N	10N	150	10L	50N	50	200N	10N	100N
36	SC030R8	5N	10N	100N	5N	10N	150	10L	50N	50	200N	10N	100N
37	SC030R9	5N	10N	100N	5N	10N	150	10L	50N	70	200N	10N	100N
38	SC031R4	5N	10N	100N	5N	10N	100	10L	50N	50	200N	10N	100N
39	SC032R2	5N	10N	100N	5N	10N	150	10L	50N	30	200N	10N	100N
40	SC034R1	5N	10N	100N	5N	10N	150	10L	50N	50	200N	10N	100N

Appendix D (continued).

	SAMPLE	Ni ppm	Pb ppm	Sb ppm	Sc ppm	Sn ppm	Sr ppm	V ppm	W ppm	Y ppm	Zn ppm	Zr ppm	Th ppm
41	SC034R2	5N	10N	100N	5N	10N	150	10L	50N	100	200N	10N	100N
42	SC034R3	5N	10N	100N	5N	10N	100	10L	50N	100	200N	10N	100N
43	SC035H1	5N	10N	100N	5N	10N	100	10L	50N	70	200N	10L	100N
44	SC035H2	5N	10N	100N	5N	10N	150	10L	50N	70	200N	30	100N
45	SC037H1	5N	10N	100N	5N	10N	100	10L	50N	70	200N	10N	100N
46	SC038H2	5N	10L	100N	5N	10N	100	10L	50N	100	200N	10N	100N
47	SC039H	5N	10	100N	5N	10N	150	10L	50N	70	200N	10N	100N
48	SC040R2	5N	10N	100N	5N	10N	150	10L	50N	10	200N	10N	100N
49	SC040R5	5N	10N	100N	5N	10N	150	10L	50N	10N	200N	10N	100N
50	SC041H	5N	10L	100N	5N	10N	100	10L	50N	30	200N	10L	100N
51	SC042R1	5N	10N	100N	5N	10N	100L	10	50N	150	200N	10N	100N
52	SC043R3	5N	10L	100N	5N	10N	100	10L	50N	150	200N	20	100N
53	SC044R1	5N	10N	100N	5N	10N	100	10L	50N	30	200N	10L	100N
54	SC045H	5N	10N	100N	5N	10N	100L	10L	50N	300	200N	10N	100N
55	SC046R1	5N	30	100N	5N	10N	100L	10L	50N	70	200N	10N	100N
56	SC046R3	5N	30	100N	5N	10N	100	10L	50N	70	200N	10N	100N
57	SC047R1	5N	10N	100N	5N	10N	100L	10L	50N	50	200N	10L	100N
58	SC048H	5N	10N	100N	5N	10N	100L	10L	50N	30	200N	10N	100N
59	SC049H	5N	10N	100N	5N	10N	100L	10L	50N	70	200N	10N	100N
60	SC050R1	5N	10N	100N	5N	10N	100	10L	50N	50	200N	10N	100N
61	SC051R1	5N	10N	100N	5N	10N	100	10L	50N	150	200N	30	100N
62	SC051R4	5N	10L	100N	5N	10N	150	10L	50N	30	200N	10N	100N
63	SC052R1	5N	10N	100N	5N	10N	100	10L	50N	70	200N	10N	100N
64	SC053H	5N	100	100N	5N	10N	100	10L	50N	70	200N	20	100N
65	SC054R1	5N	10L	100N	5N	10N	100	10L	50N	10	200N	10L	100N
66	SC055R1	5N	10N	100N	5N	10N	100	10L	50N	10L	200N	10L	100N
67	SC056R1	5N	10N	100N	5N	10N	100L	10L	50N	70	200N	10N	100N
68	SC056R3	5N	10N	100N	5N	10N	100L	10L	50N	100	200N	10N	100N
69	SC057H1	5N	10N	100N	5N	10N	100	10L	50N	100	200N	10	100N
70	SC057H2	5N	10N	100N	5N	10N	100	10L	50N	70	200N	10L	100N
71	SC058R1	5N	10N	100N	5N	10N	100L	10L	50N	150	200N	10L	100N
72	SC059R1	5N	10N	100N	5N	10N	150	10L	50N	30	200N	10N	100N
73	SC059R3	5N	10N	100N	5N	10N	150	10L	50N	15	200N	10N	100N
74	SC060H	5N	10L	100N	5N	10N	100L	10L	50N	15	200N	10N	100N
75	SC061R1	5N	10N	100N	5N	10N	150	10L	50N	30	200N	10L	100N
76	SC062H	5N	2000	100N	5N	10N	100L	30	200	70	200L	10N	100N
77	SC063H	5N	200	100N	5N	10N	150	15	50N	70	200N	30	100N
78	SC064R1	5N	10N	100N	5N	10N	100	10L	50N	20	200N	10N	100N
79	SC107R1	5N	10N	100N	5N	10N	100L	10L	50N	10N	200N	10N	100N
80	SC107R2	5N	10N	100N	5N	10N	100L	10L	50	10N	200N	10N	100N

Appendix D (continued).

	SAMPLE	Ni ppm	Pb ppm	Sb ppm	Sc ppm	Sn ppm	Sr ppm	V ppm	W ppm	Y ppm	Zn ppm	Zr ppm	Th ppm
81	SC126R1	5N	10N	100N	5N	10N	100L	10L	50N	50	200N	10L	100N
82	SC126R2	5N	10N	100N	5N	10N	100	10L	50N	30	200N	10N	100N
83	SC128R4	5N	10N	100N	5N	10N	100	10L	50N	200	200N	10L	100N
84	SC110R2	5N	10N	100N	5N	10N	100	10L	50N	500	200N	10L	100N
85	SC128R5	5N	20	100N	5N	10N	100	10L	50N	70	200N	10N	100N
86	SC110R1	5N	10N	100N	5N	10N	100	10L	50N	50	200N	10N	100N
87	SC130R1	5N	10N	100N	5N	10N	150	10L	50N	50	200N	10	100N
88	SC130R7	5N	10N	100N	5N	10N	150	10L	50N	30	200N	10N	100N
89	SC130R3	5N	10N	100N	5N	10N	150	10L	50N	30	200N	10N	100N
90	SC130R8	5N	10N	100N	5N	10N	150	10L	50N	30	200N	10N	100N
91	SC130R5	5N	10N	100N	5N	10N	100	10L	50N	50	200N	10N	100N
92	SC130R9	5N	10N	100N	5N	10N	150	10L	50N	70	200N	10N	100N
93	SC135H1	5N	10N	100N	5N	10N	100	10L	50N	70	200N	10L	100N
94	SC135H2	5N	10N	100N	5N	10N	100	10L	50N	50	200N	10L	100N
95	SC156R1	5N	10N	100N	5N	10N	100L	10L	50N	100	200N	10N	100N
96	SC156R3	5N	10N	100N	5N	10N	100L	10L	50N	100	200N	10N	100N
97	SC157H1	5N	10N	100N	5N	10N	100	10L	50N	70	200N	10	100N
98	SC157H2	5N	10N	100N	5N	10N	100	10L	50N	100	200N	10L	100N
99	SC020R3	N	N	N	L	N	L	10	N	10	200	N	N
100	SC021H	10N	20N	200N	10L	20N	200L	20L	100N	500	700	20L	200N
101	SC022R1	20N	50N	500N	20L	50N	500L	50L	200N	50	1000N	50L	500N
102	SC036H	L	N	N	N	N	N	L	N	N	N	N	N
103	SC037H2	10N	20N	200N	10N	20N	200	20N	100N	70	500N	20L	200N

Appendix E. Physical property data for fluorite samples.

Explanation of number codes.

This appendix lists several physical features identified in fluorite samples using a binocular reflected light microscope, a binocular polarizing transmitted light microscope, and short- and long-wave ultraviolet (uV) lamps.

Deposit types are coded as follows:
1 Au-Ag vein
2 Ba-Pb vein
3 "Barren" vein
4 W-Be skarn
5 "Questionable" deposit type.

Color in fluorite (white light) is coded as follows:
1 colorless
2 light green
3 dark green
4 light purple
5 dark purple
7 mixed colorless and light green
8 mixed colorless and dark green
9 mixed colorless and dark purple.

Both short- and long-wave ultraviolet fluorescence colors are coded as follows:
0 no data
1 none observed
2 dull purple
3 purple-white blue to blue-white
5 pale orange
6 bright orange
7 orange-tan
9 yellow-tan.

Relative amounts of extremely tiny anisotropic inclusions observed in fluorite are coded as follows:
1 none
2 trace amount (<10)
3 moderate amount (10-50)
4 abundant (>50).

Appendix E (continued).

	SAMPLE	Latitude	Longitude	Deposit Type	Color	Shortwave uV Light	Longwave uV Light	Anisotropic Inclusions
1	SC002H	33,29,02	107,45,06	1	1	2,1	1,4	2
2	SC002R	33,29,35	107,45,06	1	1	2	2,4	2
3	SC005R	33,28,13	107,38,28	4	1	5,6	1	3
4	SC006H	33,28,17	107,38,40	4	1	1	1	2
5	SC007R1	33,28,17	107,38,22	4	1	2	1	1
6	SC007R2	33,28,17	107,38,22	4	1	2	1	1
7	SC008R	33,27,22	107,38,31	4	1	2,7	2,4	1
8	SC009R1	33,23,41	107,36,39	3	1	2	1,4	1
9	SC009R2	33,23,41	107,36,39	3	3	2	2,4	1
10	SC010R1	33,24,04	107,36,43	3	5	1,2	2	2
11	SC010R2	33,24,04	107,36,43	3	2	2	2,4	1
12	SC010R4	33,24,04	107,36,43	3	2	2	2,4	1
13	SC010R5	33,24,04	107,36,43	3	1	2	4	2
14	SC011H	33,23,55	107,36,50	3	1	2,7	2,4	2
15	SC012R	33,22,12	107,36,17	5	1	2	2	3
16	SC013R	33,21,51	107,36,07	5	2	2	2,4	4
17	SC014R5	33,29,02	107,45,32	1	1	0	0	2
18	SC014R6	33,29,02	107,45,32	1	2	2	2	2
19	SC015R2	33,28,45	107,45,28	1	1	2	2	2
20	SC017R1	33,29,35	107,45,06	1	2	2	2,4	3
21	SC017H	33,29,35	107,45,06	1	7	2	2,4	2
22	SC018R1	33,30,10	107,44,31	1	7	2	2,4	2
23	SC019R1	33,27,22	107,38,31	4	1	1	1	2
24	SC024R2	33,23,15	107,36,30	3	1	2	2	2
25	SC026R1	33,23,10	107,36,34	3	7	2	2	3
26	SC026R2	33,23,10	107,36,34	3	7	2	2	3
27	SC027R2	33,23,19	107,36,37	3	1	2	2	1
28	SC027R3	33,23,19	107,36,37	3	1	2	2	3
29	SC028R4	33,24,04	107,36,43	3	3	1	1,2	2
30	SC028R5	33,24,04	107,36,43	3	5	2	2	4
31	SC029H	33,23,37	107,36,44	3	1	1	2	3
32	SC030R1	33,21,50	107,32,17	3	2	2	2,4	4
33	SC030R3	33,21,50	107,32,17	3	1	2,3	2,3	4
34	SC030R5	33,21,50	107,32,17	3	2	2,3	2,3	4
35	SC030R7	33,21,50	107,32,17	3	7	2,3	2,3	4
36	SC030R8	33,21,50	107,32,17	3	1	2,3	2,3	4
37	SC030R9	33,21,50	107,32,17	3	2	2,3	2,3	3
38	SC031R4	33,21,43	107,32,18	3	7	2	2,3	3
39	SC032R2	33,21,41	107,32,20	3	7	2,3	2,3	4
40	SC034R1	33,21,45	107,32,31	3	7	2,3	2,3	2

Appendix E (continued).

	SAMPLE	Latitude	Longitude Type	Deposit	Color uV Light	Shortwave uV Light	Longwave uV Light	Anisotropic Inclusions
41	SC034R2	33,21,45	107,32,31	3	3	2,3	2,3	3
42	SC034R3	33,21,45	107,32,31	3	7	2,3	2,3	2
43	SC035H1	33,21,50	107,32,20	3	1	2,3	2,3	3
44	SC035H2	33,21,50	107,32,20	3	1	2,3	2,3	3
45	SC037H1	33,28,54	107,45,21	1	1	1	1	3
46	SC038H2	33,28,46	107,45,24	1	1	1,2	1,2	3
47	SC039H	33,30,11	107,44,33	1	1	1,2	1,2	2
48	SC040R2	33,28,26	107,44,40	1	1	2	2	4
49	SC040R5	33,28,26	107,44,40	1	1	2	2	3
50	SC041H	33,28,28	107,44,36	1	8	2	2	3
51	SC042R1	33,28,33	107,44,43	1	7	2	2	2
52	SC043R3	33,28,51	107,44,57	1	1	1,2	1,2	2
53	SC044R1	33,28,45	107,44,53	1	1	2	2	3
54	SC045H	33,28,17	107,38,35	4	9	2,5,6	2	4
55	SC046R1	33,05,35	107,13,47	2	1	2	2	2
56	SC046R3	33,05,35	107,13,47	2	1	2	2	2
57	SC047R1	33,05,01	107,13,39	2	1	2	2	2
58	SC048H	33,05,02	107,13,44	2	1	2	2	4
59	SC049H	33,05,32	107,13,57	2	1	2	2	3
60	SC050R1	33,22,12	107,36,17	5	8	2	2	2
61	SC051R1	33,21,51	107,36,07	5	2	2	2	2
62	SC051R4	33,21,51	107,36,07	5	9	2	2	2
63	SC052R1	33,21,52	107,36,05	3	7	2	2	2
64	SC053H	33,21,48	107,36,14	5	1	1,2	2	2
65	SC054R1	33,21,12	107,35,49	5	1	2,9	2	3
66	SC055R1	33,21,10	107,35,47	5	1	2	2	3
67	SC056R1	33,16,29	107,34,39	3	7	2,3	2,3	3
68	SC056R3	33,16,29	107,34,39	3	7	2,3	2,3	3
69	SC057H1	33,16,30	107,34,45	3	1	2,5	2	3
70	SC057H2	33,16,30	107,34,45	3	1	2,7	2	3
71	SC058R1	33,16,12	107,34,34	3	7	2,3	2,3	3
72	SC059R1	33,15,37	107,34,07	3	7	2,3	2,3	3
73	SC059R3	33,15,37	107,34,07	3	1	2	2	2
74	SC060H	33,15,40	107,34,07	3	1	2	2	3
75	SC061R1	33,16,15	107,34,17	3	1	2	2	3
76	SC062H	33,20,20	107,34,36	5	1	2,5	2	2
77	SC063H	33,21,16	107,35,23	5	1	2	2	2
78	SC064R1	33,21,16	107,35,24	3	1	2	2	3
79	SC107R1	33,28,17	107,38,22	4	1	2	1	1
80	SC107R2	33,28,17	107,38,22	4	1	2	1	1

Appendix E (continued).

	SAMPLE	Latitude	Longitude Type	Deposit	Color uV Light	Shortwave uV Light	Longwave uV Light	Anisotropic Inclusions
81	SC126R1	33,23,10	107,36,34	3	7	2	2	3
82	SC126R2	33,23,10	107,36,34	3	7	2	2	3
83	SC128R4	33,24,04	107,36,43	3	3	1,2	1,2	2
84	SC110R2	33,24,04	107,36,43	3	2	2	2,4	1
85	SC128R5	33,24,04	107,36,43	3	5	2	1,2	4
86	SC110R1	33,24,04	107,36,43	3	5	1,2	2	2
87	SC130R1	33,21,50	107,32,17	3	2	2,4	2,4	4
88	SC130R7	33,21,50	107,32,17	3	7	2,3	2,3	4
89	SC130R3	33,21,50	107,32,17	3	1	2,3	2,3	4
90	SC130R8	33,21,50	107,32,17	3	1	2,3	2,3	4
91	SC130R5	33,21,50	107,32,17	3	2	2,3	2,3	4
92	SC130R9	33,21,50	107,32,17	3	2	2,3	2,3	3
93	SC135H1	33,21,50	107,32,20	3	1	2,3	2,3	3
94	SC135H2	33,21,50	107,32,20	3	1	2,3	2,3	3
95	SC156R1	33,16,29	107,34,39	3	7	2,3	2,3	3
96	SC156R3	33,16,29	107,34,39	3	7	2,3	2,3	3
97	SC157H1	33,16,30	107,34,45	3	1	2,5	2	3
98	SC157H2	33,16,30	107,34,45	3	1	2,7	2	3
99	SC020R3	33,27,24	107,38,31	4	1	2	2	4
100	SC021H	33,27,22	107,38,33	4	1	2,7	2	3
101	SC022R1	33,26,32	107,38,06	4	1	2	2	3
102	SC036H	33,28,52	107,45,30	1	1	1	1	1
103	SC037H2	33,28,54	107,45,21	1	1	1	1	3

Appendix F.--Chondrite-normalized rare earth element plots. Chondrite rare earth element values are from Wakita and others, 1971.

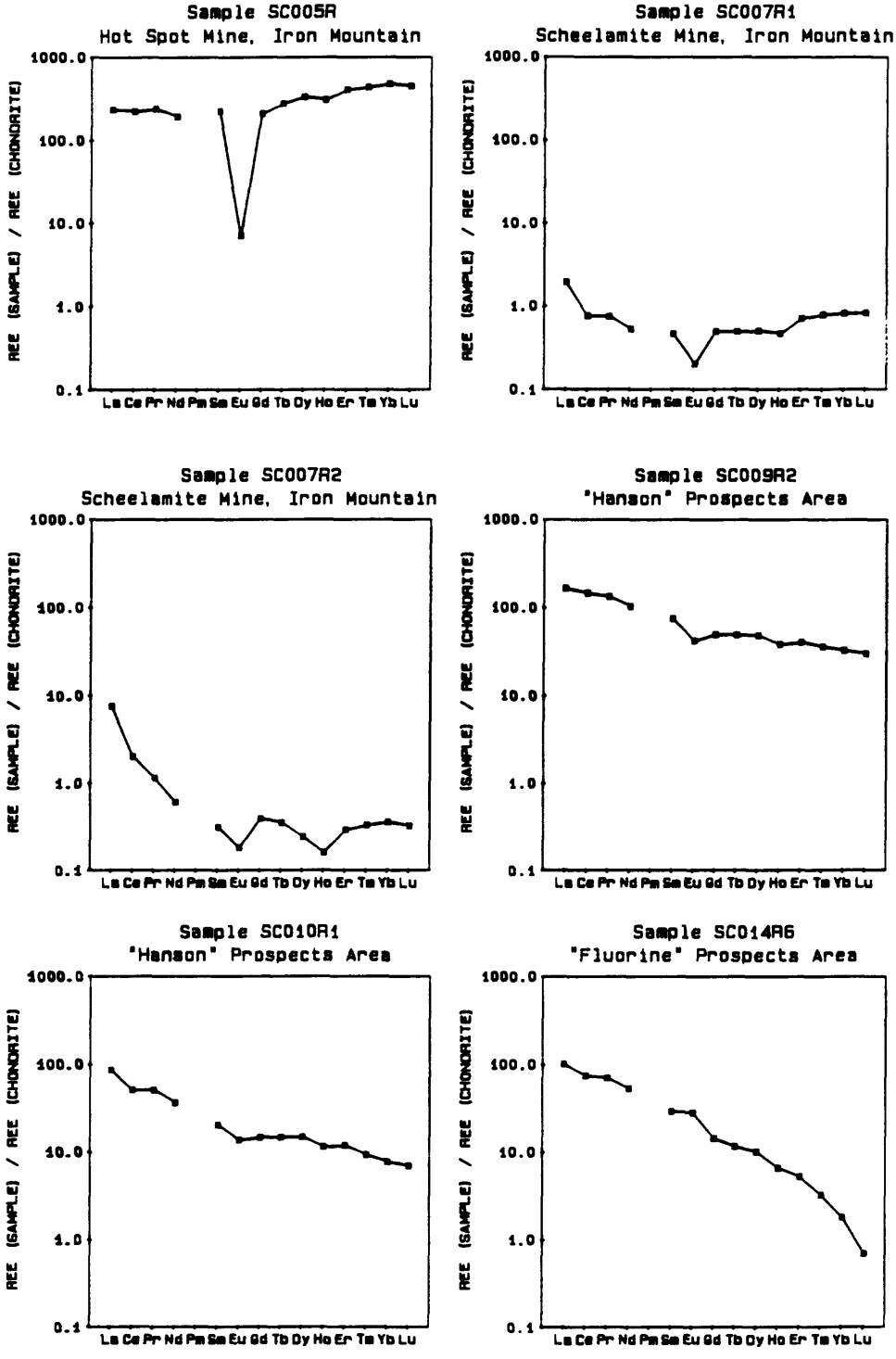

Appendix F (continued).

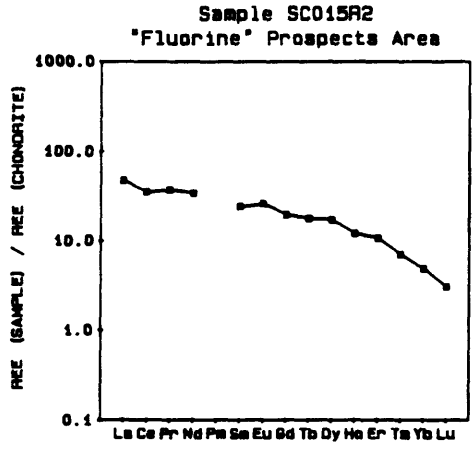

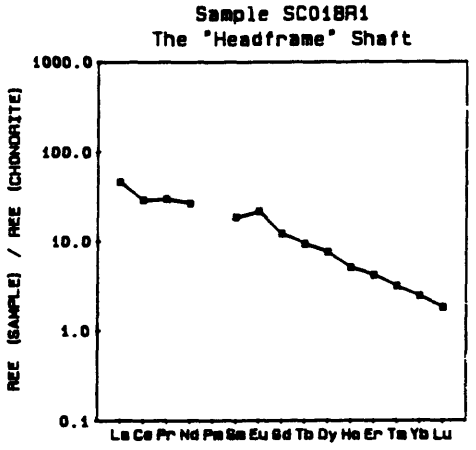

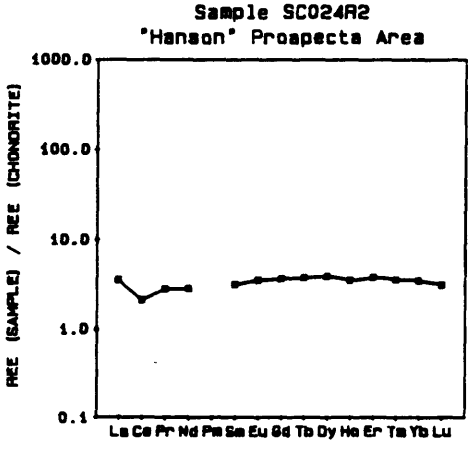

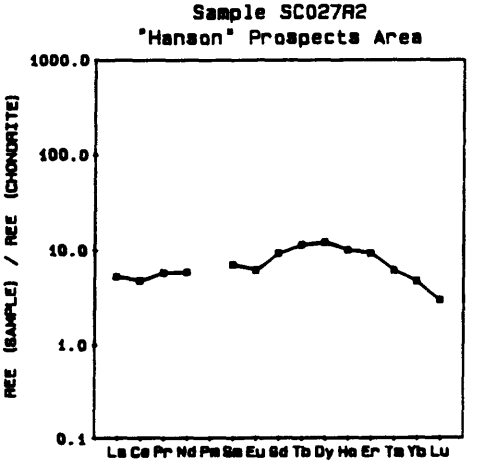

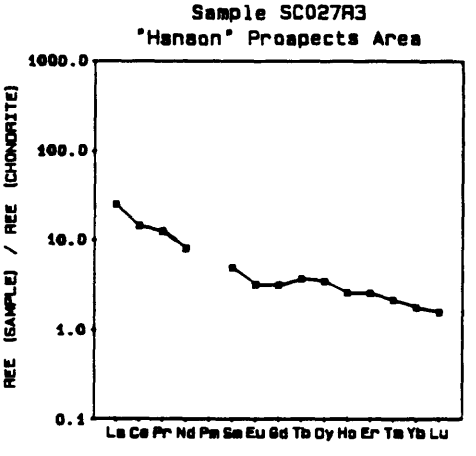

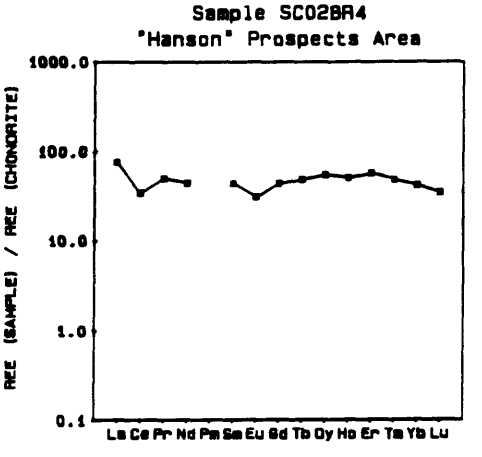

Appendix F (continued).

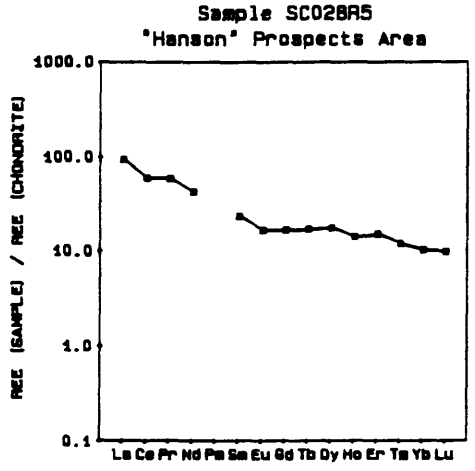

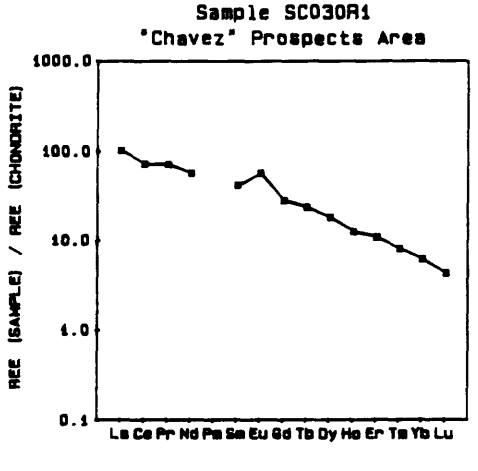

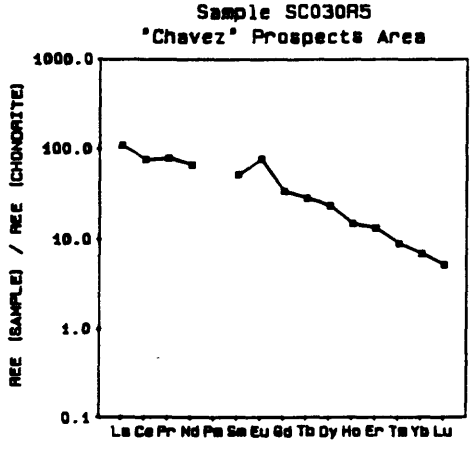

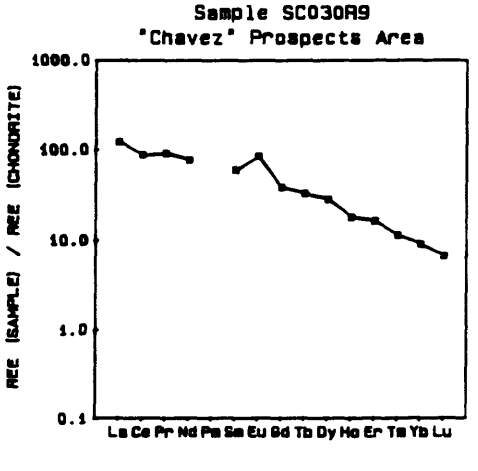

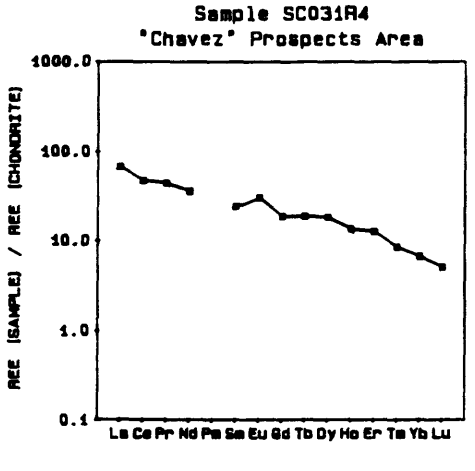

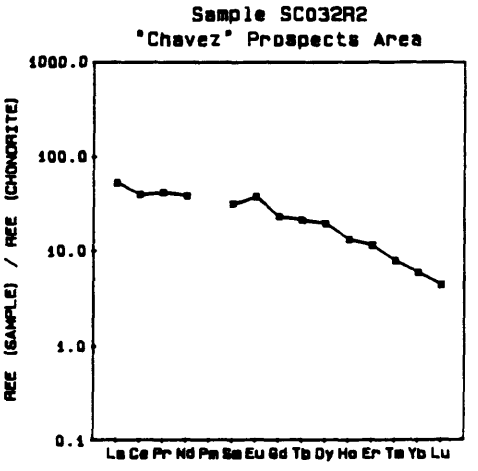

Appendix F (continued).

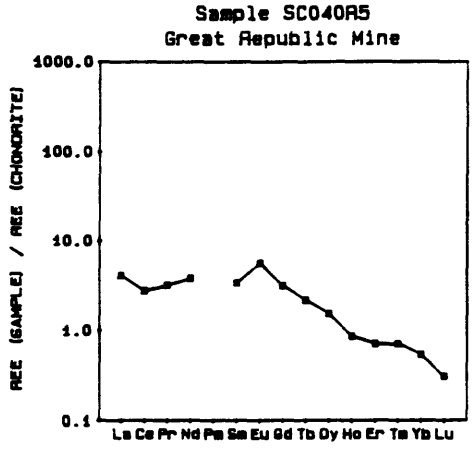

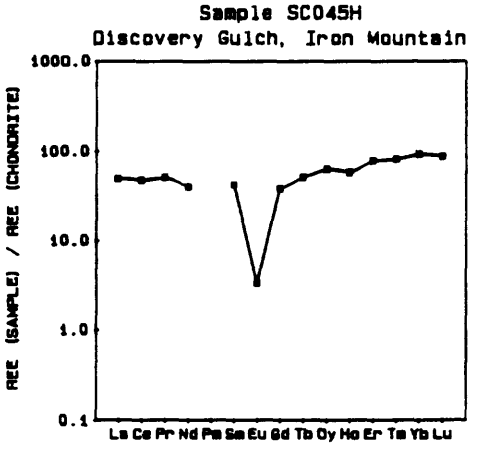

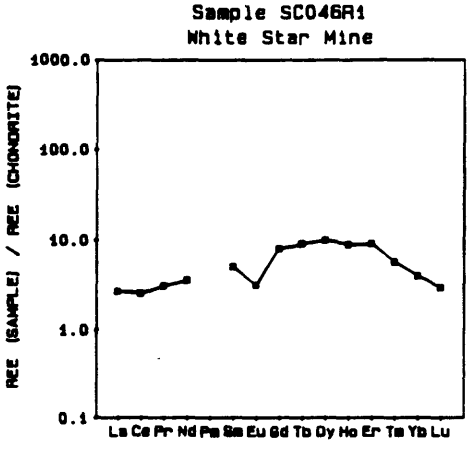

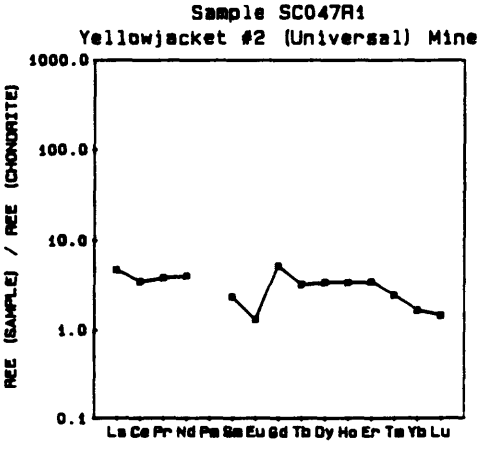

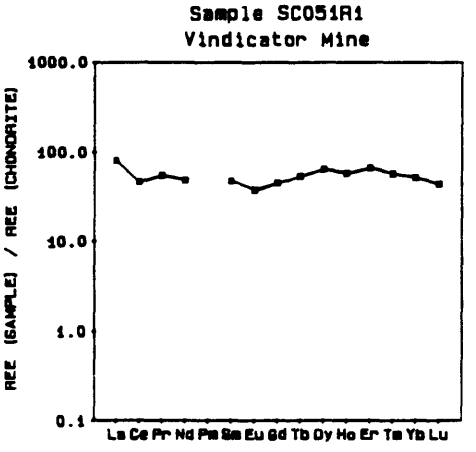

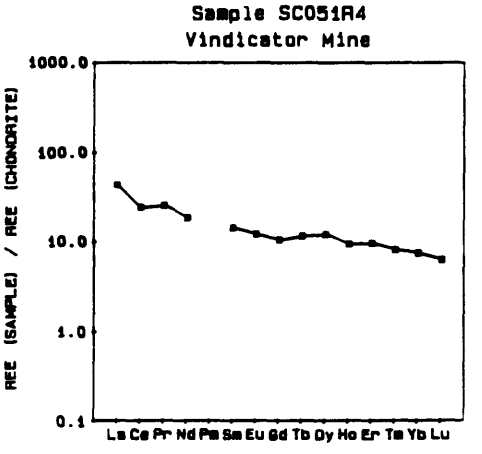

Appendix F (continued).

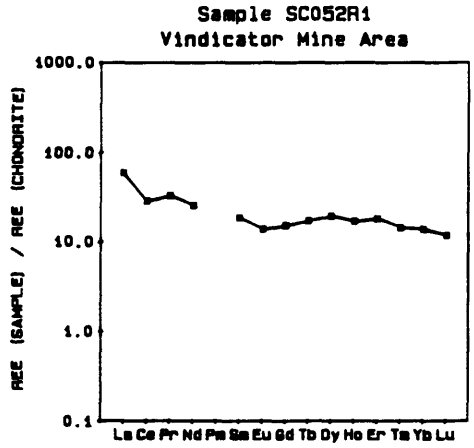

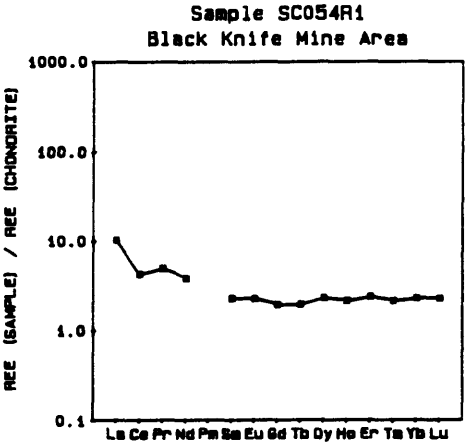

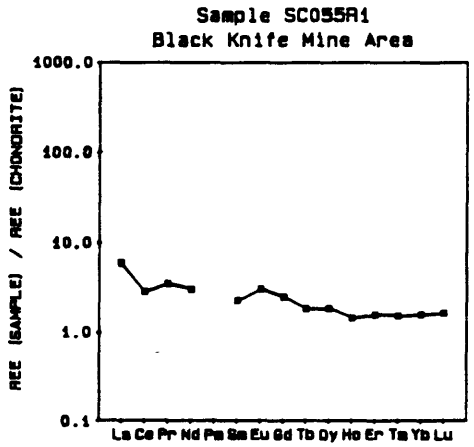

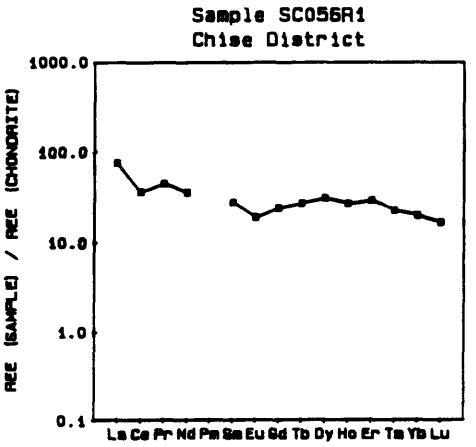

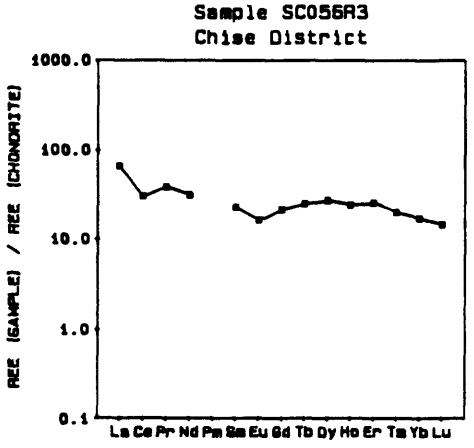

Appendix G.--Histograms for selected elements determined by ICP-AES. All values are in ppm, except for Al and Ca, which are in percent.

CLASS LIMIT - UPPER	OBS FRQ	CUM FRQ	PER FRQ	CUM FRQ	CLASS MIDPOINT	DISTRIBUTION
Aluminum						
N	0	0	.0	.0		
8.000E-01- 8.290E-01	2	2	6.9	6.9	8.145E-01	XX
8.290E-01- 8.580E-01	0	2	.0	6.9	8.435E-01	
8.580E-01- 8.870E-01	0	2	.0	6.9	8.725E-01	
8.870E-01- 9.160E-01	25	27	86.2	93.1	9.015E-01	XXXXX XXXXX XXXXX XXXXX XXXXX
9.160E-01- 9.450E-01	0	27	.0	93.1	9.305E-01	
9.450E-01- 9.740E-01	0	27	.0	93.1	9.595E-01	
9.740E-01- 1.003E+00	2	29	6.9	100.0	9.885E-01	XX
Calcium						
N	0	0	.0	.0		
5.070E+01- 5.200E+01	1	1	3.4	3.4	5.135E+01	X
5.200E+01- 5.330E+01	0	1	.0	3.4	5.265E+01	
5.330E+01- 5.460E+01	2	3	6.9	10.3	5.395E+01	XX
5.460E+01- 5.590E+01	4	7	13.8	24.1	5.525E+01	XXXX
5.590E+01- 5.720E+01	5	12	17.2	41.4	5.655E+01	XXXXX
5.720E+01- 5.850E+01	10	22	34.5	75.9	5.785E+01	XXXXX XXXXX
5.850E+01- 5.980E+01	7	29	24.1	100.0	5.915E+01	XXXXX XX
Iron						
N	8	8	27.6	27.6		XXXXX XXX
7.500E+01- 1.000E+02	5	13	17.2	44.8	8.750E+01	XXXXX
1.000E+02- 1.250E+02	7	20	24.1	69.0	1.125E+02	XXXXX XX
1.250E+02- 1.500E+02	5	25	17.2	86.2	1.375E+02	XXXXX
1.500E+02- 1.750E+02	0	25	.0	86.2	1.625E+02	
1.750E+02- 2.000E+02	1	26	3.4	89.7	1.875E+02	X
2.000E+02- 2.250E+02	0	26	.0	89.7	2.125E+02	
2.250E+02- 2.500E+02	0	26	.0	89.7	2.375E+02	
2.500E+02- 2.750E+02	0	26	.0	89.7	2.625E+02	
2.750E+02- 3.000E+02	0	26	.0	89.7	2.875E+02	
3.000E+02- 3.250E+02	0	26	.0	89.7	3.125E+02	
3.250E+02- 3.500E+02	0	26	.0	89.7	3.375E+02	
3.500E+02- 3.750E+02	1	27	3.4	93.1	3.625E+02	X
3.750E+02- 4.000E+02	0	27	.0	93.1	3.875E+02	
4.000E+02- 4.250E+02	0	27	.0	93.1	4.125E+02	
4.250E+02- 4.500E+02	0	27	.0	93.1	4.375E+02	
4.500E+02- 4.750E+02	1	28	3.4	96.6	4.625E+02	X
(break in scale)				(break in scale)		
1.875E+03- 2.175E+03	1	29	3.4	100.0	2.025E+03	X

Appendix G (continued).

LIMIT - UPPER	OBS FRQ	CUM FRQ	PER FRQ	CUM FRQ	CLASS MIDPOINT	DISTRIBUTION
Magnesium						
N	0	0	.0	.0		
1.400E+02- 1.670E+02	5	5	17.2	17.2	1.535E+02	XXXXX
1.670E+02- 1.940E+02	0	5	.0	17.2	1.805E+02	
1.940E+02- 2.210E+02	1	6	3.4	20.7	2.075E+02	X
2.210E+02- 2.480E+02	0	6	.0	20.7	2.345E+02	
2.480E+02- 2.750E+02	10	16	34.5	55.2	2.615E+02	XXXXX XXXXX
2.750E+02- 3.020E+02	12	28	41.4	96.6	2.885E+02	XXXXX XXXXX XX
3.020E+02- 3.290E+02	0	28	.0	96.6	3.155E+02	
3.290E+02- 3.560E+02	1	29	3.4	100.0	3.425E+02	X
Potassium						
N	0	0	.0	.0		
4.500E+03- 4.990E+03	3	3	10.3	10.3	4.745E+03	XXX
4.990E+03- 5.480E+03	17	20	58.6	69.0	5.235E+03	XXXXX XXXXX XXXXX XX
5.480E+03- 5.970E+03	4	24	13.8	82.8	5.725E+03	XXXX
5.970E+03- 6.460E+03	1	25	3.4	86.2	6.215E+03	X
6.460E+03- 6.950E+03	3	28	10.3	96.6	6.705E+03	XXX
6.950E+03- 7.440E+03	0	28	.0	96.6	7.195E+03	
7.440E+03- 7.930E+03	1	29	3.4	100.0	7.685E+03	X
Sodium						
N	0	0	.0	.0		
1.200E+04- 1.243E+04	2	2	6.9	6.9	1.222E+04	XX
1.243E+04- 1.286E+04	0	2	.0	6.9	1.265E+04	
1.286E+04- 1.329E+04	6	8	20.7	27.6	1.308E+04	XXXXX X
1.329E+04- 1.372E+04	0	8	.0	27.6	1.351E+04	
1.372E+04- 1.415E+04	18	26	62.1	89.7	1.394E+04	XXXXX XXXXX XXXXX XXX
1.415E+04- 1.458E+04	0	26	.0	89.7	1.437E+04	
1.458E+04- 1.501E+04	3	29	10.3	100.0	1.480E+04	XXX
Barium						
N	0	0	.0	.0		
3.700E+01- 4.100E+01	2	2	6.9	6.9	3.900E+01	XX
4.100E+01- 4.500E+01	17	19	58.6	65.5	4.300E+01	XXXXX XXXXX XXXXX XX
4.500E+01- 4.900E+01	6	25	20.7	86.2	4.700E+01	XXXXX X
4.900E+01- 5.300E+01	2	27	6.9	93.1	5.100E+01	XX
5.300E+01- 5.700E+01	0	27	.0	93.1	5.500E+01	
5.700E+01- 6.100E+01	0	27	.0	93.1	5.900E+01	
6.100E+01- 6.500E+01	1	28	3.4	96.6	6.300E+01	X
(break in scale)				(break in scale)		
3.800E+02- 4.290E+02	1	29	3.4	100.0	4.045E+02	X

Appendix G (continued).

LIMIT - UPPER	OBS FRQ	CUM FRQ	PER FRQ	CUM FRQ	CLASS MIDPOINT	DISTRIBUTION
Beryllium						
N	0	0	.0	.0		
1.000E+00- 1.490E+00	22	22	75.9	75.9	1.245E+00	XXXXX XXXXX XXXXX XXXXX XX
1.490E+00- 1.980E+00	1	23	3.4	79.3	1.735E+00	X
1.980E+00- 2.470E+00	4	27	13.8	93.1	2.225E+00	XXXX
2.470E+00- 2.960E+00	1	28	3.4	96.6	2.715E+00	X
2.960E+00- 3.450E+00	0	28	.0	96.6	3.205E+00	
3.450E+00- 3.940E+00	0	28	.0	96.6	3.695E+00	
3.940E+00- 4.430E+00	1	29	3.4	100.0	4.185E+00	X
Copper						
N	17	17	58.6	58.6		XXXXX XXXXX XXXXX XX
2.100E+00- 4.300E+00	9	26	31.0	89.7	3.200E+00	XXXXX XXXX
4.300E+00- 6.500E+00	0	26	.0	89.7	5.400E+00	
6.500E+00- 8.700E+00	1	27	3.4	93.1	7.600E+00	X
8.700E+00- 1.090E+01	0	27	.0	93.1	9.800E+00	
1.090E+01- 1.310E+01	1	28	3.4	96.6	1.200E+01	X
1.310E+01- 1.530E+01	1	29	3.4	100.0	1.420E+01	X
Lanthanum						
N	15	15	51.7	51.7		XXXXX XXXXX XXXXX
8.000E+00- 1.620E+01	7	22	24.1	75.9	1.210E+01	XXXXX XX
1.620E+01- 2.440E+01	4	26	13.8	89.7	2.030E+01	XXXX
2.440E+01- 3.260E+01	1	27	3.4	93.1	2.850E+01	X
3.260E+01- 4.080E+01	1	28	3.4	96.6	3.670E+01	X
4.080E+01- 4.900E+01	0	28	.0	96.6	4.490E+01	
4.900E+01- 5.720E+01	1	29	3.4	100.0	5.310E+01	X
Strontium						
N	1	1	3.4	3.4		X
2.000E+00- 1.600E+01	2	3	6.9	10.3	9.000E+00	XX
1.600E+01- 3.000E+01	2	5	6.9	17.2	2.300E+01	XX
3.000E+01- 4.400E+01	3	8	10.3	27.6	3.700E+01	XXX
4.400E+01- 5.800E+01	5	13	17.2	44.8	5.100E+01	XXXXX
5.800E+01- 7.200E+01	3	16	10.3	55.2	6.500E+01	XXX
7.200E+01- 8.600E+01	4	20	13.8	69.0	7.900E+01	XXXX
8.600E+01- 1.000E+02	5	25	17.2	86.2	9.300E+01	XXXXX
1.000E+02- 1.140E+02	4	29	13.8	100.0	1.070E+02	XXXX

Appendix G (continued).

LIMIT - UPPER	OBS FRQ	CUM FRQ	PER FRQ	CUM FRQ	CLASS MIDPOINT	DISTRIBUTION
Titanium						
N	0	0	.0	.0		
4.000E+00- 1.190E+01	25	25	86.2	86.2	7.950E+00	XXXXX XXXXX XXXXX XXXXX XXXXX
1.190E+01- 1.980E+01	2	27	6.9	93.1	1.585E+01	XX
1.980E+01- 2.770E+01	1	28	3.4	96.6	2.375E+01	X
2.770E+01- 3.560E+01	0	28	.0	96.6	3.165E+01	
3.560E+01- 4.350E+01	0	28	.0	96.6	3.955E+01	
4.350E+01- 5.140E+01	0	28	.0	96.6	4.745E+01	
5.140E+01- 5.930E+01	1	29	3.4	100.0	5.535E+01	X
Yttrium						
N	2	2	6.9	6.9		XX
2.300E+00- 1.123E+02	23	25	79.3	86.2	5.730E+01	XXXXX XXXXX XXXXX XXXXX XXX
1.123E+02- 2.223E+02	3	28	10.3	96.6	1.673E+02	XXX
2.223E+02- 3.323E+02	0	28	.0	96.6	2.773E+02	
3.323E+02- 4.423E+02	0	28	.0	96.6	3.873E+02	
4.423E+02- 5.523E+02	0	28	.0	96.6	4.973E+02	
5.523E+02- 6.623E+02	0	28	.0	96.6	6.073E+02	
6.623E+02- 7.723E+02	1	29	3.4	100.0	7.173E+02	X
Zinc						
N	2	2	6.9	6.9		XX
2.800E+00- 4.500E+00	9	11	31.0	37.9	3.650E+00	XXXXX XXXX
4.500E+00- 6.200E+00	9	20	31.0	69.0	5.350E+00	XXXXX XXXX
6.200E+00- 7.900E+00	1	21	3.4	72.4	7.050E+00	X
7.900E+00- 9.600E+00	3	24	10.3	82.8	8.750E+00	XXX
9.600E+00- 1.130E+01	2	26	6.9	89.7	1.045E+01	XX
1.130E+01- 1.300E+01	1	27	3.4	93.1	1.215E+01	X
1.300E+01- 1.470E+01	0	27	.0	93.1	1.385E+01	
1.470E+01- 1.640E+01	2	29	6.9	100.0	1.555E+01	XX
Zirconium						
N	0	0	.0	.0		
8.000E+00- 9.700E+00	1	1	3.4	3.4	8.850E+00	X
9.700E+00- 1.140E+01	0	1	.0	3.4	1.055E+01	
1.140E+01- 1.310E+01	10	11	34.5	37.9	1.225E+01	XXXXX XXXXX
1.310E+01- 1.480E+01	4	15	13.8	51.7	1.395E+01	XXXX
1.480E+01- 1.650E+01	7	22	24.1	75.9	1.565E+01	XXXXX XX
1.650E+01- 1.820E+01	4	26	13.8	89.7	1.735E+01	XXXX
1.820E+01- 1.990E+01	2	28	6.9	96.6	1.905E+01	XX
1.990E+01- 2.160E+01	1	29	3.4	100.0	2.075E+01	X